BLEJSKE DELAVNICE IZ FIZIKE LETNIK 12, ŠT. 1
BLED WORKSHOPS IN PHYSICS VOL. 12, NO. 1

ISSN 1580-4992

Proceedings of the Mini-Workshop

Understanding hadronic spectra

Bled, Slovenia, July 3 – 10, 2011

Edited by

Bojan Golli
Mitja Rosina
Simon Širca

University of Ljubljana and Jožef Stefan Institute

DMFA – ZALOŽNIŠTVO
LJUBLJANA, NOVEMBER 2011

The Mini-Workshop *Understanding hadronic spectra*

was organized by

Jožef Stefan Institute, Ljubljana
Department of Physics, Faculty of Mathematics and Physics, University of Ljubljana

and sponsored by

Slovenian Research Agency
Department of Physics, Faculty of Mathematics and Physics, University of Ljubljana
Society of Mathematicians, Physicists and Astronomers of Slovenia

Organizing Committee

Mitja Rosina, Bojan Golli, Simon Širca

List of participants

Luis Alvarez Ruso, Valencia, alvarez@teor.fis.uc.pt
Enrique Ruiz Arriola, Granada, earriola@ugr.es
Wojtek Broniowski, Krakow, b4bronio@cyf-kr.edu.pl
Marko Bračko, Ljubljana, marko.bracko@ijs.si
Joseph Day, Graz, jday21@gmail.com
Veljko Dmitrašinović, Belgrade, dmitrasin@yahoo.com
Bojan Golli, Ljubljana, bojan.golli@ijs.si
Regina Kleinhappel, Graz, regina.kleinhappel@gmx.at
Daniel Kupelwieser, Graz, daniel.kupelwieser@uni-graz.at
Willi Plessas, Graz, willibald.plessas@uni-graz.at
Martin Rohrmoser, Graz, martin.rohrmoser@edu.uni-graz.at
Saša Prelovšek, Ljubljana, Sasa.Prelovsek@ijs.si
Mitja Rosina, Ljubljana, mitja.rosina@ijs.si
Wolfgang Schweiger, Graz, wolfgang.schweiger@uni-graz.at
Vikram Soni, New Delhi, v.soni@airtelmail.in
Ica Stancu, Liege, fstancu@ulg.ac.be
Simon Širca, Ljubljana, simon.sirca@fmf.uni-lj.si

Electronic edition

http://www-f1.ijs.si/BledPub/

Contents

Preface

With the MiniWorkshop behind us, do we now better understand hadronic spectra? Or rather, will these Proceedings remind you that at our meeting, as many new problems have been opened as old ones resolved? But it is clear that we made progress on several fronts, and have learned a lot from each other.

Electroexcitation of baryons continues to be a fruitful source of information about the structure and spectra of light baryons. It is encouraging that many ideas, especially about pion clouds, are applicable also at higher energies, in deep inelastic scattering. The role of relativity has been further documented in understanding strange baryon spectra. The problem of theoretically underestimated resonance widths persists, while coupled-channels approaches instill some hope in its ultimate resolution.

Lattice QCD has become a respectable operational theory, and now even quark modelists can resort to it to obtain some insights, for example, into pion-pion scattering or transverse structure of the pion. The $1/N_c$ expansion has also gained some appreciation by suggesting, among other things, a $SU(2N_f)$ classification of baryon multiplets (for N_c colours and N_f flavours). This expansion also helps to understand scalar mesons and their mixing with glueballs.

New resonances in the charmonium spectrum still excite interaction between experimentalists and theorists (as much as the interaction between dimeson and tetraquark configurations). Our eyes should thus also be aimed at Heaven: perhaps new surprises about stability of 3-quark clusters in dense nuclear matter are hidden in the clues provided by the heavy magnetars?

Therefore, we need you at Bled again, next year.

Ljubljana, November 2011

M. Rosina
B. Golli
S. Širca

Predgovor

Ko se oziramo nazaj na letošnjo Blejsko delavnico iz fizike, ali se nam zdi, da sedaj bolje razumemo hadronske spektre? Ali pa nas bo ta Zbornik opomnil, da smo na našem srečanju odprli vsaj toliko novih problemov, kot smo rešili starih? Jasno pa nam je, da smo napredovali na mnogih frontah in da smo se veliko naučili drug od drugega. Ta predgovor v slovenščini naj služi tudi kot kratek povzetek naših aktivnosti in dosežkov.

Vzbujanje barionov s trki elektronov je še vedno ploden vir informacij o zgradbi in spektrih lahkih barionov. Vzpodbudno je, da veljajo mnoge ideje, zlasti o pionskih oblakih, tudi pri visokih energijah pri globoko neelastičnem sipanju. Vedno močneje se zavedamo vloge relativnosti, ki se je izkazala kot neizogibni sestavni del pristopov k razumevanju spektrov čudnih barionov. Vseeno nas še vedno skrbijo problemi s širinami resonanc, saj enostavni teoretični modeli napovedujejo premajhne širine; rešitev pričakujemo šele od računov s sklopljenimi razpadnimi kanali.

Kromodinamika na mreži si je pridobila ugled, da vsaj kvalitativno uspešno simulira lastnosti marsikaterih količin. Celo mojstri kvarkovskih modelov lahko iz nje dobijo koristne vpoglede, recimo v sipanje piona na pionu ali v transverzalno zgradbo piona. Razvoj po recipročnem številu barv je bil tudi odmeven. Med drugim je sugeriral klasifikacijo barionskih multipletov z grupo $SU(2N_f)$ v zvezi z okusi kvarkov, pomagal pa je tudi razumeti mešanje skalarnih mezonov med seboj in z gluonijem.

Nove resonance v spektru čarmonija še vzpodbujajo sodelovanje med eksperimentalci in teoretiki (kakor tudi med dimezonskimi in tetrakvarkovskimi konfiguracijami). Ozirati pa se moramo tudi v nebo: morda nas čakajo presenečenja o stabilnosti trokvarkovskih gruč znotraj goste jedrske snovi, ki jih skrivajo težke magnetne zvezde, magnetarji.

Torej vas drugo leto spet potrebujemo na Bledu!

Ljubljana, novembra 2011

M. Rosina
B. Golli
S. Širca

Workshops organized at Bled

- *What Comes beyond the Standard Model* (June 29–July 9, 1998), Vol. **0** (1999) No. 1
- *Hadrons as Solitons* (July 6–17, 1999)
- *What Comes beyond the Standard Model* (July 22–31, 1999)
- *Few-Quark Problems* (July 8–15, 2000), Vol. **1** (2000) No. 1
- *What Comes beyond the Standard Model* (July 17–31, 2000)
- *Statistical Mechanics of Complex Systems* (August 27–September 2, 2000)
- *Selected Few-Body Problems in Hadronic and Atomic Physics* (July 7–14, 2001), Vol. **2** (2001) No. 1
- *What Comes beyond the Standard Model* (July 17–27, 2001), Vol. **2** (2001) No. 2
- *Studies of Elementary Steps of Radical Reactions in Atmospheric Chemistry*
- *Quarks and Hadrons* (July 6–13, 2002), Vol. **3** (2002) No. 3
- *What Comes beyond the Standard Model* (July 15–25, 2002), Vol. **3** (2002) No. 4
- *Effective Quark-Quark Interaction* (July 7–14, 2003), Vol. **4** (2003) No. 1
- *What Comes beyond the Standard Model* (July 17–27, 2003), Vol. **4** (2003) Nos. 2-3
- *Quark Dynamics* (July 12–19, 2004), Vol. **5** (2004) No. 1
- *What Comes beyond the Standard Model* (July 19–29, 2004), Vol. **5** (2004) No. 2
- *Exciting Hadrons* (July 11–18, 2005), Vol. **6** (2005) No. 1
- *What Comes beyond the Standard Model* (July 18–28, 2005), Vol. **6** (2005) No. 2
- *Progress in Quark Models* (July 10–17, 2006), Vol. **7** (2006) No. 1
- *What Comes beyond the Standard Model* (September 16–29, 2006), Vol. **7** (2006) No. 2
- *Hadron Structure and Lattice QCD* (July 9–16, 2007), Vol. **8** (2007) No. 1
- *What Comes beyond the Standard Model* (July 18–28, 2007), Vol. **8** (2007) No. 2
- *Few-Quark States and the Continuum* (September 15–22, 2008), Vol. **9** (2008) No. 1
- *What Comes beyond the Standard Model* (July 15–25, 2008), Vol. **9** (2008) No. 2
- *Problems in Multi-Quark States* (June 29–July 6, 2009), Vol. **10** (2009) No. 1
- *What Comes beyond the Standard Model* (July 14–24, 2009), Vol. **10** (2009) No. 2
- *Dressing Hadrons* (July 4–11, 2010), Vol. **11** (2010) No. 1
- *What Comes beyond the Standard Model* (July 12–22, 2010), Vol. **11** (2010) No. 2
- *Understanding hadronic spectra* (July 3–10, 2011), Vol. **12** (2011) No. 1
- *What Comes beyond the Standard Model* (July 11–21, 2011), Vol. **12** (2011) No. 2

Also published in this series

- Book of Abstracts, *XVIII European Conference on Few-Body Problems in Physics*, Bled, Slovenia, September 8–14, 2002, Edited by Rajmund Krivec, Bojan Golli, Mitja Rosina, and Simon Širca, Vol. **3** (2002) No. 1–2

BLED WORKSHOPS
IN PHYSICS
VOL. 12, NO. 1
p. 1

Proceedings of the Mini-Workshop
Understanding hadronic spectra
Bled, Slovenia, July 3 - 10, 2011

Meson dynamics in the vector-scalar sector*

L. Alvarez-Ruso[a], J. A. Oller[b], J. M. Alarcón[b]

[a] Instituto de Física Corpuscular, UVEG-CSIC, Valencia, Spain
[b] Departamento de Física, Universidad de Murcia, Murcia, Spain

Abstract. We have studied the $\phi(1020)f_0(980)$ and $\phi(1020)a_0(980)$ S-wave scattering at threshold energies employing chiral Lagrangians coupled to vector mesons by minimal coupling. The $\phi\, f_0$ ($\phi\, a_0$) interaction kernel is obtained by treating the $f_0(980)$ [$a_0(980)$] as bound (dynamically generated) state and resuming unitarity loops. We are able to describe the $e^+e^- \to \phi(1020)f_0(980)$ recent scattering data concluding that the $Y(2175)$ resonance has a large $\phi(1020)f_0(980)$ component. We also predict a strong $\phi(1020)a_0(980)$ interaction that can be studied in $e^+e^- \to \phi\pi^0\eta$. For some sets of parameters a clear resonant peak indicates the presence of an isovector companion of the $Y(2175)$.

1 Introduction

A new hadronic spectroscopy has emerged in the last decade thanks to the experimental activity carried out meanly at e^+e^- facilities (BES at IHEP, CLEO at LEPP, BABAR in SLAC, Belle at KEK) but also at $p\bar{p}$ colliders (CDF,D0 at FNAL) and in fixed target experiments such as HERA-B at DESY. Indeed, our understanding of meson spectroscopy has been challenged by the observation of several exotic states (extensive reviews can be found, for example, in Ref. [1]). These can be neutral mesons with quantum numbers that are not allowed for $q\bar{q}$ pairs ($J^{PC} = 0^{--}, 0^{+-}, 1^{-+}, 2^{+-}, \ldots$) but also states with conventional quantum numbers that cannot be easily accommodated into the constituent quark model. One such a state is the resonance $\phi(2170)$ (or $Y(2175)$, as we will refer to it from now on), a light unflavored meson with quantum numbers $J^{PC} = 1^{--}$, $I^G = 0^-$, mass of 2175 ± 15 MeV and width $\Gamma_Y = 61 \pm 18$ MeV (PDG estimates [2]). It was first observed by the BABAR Collaboration [3, 4] in the initial-state radiation process $e^+e^- \to \phi\, f_0(980)\, \gamma \to K^+K^-\pi\pi\gamma$ and also found by BES in $J/\Psi \to \eta\, \phi\, f_0(980)$ decay [5]. The Belle Collaboration has performed the most precise measurements so far of the reactions $e^+e^- \to \phi\, \pi^+\pi^-$ and $e^+e^- \to \phi\, f_0(980)$ finding $M_Y = 2079 \pm 13^{+79}_{-28}$ MeV and $\Gamma_Y = 192 \pm 23^{+25}_{-61}$ MeV [6]. The obtained width is larger than in previous measurements but the error is also large.

These experimental findings have triggered a considerable theoretical activity aimed at unraveling the nature and properties of the $Y(2175)$. It has been interpreted as a tetraquark [7–9], with a mass of 2.21 ± 0.09 GeV [7] or 2.3 ± 0.4 GeV [8] calculated using QCD sum rules with meson-meson $(s\bar{s})(s\bar{s})$ currents [7] and

* Talk delivered by L. Alvarez-Ruso

adding diquark-antidiquark $(ss)(\bar{s}\bar{s})$ ones [8]. In the diquark-antidiquark picture a prominent $Y(2175) \to \Lambda\bar{\Lambda}$ decay mode appears [9]. The $Y(2175)$ has also been identified with the lightest hybrid $s\bar{s}g$ state [10] with $K_1(1400)\,K$ and $K_1(1270)\,K$ as dominant decay channels. Conventional $s\bar{s}$ states in 2^3D_1 or 3^3S_1 configurations have been considered as their masses are expected to be compatible with the $Y(2175)$ [11] although the estimated widths are too large. Reference [12] studies the three-body $K\bar{K}\phi(1020)$ scattering with two-body pseudoscalar-pseudoscalar and vector-pseudoscalar interactions taken from unitarized chiral perturbation theory [13,14]. A resonance with 2170 MeV mass is generated albeit with a width of only 20 MeV.

2 $\phi(1020)$ $f_0(980)$ scattering

In Ref. [15] we have studied the S-wave scattering of the vector meson $\phi(1020)$ with the scalar $f_0(980)$, the channel with the same quantum numbers as the $Y(2175)$. This is feasible because both the $\phi(1020)$ and the $f_0(980)$ are rather narrow resonances.

First we derive the kernel of the $\phi\, f_0$ interaction. For this we take advantage of the fact that the $f_0(980)$ scalar meson is successfully described as a $K\bar{K}$ bound state [13,16]. This means that in the second Riemann sheet, in the vicinity of the $f_0(980)$ pole

$$-iT_{K\bar{K}} = \frac{\gamma_0^2}{k^2 - M_{f_0}^2} + \gamma_1 + \gamma_2(M_{f_0}^2 - k^2) + \dots \,, \text{ and } \lim_{k^2 \to M_{f_0}^2} (M_{f_0}^2 - k^2)(-iT_{K\bar{K}}) = \gamma_0^2 \,. \tag{1}$$

Therefore, the $\phi(1020)f_0(980)$ interaction can be obtained from the $\phi(1020)K\bar{K}$ one by extracting the residue at the $f_0(980)$ double pole position that arises from the initial and final $K\bar{K}$ rescatterings.

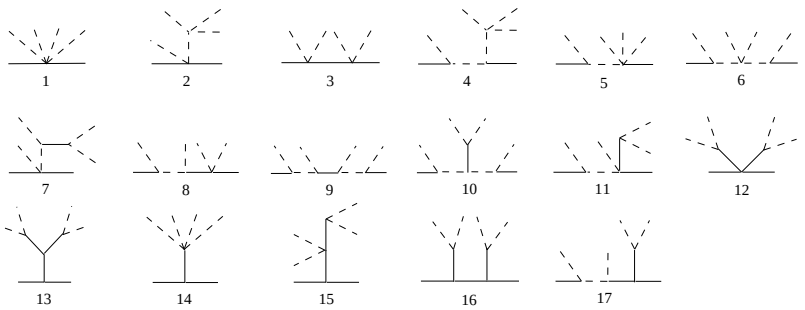

Fig. 1. Feynman diagrams for $\phi K\bar{K}$ scattering. Dashed lines denote kaons and solid ones, vector mesons.

The contributions to the $\phi(K\bar{K})_{I=0} \to \phi(K\bar{K})_{I=0}$ amplitude, determined with chiral Lagrangians coupled to vector mesons are depicted in Fig. 1. It can be shown [15] that close to the $\phi K\bar{K}$ threshold and taking into account that the

$f_0(980)$ is also close to the $K\bar{K}$ threshold, the dominant term is given by diagram 2.

The rescattering of initial and final $K\bar{K}$ pairs in this dominant amplitude gives rise to the diagram on the left hand side of Fig. 2. For the $(K\bar{K})^2$ vertices we take

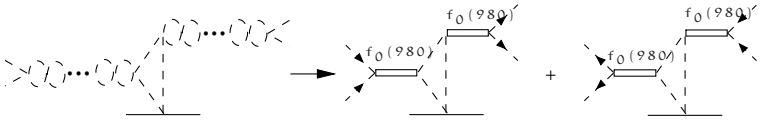

Fig. 2. Dominant contribution to the $\phi(K\bar{K})_{I=0}$ amplitude with $K\bar{K}$ initial and final state interactions that contain $f_0(980)$ poles.

only on-shell amplitudes. The off-shell parts are proportional to the inverse of kaon propagators and cancel with them in the calculation of the loop, resulting in amplitudes that do not correspond anymore to the dominant triangular kaon-loop but to other topologies. After projecting into S-waves

$$\mathcal{M}^S_{I=0} = -t_{\phi K}\, T_{K\bar{K}}(k^2)\, T_{K\bar{K}}(k'^2)\, L_S \tag{2}$$

where $t_{\phi K}$ and $T_{K\bar{K}}$ are the full scattering amplitudes, $k^2(k'^2)$ is the initial (final) $K\bar{K}$ invariant mass and

$$L_S = \frac{1}{4\pi^2}\int_{-1}^{+1}\frac{d\cos\rho}{Q^2}\int_0^{1/2} dx \frac{1}{c}\left[\log(1-2x/c) - \log(1+2x/c)\right], \tag{3}$$

with

$$c^2 = \frac{4}{Q^2}\left[x^2Q^2 + 2k^2x(1-2x) - m_K^2 + i\epsilon\right]. \tag{4}$$

Here $Q^2 = -2\mathbf{p}^2(1-\cos\rho)$ in terms of the relative angle ρ between the incoming $\mathbf{p}$ and outgoing $\mathbf{p}'$ ϕ three-momenta in the ϕf_0 CM frame.

The residue at the $f_0(980)$ double pole is the $f_0(980)\phi(1020)$ potential

$$V_{\phi f_0} = \frac{1}{\gamma_0^2}\lim_{k^2,k'^2\to M^2_{f_0}}(k^2 - M^2_{f_0})(k'^2 - M^2_{f_0})M^S_{I=0} = -t_{\phi K}\,\gamma_0^2\, L_S, \tag{5}$$

which is unitarized as schematically shown in Fig. 3 leading to the full ϕf_0 amplitude

$$T_{\phi f_0} = \frac{V_{\phi f_0}}{1 + V_{\phi f_0}\, G_{\phi f_0}}. \tag{6}$$

The loop function $G_{\phi f_0}$ is expressed in terms of a renormalization scale fixed to the ρ meson mass $\mu = 770$ MeV and a subtraction constant a_1 to be fitted to data [15].

We have performed fits to the $e^+e^- \to \phi f_0(980)$ BABAR and Belle data [4, 6]. The $\phi(1020)\, f_0(980)$ strong scattering amplitude is employed to correct the production process by final state interactions (FSI)

$$\sigma(s) = \frac{\sigma_{BG}(s)}{|1 + V_{\phi f_0} G_{\phi f_0}|^2}. \tag{7}$$

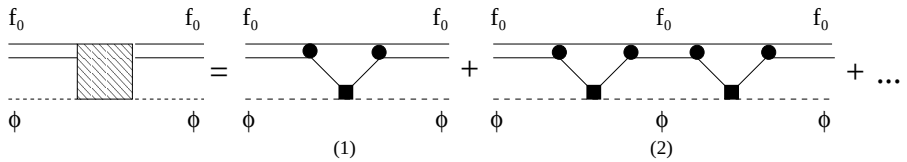

Fig. 3. Diagrammatic representation of the full $\phi f_0(980)$ amplitude.

For the nonresonant background production cross section the Belle fit (Fig. 6(b) of Ref. [6]) has been adopted. In our fits the $f_0(980)$ properties, pole position M_{f_0} and residue γ_0^2 are taken from two different studies [17, 18]; $t_{\phi K}$ and a_1 are free parameters. The results are presented in Table 1 and Fig. 4

	M_{f_0} [MeV] (fixed)	γ_0^2 [GeV^2] (fixed)	$t_{\phi f_0}$	a_1
Fit 1	980	16	-54 ± 4	-2.41 ± 0.14
Fit 2	988	13.2	-27 ± 1	-2.61 ± 0.14

Table 1. Fits to the $e^+e^- \to \phi(1020) f_0(980)$ BABAR [4] and Belle [6] data.

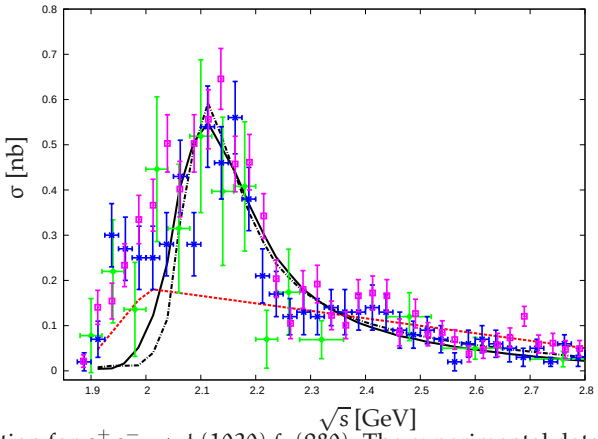

Fig. 4. Cross section for $e^+e^- \to \phi(1020)\, f_0(980)$. The experimental data are from Ref. [4] (diamonds and crosses) and Ref. [6] (empty boxes). The solid and dash-dotted lines correspond to the first and second fits of Table 1. The dashed line shows the background.

The description of the data is satisfactory, particularly the peak position and width. Worse is the agreement at $\sqrt{s} < 2$ GeV: the suppression of the theoretical curves happens because the $V_{\phi f_0}$ potential is large due to the $1/Q^2$ factor. We obtain negative values for a_1 as it should be for a dynamically generated resonance. Moreover, the resulting scale $\Lambda = (4\pi f)/\sqrt{|a_1|} \simeq 0.75$ GeV, preserves a natural size around M_ρ. The interpretation of the $t_{\phi K}$ values is more difficult due to the

lack of information about the ϕK interaction close to threshold. Nevertheless one should recall that the $K_1(1400)$ resonance is only 100 MeV below this threshold. Therefore, the assumption that ϕK scattering is dominated by the $K_1(1400)$ would explain the negative sign of $t_{\phi K}$ because

$$t_{\phi K} \sim \frac{\gamma^2_{K_1 \phi K}}{M^2_{K_1} - (M_\phi + m_K)^2} < 0\,. \tag{8}$$

Our fitted $t_{\phi K}$ values are very different from those used in Ref. [12], taken from Ref. [14] which does not contain the $K_1(1400)$. With a $t_{\phi K} \sim 12 - 7\,i$ as in Ref. [14] we would not describe the $e^+e^- \to \phi(1020)\,f_0(980)$ data. This means that even if the results of both Refs. [12,15] support the interpretation of the $Y(2175)$ as a dynamically generated resonance, the two descriptions are quantitatively different.

3 $\phi(1020)$ $a_0(980)$ scattering

In the present contest, it is relevant to establish whether there is an isovector companion of the isoscalar $Y(2175)$. It will help constraining theoretical models. In particular, the calculation of Ref. [12] does not find any resonance in the isovector $\phi(1020)a_0(980)$ S-wave channel. Experimentally, this resonance could show up in $e^+e^- \to \phi(1020)a_0(980) \to \phi(1020)\pi^0\eta$, as suggested in Ref. [19] or in $e^+e^- \to \phi(1020)a_0(980) \to \phi(1020)K^+K^-$ [20]. Our study of the $\phi(1020)a_0(980)$ [21] interaction proceeds as described in the previous section but replacing the scalar-isoscalar $f_0(980)$ by the scalar-isovector $a_0(980)$. The latter is treated as a dynamical resonance in coupled channels (mainly $K\bar{K}$ and $\pi^0\eta$) whose properties depend on the adopted approach (see Table 2). No new free parameters need to be introduced if one demands that the $e^+e^- \to \phi(1020)\,f_0(980)$ cross section is reproduced and takes $t_{\phi K}$, a_1 from Table 1.

	M_{a_0} [GeV]	$\gamma^2_{K\bar{K}}$ [GeV^2]
BS	$1.009 + i\,0.056$	$24.73 - i\,10.82$
N/D	$1.055 + i\,0.025$	$17.37 - i\,24.77$

Table 2. $a_0(980)$ properties, pole position M_{a_0} and residue $\gamma^2_{K\bar{K}}$, as obtained with the Bethe-Salpeter (BS) equation [13] and the N/D method [18].

We have investigated the corrections to the $e^+e^- \to \phi(1020)a_0(980) \to \phi(1020)\pi^0\eta$ reaction that arise from $\phi(1020)a_0(980)$ FSI finding strong modifications (see Fig. 5). If the $a_0(980)$ properties from the N/D method are taken, a strong peak around 2.03 GeV is observed, signaling the presence of the dynamically generated isovector 1^{--} resonance. For the BS pole no peak is generated but a strong reduction of the cross-section takes place. This result further supports the idea that a study of the $e^+e^- \to \phi(1020)a_0(980)$ reaction, which should be accessible at present e^+e^- factories, may provide novel relevant information about hadronic structure and interactions in the 2 GeV region.

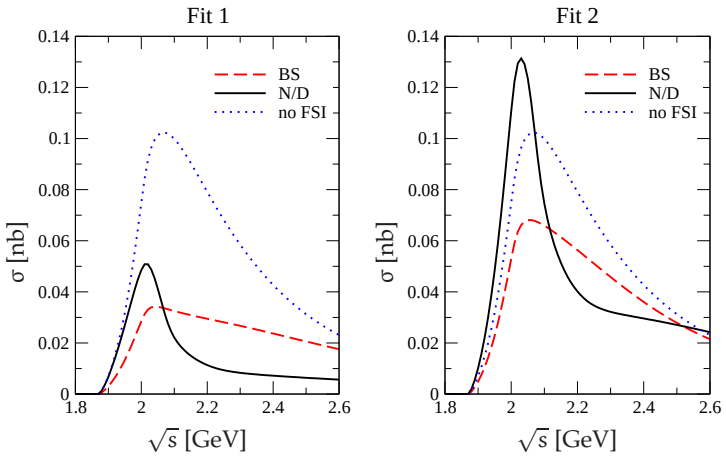

Fig. 5. $e^+e^- \to \phi(1020)a_0(980) \to \phi(1020)\pi^0\eta$ cross section. The dotted lines in both plots is the result of Ref. [19] where final state $\phi(1020)a_0(980)$ rescattering was not considered. The rest of the lines include FSI for the sets of parameters given in Tables 1, 2.

References

1. S. L. Zhu, Int. J. Mod. Phys. E **17** (2008) 283; N. Drenska *et al.*, Riv. Nuovo Cim. **033** (2010) 633-712; N. Brambilla *et al.*, Eur. Phys. J. **C71** (2011) 1534.
2. C. Amsler *et al.* [Particle Data Group], Phys. Lett. B **667** (2008) 1.
3. B. Aubert *et al.* [BABAR Collaboration], Phys. Rev. D **74** (2006) 091103.
4. B. Aubert *et al.* [BABAR Collaboration], Phys. Rev. D **76** (2007) 012008.
5. M. Ablikim, *et al.* [BES Collaboration], Phys. Rev. Lett. **100** (2008) 102003.
6. C. P. Shen *et al.* [Belle Collaboration], Phys. Rev. D **80** (2009) 031101.
7. Z. G. Wang, Nucl. Phys. A **791** (2007) 106.
8. H.-X. Chen, X. Liu, A. Hosaka and S.-L. Zhu, Phys. Rev. D **78** (2008) 034012.
9. N. V. Drenska, R. Faccini and A. D. Polosa, Phys. Lett. B **669** (2008) 160.
10. G.-J. Ding and M.-L. Yan, Phys. Lett. B **650** (2007) 390.
11. G.-J. Ding and M.-L. Yan, Phys. Lett. B **657** (2007) 49; T. Barnes, N. Black and P. R. Page, Phys. Rev. D **68** (2003) 054014.
12. A. Martinez Torres *et al.*, Phys. Rev. D **78** (2008) 074031.
13. J. A. Oller and E. Oset, Nucl. Phys. A **620** (1997) 438; (E)-ibid. A **652** (1999) 407.
14. L. Roca, E. Oset and J. Singh, Phys. Rev. D **72** (2005) 014002.
15. L. Alvarez-Ruso, J. A. Oller and J. M. Alarcón, Phys. Rev. D **80** (2009) 054011.
16. J. D. Weinstein and N. Isgur, Phys. Rev. Lett. **48** (1982) 659.
17. M. Albaladejo and J. A. Oller, Phys. Rev. Lett. **101** (2008) 252002.
18. J. A. Oller and E. Oset, Phys. Rev. D **60** (1999) 074023.
19. C. A. Vaquera-Araujo and M. Napsuciale, Phys. Lett. B **681** (2009) 434.
20. S. Gomez-Avila, M. Napsuciale and E. Oset, Phys. Rev. D **79** (2009) 034018.
21. L. Alvarez-Ruso, J. A. Oller and J. M. Alarcon, Phys. Rev. D **82** (2010) 094028.

BLED WORKSHOPS
IN PHYSICS
VOL. 12, NO. 1
p. 7

Proceedings of the Mini-Workshop
Understanding hadronic spectra
Bled, Slovenia, July 3 - 10, 2011

0^{++} states in a large-N_c Regge approach*

Enrique Ruiz Arriola[a] and Wojciech Broniowski [b]

[a]Departamento de Física Atómica, Molecular y Nuclear and Instituto Carlos I de Física Teórica y Computacional, Universidad de Granada, E-18071 Granada, Spain
[b]The H. Niewodniczański Institute of Nuclear Physics PAN, PL-31342 Kraków, Poland, and Institute of Physics, Jan Kochanowski University, PL-25406 Kielce, Poland

Abstract. Scalar-isoscalar states ($J^{PC} = 0^{++}$) are discussed within the large-N_c Regge approach. We find that the lightest $f_0(600)$ scalar-isoscalar state fits very well into the pattern of the radial Regge trajectory where the resonance nature of the states is advantageously used. We confirm the obtained mass values from an analysis of the pion and nucleon spin-0 gravitational form factors, recently measured on the lattice. We provide arguments suggesting an alternating meson-glueball pattern of the 0^{++} states, which is supported by the pseudoscalar-isovector 0^{+-} excited spectrum and asymptotic chiral symmetry. Finally, matching to the OPE requires a fine-tuned mass condition of the vanishing dimension-2 condensate in the Regge approach with infinitely many scalar-isoscalar states.

1 Introduction

The goal of this talk is to discuss various intriguing aspects of the spectrum of scalar-isoscalar states. Approaches developed in recent years may shed new light on this long-elaborated problem in hadronic physics.

Subsequent hadron resonances listed in the Particle Data Group (PDG) tables increase their mass up to the upper experimental limit of 2.5 GeV, while their width remains bound within 500 MeV. In Fig. 1 we show separately the widths of all baryons and mesons listed in the PDG tables [1] as functions of the mass of the state. One naturally expects that broad resonances, i.e., with $\Gamma \sim m$, escape phenomenological analysis; even if they existed, they might be missing from the PDG as difficult to assess experimentally. Note, however, that with the exception of the notorious $f_0(600)$ resonance and a few baryon and meson states, the ratio is bound by the line $\Gamma/m \sim 1/3$ (the dashed line in Fig. 2).

A natural and model-independent framework to understand this feature is provided by the limit of large number of colors in QCD. Indeed, in this large-N_c limit, with $g^2 N_c$ fixed, baryons are heavy with mass $m = \mathcal{O}(N_c)$ and width $\Gamma = \mathcal{O}(N_c^0)$ [2,3], while mesons and glueballs are stable, with mass independent of N_c, namely $m = \mathcal{O}(N_c^0)$, and width Γ suppressed as $1/N_c$ and $1/N_c^2$, respectively. This means that Γ/m is suppressed (see, e.g., [4] for a review). In particular, one has $\Gamma/m \sim N_c^{-1}$ for mesons and baryons, while $\Gamma/m \sim N_c^{-2}$ for glueballs.[1]

* Talk delivered by Enrique Ruiz Arriola

[1] Fig. 1 suggests that it is reasonable to assume that excited states in the spectrum follow a more accurate large-N_c pattern than the ground state.

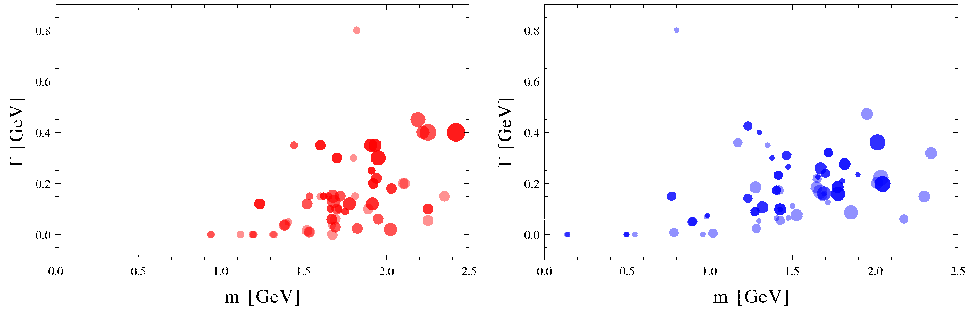

Fig. 1. Width of *all* baryons (left panel) and mesons (right panel) listed in the PDG tables [1] as a function of the hadron mass (in GeV). The surface of each point is proportional to the $(2J+1)$ spin degeneracy, while the intensity is proportional to the isospin degeneracy $(2I+1)$.

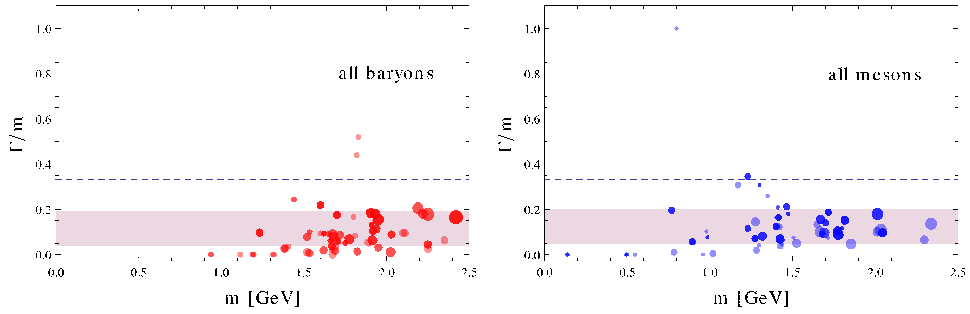

Fig. 2. Same as Fig. 1 for the width/mass ratio. The large-N_c limit predicts $\Gamma/m \sim \mathcal{O}(N_c^{-1})$. The dashed horizontal line corresponds to $1/3$. The gray bands reflect the uncertainties of the fit $\Gamma/m = 0.12(8)$.

On the other hand, at high excitations mesons are expected to resemble strings of length $l \sim m/\sigma$, with σ denoting the string tension (see, e.g., Ref. [5] and references therein). Actually, the decay rate of a string per unit time, Γ, is estimated to be proportional to the length [6,7], which immediately yields constant Γ/m.[2] In Fig. 2 we show the ratio of widths to masses of *all* baryons and mesons listed in the PDG tables [1], plotted as functions of the mass of the state. If we compute the average weighted with the $(2J+1)$ spin degeneracy and its spread, we find (α are the remaining quantum numbers, including isospin)

$$\frac{\Gamma}{m} \equiv \sum_{J,\alpha} (2J+1) \frac{\Gamma_{J,\alpha}}{m_{J,\alpha}} = 0.12(8) \tag{1}$$

for both baryons and mesons! This rather small ratio, complying to the large-N_c and string-model arguments, suggests that this is a generic feature of the hadronic spectrum rather than a lack of experimental ability to resolve too broad states. One may thus assert in this regard that the PDG spectrum is fairly complete.

[2] The argument directly carries over to baryons, treated as a quark-diquark string.

2 Masses of resonances

A resonance may be interpreted as a superposition of states with a given mass distribution, approximately spanning the $m \pm \Gamma/2$ interval. Of course, the shape of the distribution depends on the particular process where the resonance is produced, and thus on the background. The rigorous quantum-mechanical definition of the resonance corresponds to a pole in the second Riemann sheet in the partial-wave amplitude of the corresponding decay channel, which becomes independent of the background. However, although quoting the pole is highly desirable, with a few exceptions this is *not* what one typically finds in the PDG.

As a matter of fact, several definitions are used: pole in the second Riemann sheet, pole in the K-matrix, Breit-Wigner resonance, maximum in the speed plot, time delay, etc. (see, e.g., [8, 9]). Clearly, while all these definitions converge for narrow resonances, even for broad states we expect the masses to be compatible within their corresponding $m \pm \Gamma/2$ intervals. As mentioned, the values listed in the PDG for a given resonance correspond to different choices and/or processes, but mostly the results are compatible within the estimated width differences.

The lowest resonance in QCD is the 0^{++} state $f_0(600)$ or the σ—meson. It appears as a complex pole in the second Riemann sheet of the $\pi\pi$ scattering amplitude at $\sqrt{s_\sigma} = m_\sigma - i\Gamma_\sigma/2$ with $m_\sigma = 441^{+16}_{-8}$ and $\Gamma_\sigma = 544^{+18}_{-24}$ MeV [10] (see also Ref. [11]). While these are remarkably accurate, it is unclear whether these numbers can be directly used in hadronic physics. An analysis of the role played by the σ as a correlated 2π exchange in the central component to the NN force shows that the complex-pole exchange does not accurately describe this effect in the range 1 fm $< r <$ 5 fm, but prefers a value in between the pole and the Breit-Wigner approximation, $m_\sigma = 600(50)$ MeV [12]. The Breit-Wigner parameters are $(m_\sigma, \Gamma_\sigma) = (841(5), 820(20))$ MeV [13]. For the time delay method we obtain $(m_\sigma, \Gamma_\sigma) \sim (475, 630)$ MeV. As we see, the different determinations agree within the wide $m_\sigma \pm \Gamma_\sigma/2$ interval.

3 Scalar Regge spectrum

Higher 0^{++} states listed in the PDG [1] follow roughly the general pattern of increasing mass but not their width. Radial and rotational Regge trajectories were analyzed in Ref. [14]. For scalar states [15] two parallel radial trajectories could then be identified, including three states per trajectory. In a recent work [16, 17] (see also [18]) we have analyzed all the 0^{++} states which appear in the PDG tables (see Fig. 3) and found that *all* fit into a single radial Regge trajectory of the form

$$M_S(n)^2 = \frac{a}{2} n + m_\sigma^2. \tag{2}$$

The mass of the σ state can be deduced from this trajectory as the mass of the lowest state. The resonance nature of these states suggests to use the corresponding half-width as the mass uncertainty in the χ^2 fit:

$$\chi^2 = \sum_n \left(\frac{M_{f,n} - M_S(n)}{\Gamma_{f,n}/2} \right)^2 . \tag{3}$$

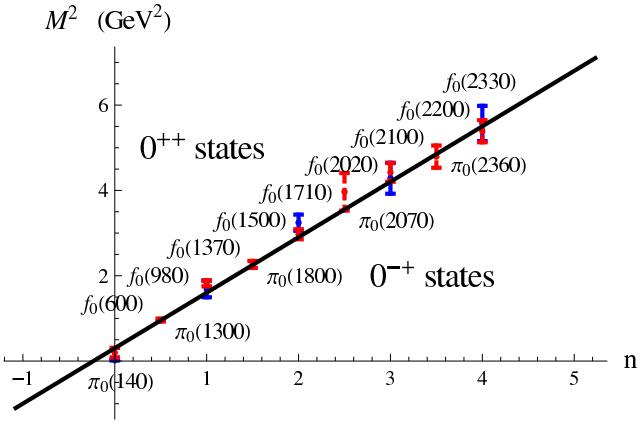

Fig. 3. Radial Regge trajectory corresponding to the squared mass of all $J^{PC} = 0^{++}$ scalar-isoscalar and $J^{PC} = 0^{-+}$ pseudoscalar-isovector states listed in the PDG tables [1]. The four heaviest 0^{++} and two 0^{-+} states are not yet well established and are omitted from the PDG summary tables. The error bars correspond to the errors in the determination of the square of mass as $\Delta m^2 = m\Gamma$ with Γ from [1]. The straight line is the result of our joined fit. Labels of 0^{++} states are above their mark whereas labels of 0^{+-} states are below their mark.

Minimization yields $\chi^2/\mathrm{DOF} = 0.12$, with

$$a = 1.31(12)\ \mathrm{GeV}^2, \qquad m_\sigma = 556(127)\ \mathrm{MeV}. \tag{4}$$

Formula (2) is actually equivalent to two parallel radial Regge trajectories with the *standard* slope,

$$M_{S,-}(n)^2 = a\,n + m_\sigma^2, \tag{5}$$

$$M_{S,+}(n)^2 = a\,n + m_\sigma^2 + \frac{a}{2}, \tag{6}$$

where $a = 2\pi\sigma$, and σ is the string tension associated to the potential $V(r) = \sigma r$ between heavy colored sources. The value $\sqrt{\sigma} = 456(21)\,\mathrm{MeV}$ obtained from our fit agrees well with lattice determinations of $\sqrt{\sigma} = 420$ MeV [19]. Of course, one expects some of these states to correspond eventually to glueballs. However, there seems to be no obvious difference between mesons and glueballs, as far as the radial Regge spectrum is concerned. Note that Casimir scaling suggests that the string tension is $\sigma_{\mathrm{glueball}} = \frac{9}{4}\sigma_{\mathrm{meson}}$, but this holds in the case of fixed and heavy sources. The fact that we have light quarks might explain why we cannot allocate easily the Casimir scaling pattern in the light-quark scalar-isoscalar spectrum.

4 Interpolating fields

For scalar states a measure of the spectrum is given in terms of the (gauge and renorm invariant) trace of the energy momentum tensor [20]

$$\Theta^\mu_\mu \equiv \Theta = \frac{\beta(\alpha)}{2\alpha} G^{\mu\nu a} G^a_{\mu\nu} + \sum_q m_q\,[1 + \gamma_m(\alpha)]\,\bar{q}q. \tag{7}$$

Here $\beta(\alpha) = \mu^2 d\alpha/d\mu^2$ denotes the beta function, $\alpha = g^2/(4\pi)$ is the running coupling constant, $\gamma_m(\alpha) = d\log m/d\log\mu^2$ is the anomalous dimension of the current quark mass m_q, and $G^a_{\mu\nu}$ is the field strength tensor of the gluon field.

It is interesting to consider the situation of massless quarks, where things become somewhat simpler. Then, we have in principle two scalar operators with smallest canonical dimensions, the gluon G^2 and the quark $\bar{q}q$. While these two operators are both scalars, they are chirally even and odd, respectively, i.e., under the $q \to \gamma_5 q$ transformation. Because the chiral symmetry is spontaneously broken, there is some mixing between G^2 and $\bar{q}q$. These operators connect scalar states to the vacuum through the matrix element

$$\langle 0|\Theta|n\rangle = m_n^2 f_n\,, \qquad \langle 0|\bar{q}q|n\rangle = m_n c_n\,. \tag{8}$$

The two-point correlators read

$$\Pi_{\Theta\Theta}(q) = i\int d^4x e^{iq\cdot x}\langle 0|T\{\Theta(x)\Theta(0)\}|0\rangle = \sum_n \frac{f_n^2 m_n^4}{m_n^2 - q^2} + \text{c.t.}\,, \tag{9}$$

$$\Pi_{\Theta S}(q) = i\int d^4x e^{iq\cdot x}\langle 0|T\{\Theta(x)\bar{q}q(0)\}|0\rangle = \sum_n \frac{f_n^2 m_n^2 c_n m_n}{m_n^2 - q^2} + \text{c.t.}\,, \tag{10}$$

$$\Pi_{SS}(q) = i\int d^4x e^{iq\cdot x}\langle 0|T\{\bar{q}q(x)\bar{q}q(0)\}|0\rangle = \sum_n \frac{c_n^2 m_n^2}{m_n^2 - q^2} + \text{c.t.}\,, \tag{11}$$

where in the r.h.s. we saturate with scalar states and c.t. stands for subtraction constants which can chosen as to replace $m_n^2 \to q^2$ in the numerator. In that scheme, in the large $-q^2 \gg \Lambda_{QCD}$ limit, a comparison with the Operator Product Expansion (OPE) [21–23] leads to the matching conditions

$$\begin{aligned}
\Pi_{\Theta\Theta}(q^2) &= q^4\, C_0\, \log(-q^2) + \ldots\,,\\
\Pi_{SS}(q^2) &= q^2\, C_0'\, \log(-q^2) + \ldots\,,\\
\Pi_{\Theta S}(q^2) &= C_0''\,\langle\bar{q}q\rangle \log(-q^2) + \ldots\,,
\end{aligned} \tag{12}$$

where $C_0 = -(2\beta(\alpha)/\alpha\pi)^2$, $C_0' = -3/(8\pi^2)$ and $C_0'' = -2\beta(\alpha)/\alpha\pi$. As we see, $\bar{q}q$ and G^2 do not mix at high q^2 values, a consequence of asymptotic chiral symmetry [20]. In these limits the sums over n can be replaced by integrals, whence the following asymptotic conditions are found:

$$f_n^2/(dm_n^2/dn) \to C_0\,, \quad c_n^2/(dm_n^2/dn) \to C_0'\,, \quad c_n f_n m_n^3/(dm_n^2/dn) \to C_0''\langle\bar{q}q\rangle \tag{13}$$

We see that the first two conditions are incompatible with the third one if m_n increases for large n, as is the case of the data. However, if we group the states in two families, as suggested by Eqs. (6) and Fig. 3, we get a compatible solution

$$c_{n,-}, f_{n,+} \to \text{const} \qquad c_{n,+}, f_{n,-} \to \text{const}/m_n^3. \tag{14}$$

This is equivalent to assuming an asymptotically alternating pattern of mesons and glueballs, coupling to chirally odd and even operators, $\bar{q}q$ and G^2, respectively. Since asymptotically $m_n^2 \sim an/2$, we find $c_{n,-}/c_{n,+}$ and $f_{n,+}/f_{n,-} \sim n^{\frac{3}{2}}$. Of course, this is not the only solution.

The situation described above suggests the existence of a hidden symmetry in the 0^{++} sector. In our case we could think of the γ_5-parity (which becomes a good quantum number for excited states) as the relevant symmetry which makes the difference between the chirally even and odd states. This, however, only explains the fact that asymptotically the slopes of the $+$ and $-$ branches are the same, but not why the intercepts accurately differ by half the slope.

5 The holographic connection

To further elaborate on this intriguing point of the accidental degeneracy, let us consider the one-dimensional harmonic oscillator with frequency ω, as an example; all states $\psi_n(z)$ with the energy $E_n = \hbar\omega(n + 1/2)$ can be separated into parity *even* and parity *odd* states, satisfying the conditions $\psi_{n,\pm}(z) = \psi_{2n}(z)$ and $\psi_{\pm,n}(-z) = \pm\psi_{\pm,n}(z)$, respectively, and having the energies $E_{+,n} = 2\hbar\omega(n+1/4)$ and $E_{-,n} = 2\hbar\omega(n + 3/4)$. These formulas display *twice* the slope of E_n. Thus, given the states with energies $E_{+,n}$ and $E_{-,n}$, we might infer that parity was a hidden symmetry of a Hamiltonian explaining the correlation between the slope and intercepts.

In the relativistic case the argument can also be made in a suggestive manner. Let us consider the Klein-Gordon action for infinitely many bosons in four dimensions, described with fields $\phi_n(x)$ of masses m_n:

$$S = \frac{1}{2}\int d^4x \sum_n \left[\partial^\mu\phi_n\partial_\mu\phi_n - m_n^2\phi_n^2\right]. \tag{15}$$

We assume the spectrum of the form $m_n^2 = an + m_0^2$. Next, we can introduce the five-dimensional field $\phi(x,z) = \sum_n \phi_n(x)\psi_n(z)$, with $\psi_n(z)$ fulfilling the auxiliary Sturm-Liouville problem in the variable $0 \le z < \infty$,

$$-\partial_z\left[p(z)\partial_z\psi_n(z)\right] + q(z)\psi_n(z) = m_n^2\rho(z)\psi_n(z), \tag{16}$$

where the functions are orthogonal with respect to the weight function $\rho(z)$, provided suitable boundary conditions

$$p(z)\left(\psi_n'(z)\psi_m(z) - \psi_n(z)\psi_m'(z)\right)|_{z=0} = 0 \tag{17}$$

and $\psi_n(\infty) \to 0$ are fulfilled. The action can then be written as

$$S = \frac{1}{2}\int d^4x \int_0^\infty dz\left[\rho(z)\partial^\mu\phi\partial_\mu\phi - p(z)(\partial_z\phi)^2 - q(z)\phi^2\right] \tag{18}$$

after some integration by parts in the variable z. This action can be written as a five-dimensional action with a non-trivial metric [24], featuring the AdS/CFT (soft-wall) approach (see [25] and references therein), with the extra dimension z playing the role of a holographic variable and the orthogonal set of functions $\psi_n(z)$ denoting the corresponding Kaluza-Klein modes. Clearly, z has the dimension of length, suggesting that $z \to 0$ corresponds to the ultraviolet and $z \to \infty$ to the infrared regime.

Turning to Eq. (16), we may take the standard Harmonic oscillator Schrödinger-like equation ($p(z) = \rho(z) = 1$, $q(z) \equiv U(z) = a^2 z^2/16$)

$$-\psi_n''(z) + \frac{1}{16} a^2 z^2 \psi_n(z) = m_n^2 \psi_n(z) \tag{19}$$

and obtain for the regular solutions at infinity the result

$$\frac{\psi_n'(0)}{\psi_n(0)} = -\sqrt{a}\, \frac{\Gamma\left(\frac{3}{4} - \frac{m_n^2}{a}\right)}{\Gamma\left(\frac{1}{4} - \frac{m_n^2}{a}\right)}, \tag{20}$$

where $\Gamma(x)$ is the Euler Gamma function, which is meromorphic and have simple poles at $x = 0, -1, -2, \ldots$. The solutions fulfilling the Dirichlet, $\psi_n(0) = 0$, and Neumann, $\psi_n'(0) = 0$, boundary conditions, respectively, have the masses

$$m_{-,n}^2 = an + \frac{a}{4}\,, \qquad m_{+,n}^2 = an + \frac{3a}{4}\,, \tag{21}$$

which can be merged into one single formula

$$m_n^2 = \frac{a}{4}(2n + 1)\,. \tag{22}$$

This yields $m_\sigma = m_{f_0}/\sqrt{3} = 566$ MeV and, for the string tension, $\sigma = m_{f_0}\sqrt{2/3\pi} = 450$ MeV with $m_{f_0} = 980$ MeV, quite reasonable values.

In this approach the symmetry in the scalar spectrum corresponds to a parity symmetry in the holographic z variable $\psi_n(-z) = \pm\psi_n(z)$. Note that usually the holographic variable z is taken to be positive[3], but if we extend it to $-\infty < z < \infty$, we may define a holographic superfield containing two different and orthogonal modes. Otherwise, in the interval $0 < z < \infty$ the Dirichlet and Neumann modes are not orthogonal to each other.

6 Pseudoscalar mesons and chiral symmetry

Discerning the nature of the σ state has been a recurrent pastime for many years. As is well known, glueballs are more weakly coupled to mesons, $\mathcal{O}(1/N_C)$, than other mesons, $\mathcal{O}(1/\sqrt{N_C})$. The minimum number of states, allowed by certain sum rules and low energy theorems, is just two. In Ref. [16] we undertake such an analysis which suggests that $f_0(600)$ (denoted as σ) is a $\bar{q}q$ meson, while $f_0(980)$ (denoted as f_0) is a glueball. This is supported by the rather small width ratio,

[3] This is supported by the light-front interpretation of Brodsky and de Teramond [26], where the holographic variable is the polar coordinate of a two dimensional vector, $z = |\zeta|$ and $\zeta = b\sqrt{x(1-x)}$, with b denoting the impact parameter and x the momentum fraction of the quark. This interpretation yields a two dimensional potential $U(\zeta) = \kappa^2\zeta^2 + 2\kappa^2(L + S - 1)$ with $J = L + S$ which, when passing to the polar variable z, generates the usual centrifugal term $(L^2 - 1/4)/z^2$ not present in our discussion, yielding $M_{n,L,S}^2 = 4\kappa^2(n + L + S/2)$ which for $J = 0$ and $L = 1$ resembles Eq. (22).

which yields $\Gamma_f/\Gamma_\sigma \sim (g^2_{f\pi\pi} m_f^3)/(g^2_{\sigma\pi\pi} m_\sigma^3) \sim 1/N_C$, thus for $m_\sigma \sim 0.8$ MeV $\sim m_f$ the ratio $g_{\sigma\pi\pi}/g_{f\pi\pi} \sim \sqrt{N_C}$ is obtained.

A further piece of evidence for the alternating meson-glueball pattern is provided by looking at the excited pion spectrum, which we show in Fig. 3. The alternating pattern was unveiled by Glozman [27], suggesting that states degenerate with the pion might not be identified with glueballs. Remarkably, the states generating doublets with pion states are $f_0(600) \leftrightarrow \pi_0(140)$, $f_0(1370) \leftrightarrow \pi_0(1300)$, $f_0(1710) \leftrightarrow \pi_0(1800)$, $f_0(2100) \leftrightarrow \pi_0(2070)$, and $f_0(2330) \leftrightarrow \pi_0(2360)$, whereas the other scalar states $f_0(980)$, $f_0(1500)$, $f_0(2020)$ and $f_0(2200)$ are not degenerate with other mesons with light u and d quarks. Our analysis is reinforced by this observation.

As a matter of fact, fitting the pion $\pi(140)$ as the $n = 0$ state of the Regge spectrum requires strong departure from a simple linear trajectory, $m_n^2 = an + m_0^2$. One may improve on this by using the holographic connection and a mixed boundary condition at $z = 0$ determined by fixing the mass of the ground state m_0 using Eq. (17) together with Eq. (20) for the harmonic oscillator case, Eq. (19). This procedure ensures the orthogonality between all states and implements linearity for large n. This can be done for the ground states $m_0 = m_\pi, m_\sigma, m_{f_0}$. The fit to all states yields $a = 1.37\text{GeV}^2$ and the mass spectra (in GeV)

π (Regge) $(0.140, 1.260, 1.730, 2.092, 2.400, \dots)$ π (PDG) $(0.140, 1.300, 1.812, 2.070, 2.360)$
σ (Regge) $(0.527, 1.297, 1.750, 2.106, 2.411, \dots)$ σ (PDG) $(0.600, 1.350, 1.724, 2.103, 2.321)$
f_0 (Regge) $(0.977, 1.513, 1.906, 2.232, 2.517, \dots)$ f_0 (PDG) $(0.980, 1.505, 1.992, 2.189)$

yielding $1/\sqrt{a}\,\psi_0'(0)/\psi_0(0) = -3.1$, -14.9, and 0.2, respectively. Note the large and small values for the σ and f_0 cases, which suggests that these boundary conditions are very close to the Dirichlet and Neumann cases. Chiral symmetry breaking corresponds to the different π and σ values.

7 Scalar dominance and heavy pions

Hadronic matrix elements of the energy-momentum tensor, the so-called gravitational form factors (GFF) of the pion and nucleon, correspond to a dominance of scalar states in the large-N_c picture, as ($u(p)$ is a Dirac spinor)

$$\langle \pi(p')|\Theta|\pi(p)\rangle = \sum_n \frac{g_{n\pi\pi} f_n q^2 m_n^2}{m_n^2 - q^2}, \tag{23}$$

$$\langle N(p')|\Theta|N(p)\rangle = \bar{u}(p')u(p) \sum_n \frac{g_{nNN} f_n m_n^2}{m_n^2 - q^2}, \tag{24}$$

where the sum rules $\sum_n g_{n\pi\pi} f_n = 1$ [28] and $M_N = \sum_n g_{nNN} f_n$ [29] hold. Unfortunately, the lattice QCD data for the pion [30] and nucleon (LHPC [31] and QCDSF [32] collaborations), picking the valence quark contribution, are too noisy as to pin down the coupling of the excited scalar-isoscalar states to the energy-momentum tensor. Nevertheless, useful information confirming the (Regge) mass estimates for the σ-meson can be extracted [16] through the use of the multiplicative QCD evolution of the GFF in the valence quark momentum fraction, $\langle x\rangle_{u+d}$,

m_π[MeV]	m_σ [MeV]	m_σ [MeV]	m_σ [MeV]	m_σ [MeV]
	GFF	GFF	$(\bar{q}q)^2$-dynam.	$(\bar{q}q)^2$-quench.
230	580(190)	620(100)	–	400(30)
342	630(190)	660(90)	–	720(20)
478	710(200)	730(90)	–	1000(20)
318	620(190)	650(90)	468(50)	–
469	700(190)	720(90)	936(13)	–
526	739(200)	750(90)	1066(13)	–

Table 1. Scalar monopole mass obtained from the nucleon gravitational form factors, extracted from the $(\bar{q}q)$ components obtained by LHPC [31] and QCDSF [32] and compared to the lattice calculation using the tetraquark $(\bar{q}q)^2$ probing fields, both for the dynamical and quenched fermions [33] .

as seen in deep inelastic scattering or on the lattice at the scale $\mu = 2$ GeV. For the pion and nucleon GFFs we obtain the fits

$$\langle x\rangle^{\pi}_{u+d} = 0.52(2), \qquad m_\sigma = 445(32)\ \text{MeV}\,, \tag{25}$$
$$\langle x\rangle^{N}_{u+d} = 0.447(14), \qquad m_\sigma = 550^{+180}_{-200}\text{MeV}. \tag{26}$$

Assuming a simple dependence of m_σ on m_π,

$$m_\sigma^2(m_\pi) = m_\sigma^2 + c\left(m_\pi^2 - m_{\pi,\text{phys}}^2\right), \tag{27}$$

yields $m_\sigma = 550^{+180}_{-200}$MeV and $c = 0.95^{+0.80}_{-0.75}$, or $m_\sigma = 600^{+80}_{-100}$MeV and $c = 0.8(2)$, depending on the choice of the lattice data [31] or [32], respectively. Note that c is close to unity. *Higher* quark masses might possibly clarify whether or not the state evolves into a glueball or a meson. For a $(\bar{q}q)^n$ system one expects $m_\sigma \to 2n m_q + \text{const}$ at large current quark mass m_q. The data from [31] or [32] are too noisy to see the difference, although for the largest pion masses we see that $m_\sigma \sim m_\pi$, as it simply corresponds to the $\bar{q}q$-component of Θ. We observe, however, that for $m_\pi \sim 500$MeV our results are not far away from the recent lattice calculation using the tetraquark probes, $(\bar{q}q)^2$ [33], which provide $m_\sigma \sim 2m_\pi$ for the largest pion masses as they should (see Table 1). From this viewpoint, and unless operator mixing is implemented, the nature of the state is predetermined by the probing operator.

8 Dimension-2 condensates

One of the problems of the large-N_c Regge models [35] and their holographic relatives [36, 37] is that they may contradict expectations from the OPE, as they involve dimension-2 condensates. For instance, the OPE for the $\Pi_{\Theta\Theta}(q^2)$ correlator in Eq.(12) gives corrections $\mathcal{O}(q^0)$, while the $\mathcal{O}(q^2)$ terms are missing [21].

This yields a one to one comparison:

$$C_0 = -\lim_{n\to\infty} \frac{f_n^2}{dm_n^2/dn} = -\frac{N_c^2-1}{2\pi^2}\left(\frac{\beta(\alpha)}{\alpha}\right)^2, \tag{28}$$

$$C_2 = \sum_n f_n^2 = 0\,, \tag{29}$$

$$C_4 = \sum_n f_n^2 m_n^2 = \left(\frac{\beta(\alpha)}{\alpha}\right)^2 \langle G^2\rangle\,. \tag{30}$$

Equation (28) requires infinitely many states, while Eq. (29) suggests a positive and non-vanishing gauge-invariant dimension-2 object, $C_2 = i\int d^4x x^2\langle\Theta(x)\Theta\rangle$, which is generally non-local, as it should not appear in the OPE. Note that $C_2 > 0$, hence is non-vanishing for a finite number of states. The infinite Regge spectrum of Eq. (2) with Eq. (28) may be modeled with a constant $f_{f_0} = f_{n,+} = \mathcal{O}(N_c)$ whereas $f_{n,-} = \mathcal{O}(\sqrt{N_c})$ goes as Eq. (14) and yields a convergent and hence positive contribution. Naively, we get $C_2 = \infty$. However, C_2 may vanish, as required by standard OPE, when infinitely many states are considered *after regularization*. The use of the ζ-function regularization [16,34] gives

$$C_2 \equiv \lim_{s\to 0}\sum f_n^2 M_S(n)^{2s} = \sum_n f_{n,-}^2 + f_{f_0}^2\left(1/2 - m_{f_0}^2/a\right)\,. \tag{31}$$

Then $C_2 = 0$ for $m_{f_0} > \sqrt{a/2} = 810(40)$ MeV, a reasonable value to $\mathcal{O}(1/N_c)$ In any case, the important remark is that while at the OPE level $C_2 = 0$ vanishes for trivial reasons, at the Regge spectrum level some fine tuning must be at work.

Acknowledgments This work is partially supported by the Polish Ministry of Science and Higher Education (grants N N202 263438 and N N202 249235), Spanish DGI and FEDER funds (grant FIS2008-01143/FIS), Junta de Andalucía (grant FQM225-05).

References

1. C. Amsler, et al., *Phys. Lett.* **B667**, 1 (2008).
2. E. Witten, Nucl. Phys. **B160**, 57 (1979).
3. W. Broniowski, Nucl. Phys. **A580**, 429 (1994), hep-ph/9402206.
4. A. Pich (2002), hep-ph/0205030.
5. A. Andrianov, D. Espriu, and A. Prats, *Int.J.Mod.Phys.* **A21**, 3337 (2006), hep-th/0507212.
6. E. Gurvich, *Phys.Lett.* **B87**, 386 (1979).
7. A. Casher, H. Neuberger, and S. Nussinov, *Phys.Rev.* **D20**, 179 (1979).
8. N. Suzuki, T. Sato, and T.-S. Lee, *Phys.Rev.* **C79**, 025205 (2009), 0806.2043.
9. R. Workman, R. Arndt, and M. Paris, *Phys.Rev.* **C79**, 038201 (2009), 0808.2176.
10. I. Caprini, G. Colangelo, and H. Leutwyler, *Phys. Rev. Lett.* **96**, 132001 (2006), hep-ph/0512364.
11. R. Garcia-Martin, R. Kaminski, J. R. Pelaez, and J. Ruiz de Elvira, *Phys. Rev. Lett.* **107**, 072001 (2011), 1107.1635.

12. A. Calle Cordon, and E. Ruiz Arriola, *Phys. Rev.* **C80**, 014002 (2009), nucl-th/0904.0421.
13. J. Nieves, A. Pich, and E. Ruiz Arriola *Phys. Rev.* **D** (2011) (in press), hep-ph/1107.3247.
14. A. V. Anisovich, V. V. Anisovich, and A. V. Sarantsev, *Phys. Rev.* **D62**, 051502 (2000), hep-ph/0003113.
15. V. V. Anisovich, *Int. J. Mod. Phys.* **A21**, 3615 (2006), hep-ph/0510409.
16. E. Ruiz Arriola, and W. Broniowski, *Phys. Rev.* **D81**, 054009 (2010), 1001.1636.
17. E. R. Arriola, W. Broniowski, AIP Conf. Proc. **1343**, 361 (2011), 1011.5176.
18. W. de Paula, and T. Frederico, *Phys.Lett.* **B693**, 287 (2010), 0908.4282.
19. O. Kaczmarek, and F. Zantow, *Phys. Rev.* **D71**, 114510 (2005), hep-lat/0503017.
20. J. F. Donoghue, and H. Leutwyler, *Z. Phys.* **C52**, 343 (1991).
21. S. Narison, *Nucl. Phys.* **B509**, 312 (1998), hep-ph/9612457.
22. S. Narison, N. Pak, N. Paver, Phys. Lett. **B147** (1984) 162.
23. D. Harnett, R. T. Kleiv, K. Moats, T. G. Steele, Nucl. Phys. **A850**, 110-135 (2011).
24. S. S. Afonin, Int. J. Mod. Phys. **A25**, 5683 (2010), 1001.3105.
25. J. Erdmenger, N. Evans, I. Kirsch, E. Threlfall, Eur. Phys. J. **A35**, 81 (2008), 0711.4467.
26. G. F. de Teramond, S. J. Brodsky, Phys. Rev. Lett. **102** (2009) 081601. [arXiv:0809.4899 [hep-ph]].
27. L. Glozman, *Eur.Phys.J.* **A19**, 153 (2004), hep-ph/0301012.
28. S. Narison, and G. Veneziano, *Int. J. Mod. Phys.* **A4**, 2751 (1989).
29. P. Carruthers, *Phys. Rept.* **1**, 1 (1971).
30. D. Brommel, et al. (2007), 0708.2249.
31. P. Hagler, et al., *Phys. Rev.* **D77**, 094502 (2008), 0705.4295.
32. M. Gockeler, et al., *Phys. Rev. Lett.* **92**, 042002 (2004), hep-ph/0304249.
33. S. Prelovsek, T. Draper, C. B. Lang, M. Limmer, K.-F. Liu, et al., *Phys.Rev.* **D82**, 094507 (2010), 1005.0948.
34. E. R. Arriola, and W. Broniowski, *Eur. Phys. J.* **A31**, 739–741 (2007), hep-ph/0609266.
35. E. Ruiz Arriola, W. Broniowski, Phys. Rev. **D73** (2006) 097502.
36. O. Andreev, Phys. Rev. **D73** (2006) 107901.
37. F. Zuo, T. Huang, [arXiv:0801.1172 [hep-ph]].

Bled Workshops
in Physics
Vol. 12, No. 1
p. 18

Proceedings of the Mini-Workshop
Understanding hadronic spectra
Bled, Slovenia, July 3 - 10, 2011

Transversity structure of the pion in chiral quark models*

W. Broniowski[a,b], E. Ruiz Arriola[c,d], A. E. Dorokhov[e,f]

[a] Institute of Nuclear Physics PAN, PL-31342 Cracow, Poland
[b] Institute of Physics, Jan Kochanowski University PL-25406 Kielce, Poland
[c] Departamento de Física Atómica, Molecular y Nuclear, Universidad de Granada, E-18071 Granada, Spain
[d] Instituto Carlos I de Fisica Teórica y Computacional, Universidad de Granada E-18071 Granada, Spain
[e] Joint Institute for Nuclear Research, Bogoliubov Laboratory of Theoretical Physics RU-141980 Dubna, Russia
[f] Institute for Theoretical Problems of Microphysics, Moscow State University RU-119899 Moscow, Russia

Abstract. We describe the chiral quark model evaluation of the transversity Generalized Parton Distributions (tGPDs) and related transversity form factors (tFFs) of the pion. The obtained tGPDs satisfy all necessary formal requirements, such as the proper support, normalization, and polynomiality. The lowest tFFs, after the necessary QCD evolution, compare favorably to the recent lattice QCD determination. Thus the transversity observables of the pion support once again the fact that the spontaneously broken chiral symmetry governs the structure of the Goldstone pion. The proper QCD evolution is crucial in these studies.

This talk is based on our two recent works [1, 2], where more details and a complete list of references may be found. Its topic concerns the transversity Generalized Parton Distribution (tGPD) of the pion, the least-known of the Generalized Parton Distributions (see [3–5] and references therein for an extensive review). The definition involves aligned parton-helicity operators (maximum-helicity case). For the case of spin-0 hadrons, tGPDs arise because of the nonzero orbital angular momentum between the initial and final state, thus allowing to study the spin structure without the inherent complications of the explicit spin degrees of freedom, as in the case of the nucleon. In that situation the analysis of the spin structure of the pion is particularly appealing, however, the quantity will be very difficult to access experimentally.

A few years ago, however, lattice simulations [6] provided the lowest-order pion quark transversity form factors (tFFs), defined as Mellin moments of tGPDs

* Talk delivered by W. Broniowski

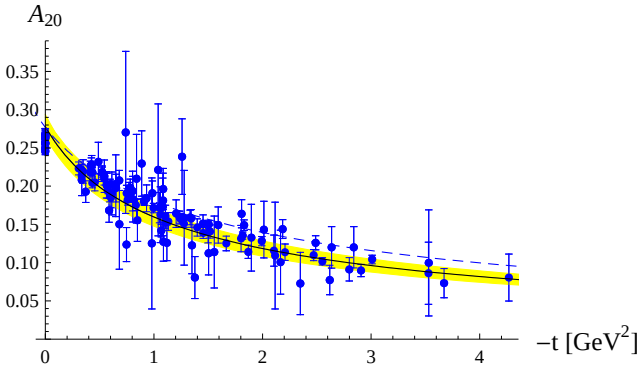

Fig. 1. The quark part of the spin-2 gravitational form factor in Spectral Quark Model (solid line) and NJL model with the Pauli-Villars regularization (dashed line), compared to the lattice data from Ref. [7,8]. The band around the Spectral Quark Model results corresponds to the model parameter uncertainty.

in the Bjorken x variable. That way lattices supply valuable information on the nontrivial spin structure of hadrons. In general, lattice calculations are capable to determine quantities that may only be dreamed off to be measured experimentally and, in that regard, are extremely useful. The results can be used to verify various theoretical approaches and models in their rich spectrum of predictions. An example is the gravitational form factor of the pion. Its lattice determination [7,8] agrees remarkably well with the evaluation in chiral quark models [9], as can be seen from Fig. 1.

Our study consist of two distinct parts: 1) the chiral quark model determination of tFFs and tGPDs of the pion and 2) the QCD evolution. For the first part we apply the standard *local* NJL model with the Pauli-Villars regularization [10] and two versions of the *nonlocal* models, where the quark mass depends on the momentum of the quark, namely, the instanton model [11] and the Holdom-Terning-Verbeek (HTV) model [12]. We stress that chiral quark models have been successfully used for the evaluation of *soft* matrix elements entering numerous high-energy processes [9, 13–40]. They also agree with the Euclidean lattice determination of moments (see, e.g., [41,42]) and direct results from the transverse lattices [43–46].

The second element, crucial in obtaining proper results, is the QCD evolution, where renorm-improved radiative gluonic corrections are appended. The method is schematically depicted in Fig. 2. One-loop (large-N_c) quark diagram, with external gauge bosons and Goldstone mesons, is evaluated. Then the renorm-improved gluon exchanges are incorporated in terms of the LO DGLAP evolution. The scale where the quark model calculation is carried out can be identified with the help of the momentum fraction carried by the quarks. According to phenomenology [47,48] or lattice calculations [49], the valence quark contribution is 47% of the total at the scale $\mu = 2$GeV. Since the quark models possess no explicit gluons, the valence quarks carry 100% of the momentum. This determines the quark model scale, denoted as μ_0, as the scale determined in such a way, that

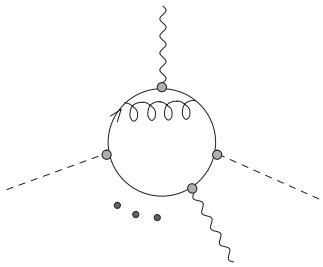

Fig. 2. One-loop (large-N_c) quark diagram, with external gauge bosons (wavy lines) and Goldstone mesons (dashed lines). The renorm-improved gluon exchanges are incorporated in terms of the LO DGLAP evolution.

when the evolution is carried out from μ_0 up to $\mu = 2$ GeV, the fraction drops to $47 \pm 2\%$. The result of the LO DGLAP evolution is

$$\mu_0 = 313^{+20}_{-10}\ \text{MeV}. \tag{1}$$

Despite the low value of this scale, the prescription has been successfully confirmed by a variety of high-energy data and lattice calculations (see [26] and references therein). Moreover, the NLO DGLAP modifications yield moderate corrections [14], supporting our somewhat strained use of perturbative QCD at low scales. To summarize, *our approach = chiral quark model + QCD evolution*.

We now come to definitions. The pion u-quark tFFs, denoted as $B^{\pi,u}_{ni}(t)$, are defined via [50]

$$\langle \pi^+(p')|\overline{u}(0) i\sigma^{\mu\nu} a_\mu b_\nu \left(i\overleftrightarrow{D}\, a\right)^{n-1} u(0)|\pi^+(p)\rangle = (a\cdot P)^{n-1} \frac{[a\cdot p\, b\cdot p']}{m_\pi} \times \sum_{\substack{i=0,\\ \text{even}}}^{n-1} (2\xi)^i B^{\pi,u}_{ni}(t)\,, \tag{2}$$

where the auxiliary vectors a and b satisfy the conditions $a^2 = (ab) = 0$ and $b^2 \neq 0$. The skewness parameter is defined as $\xi = -a\cdot q/(2a\cdot P)$, the symbol $\overleftrightarrow{D}^\beta = \overleftrightarrow{\partial}^\beta - igA^\beta$ is the covariant derivative, and $\overleftrightarrow{\partial}^\beta = \frac{1}{2}\left(\overrightarrow{\partial}^\beta - \overleftarrow{\partial}^\beta\right)$. Next, p' and p are the initial and final pion momenta, $P = \frac{1}{2}(p'+p)$, $q = p'-p$, and $t = -q^2$. The bracket denotes antisymmetrization in the vectors a and b. The corresponding definition of the tGPD is [3]

$$\langle \pi^+(p') \mid \bar{u}(-a) i\sigma^{\mu\nu} a_\mu b_\nu u(a) \mid \pi^+(p)\rangle = \frac{[a\cdot p\, b\cdot p']}{m_\pi} \int_{-1}^{1} dx\, e^{-ix\,P\cdot a} E^{\pi,u}_T(x,\xi,t), \tag{3}$$

where the presence of the gauge link operator are understood. The tFFs for the d-quarks follow from the isospin symmetry, namely $B^{\pi,d}_{ni}(t) = (-1)^n B^{\pi,u}_{ni}(t)$. The tFFs are the moments of the tGPD in the x-variable,

$$\int_{-1}^{1} dx\, x^{n-1} E^{\pi,u}_T(x,\xi,t) = \sum_{\substack{i=0,\\ \text{even}}}^{n-1} (2\xi)^i B^{\pi,u}_{ni}(t)\,. \tag{4}$$

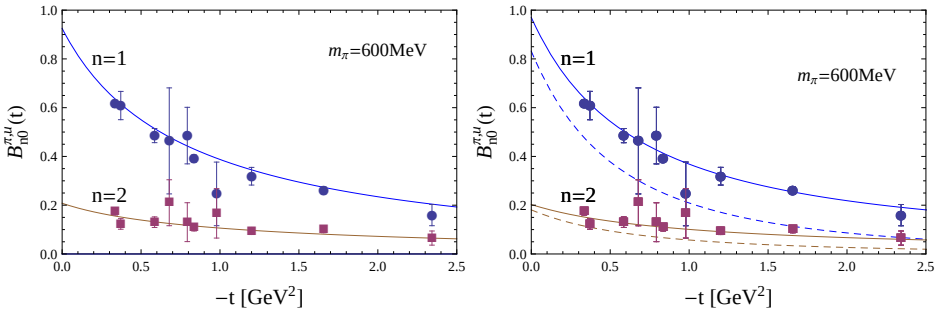

Fig. 3. The form factors $B^{\pi,u}_{10}(t)$ and $B^{\pi,u}_{20}(t)$, evaluated at $m_\pi = 600$MeV in the local NJL model (left panel) and in nonlocal models (right panel, solid line – HTV model, dashed line – instanton model). The lattice data from [6]. The local NJL and HTV models agree very well with the data.

This formula explicitly displays the desired polynomiality property. We remark that the full information carried by tGPDs is contained in the collection of the infinitely many tFFs.

The full details of the quark-model calculation as well as the QCD evolution can be found in [1, 2]. The two lowest tFFs available from the lattice data, $B^{\pi,u}_{10}$ and $B^{\pi,u}_{20}$, evolve multiplicatively in a simple way:

$$B^{\pi,u}_{n0}(t;\mu) = B^{\pi,u}_{n0}(t;\mu_0)\left(\frac{\alpha(\mu)}{\alpha(\mu_0)}\right)^{\gamma^T_n/(2\beta_0)}, \tag{5}$$

where γ^T_n are the appropriate anomalous dimensions [1, 2]. In the local model, in the chiral limit at $t = 0$ we find the very simple result:

$$B^{\pi,u}_{10}(t=0;\mu_0)/m_\pi = \frac{N_c M}{4\pi^2 f_\pi^2}, \quad \frac{B^{\pi,u}_{20}(t=0;\mu)}{B^{\pi,u}_{10}(t=0;\mu)} = \frac{1}{3}\left(\frac{\alpha(\mu)}{\alpha(\mu_0)}\right)^{8/27}, \tag{6}$$

where M is the constituent quark mass. The results of the model calculation followed by evolution are shown in Fig. 3. We note a striking agreement with the lattice data [6] for the local NJL model, as well as for the non-local HTV model.

Finally, we present the results for the full tGPD for $t = 0$ and $\xi = 1/3$ or $\xi = 0$. The evolution is different for the symmetric and antisymmetric parts of tGPDs, hence we define the isovector and isoscalar combinations:

$$E^{\pi,I=1}_T(x,\xi,Q^2) \equiv E^{\pi,S}_T(x,\xi,Q^2) = E^{\pi}_T(x,\xi,Q^2) + E^{\pi}_T(-x,\xi,Q^2),$$
$$E^{\pi,I=0}_T(x,\xi,Q^2) \equiv E^{\pi,A}_T(x,\xi,Q^2) = E^{\pi}_T(x,\xi,Q^2) - E^{\pi}_T(-x,\xi,Q^2).$$

The QCD evolution has been carried out with the method of [51–54]. The results for $\xi = 1/3$ in the NJL model are shown in Fig. 4, while in Fig. 5 we compare the result for $\xi = 0$ in the NJL model (left panel) and the nonlocal instanton model (right panel). Except for different end-point behavior, discussed in [2], the results are similar.

In conclusion we wish to stress that the absolute predictions for the multiplicatively evolved B_{10} and B_{20} agree remarkably well with the lattice results,

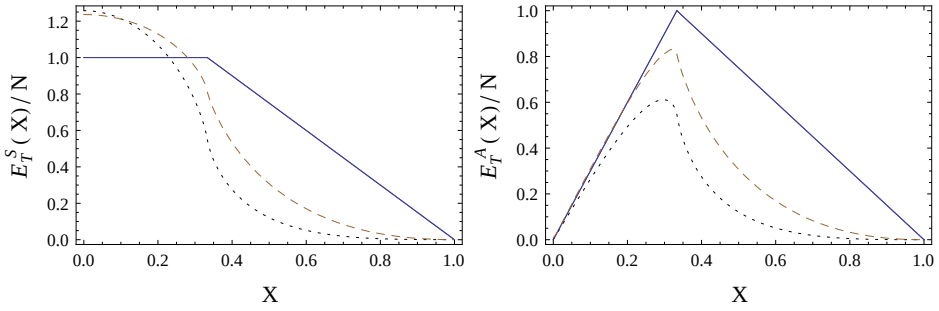

Fig. 4. The symmetric (left panel) and antisymmetric (right panel) tGPDs of the pion at $t = 0$ and $\xi = 1/3$, evaluated in the NJL model in the chiral limit at the quark-model scale $\mu_0 = 313$ MeV (solid lines) and evolved to the scales $\mu = 2$ GeV (dashed lines) and 1 TeV (dotted lines).

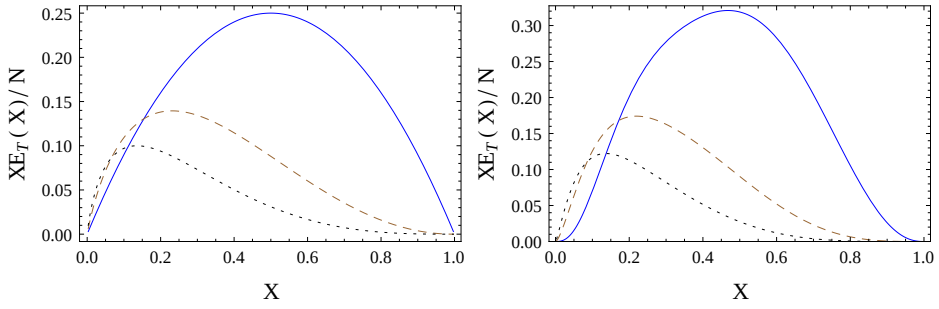

Fig. 5. The tGPD of the pion at $t = 0$ and $\xi = 0$, evaluated in the chiral limit in the local NJL model (left panel) and in the instanton model (right panel). The solid lines correspond to the quark-model scale $\mu_0 = 313$ MeV, the dashed lines to $\mu = 2$ GeV, and the dotted lines to $\mu = 1$ TeV.

supporting the assumptions of numerous other calculations following the same "chiral quark model + QCD evolution" scheme. Our study of the transversity observables of the pion support once again the feature that the spontaneously broken chiral symmetry determines the structure of the Goldstone pion.

Acknowledgments This work is supported by the Bogoliubov-Infeld program (JINR), the Polish Ministry of Science and Higher Education, grants N N202 263438 and N N202 249235, Spanish DGI and FEDER grant FIS2008-01143/FIS, Junta de Andalucía grant FQM225-05, and EU Integrated Infrastructure Initiative Hadron Physics Project, contract RII3-CT-2004-506078. AED acknowledges partial support from the Russian Foundation for Basic Research, projects No. 10-02-00368 and No. 11-02-00112.

References

1. W. Broniowski, A.E. Dorokhov and E.R. Arriola, Phys. Rev. D82 (2010) 094001, 1007.4960.

2. A.E. Dorokhov, W. Broniowski and E.R. Arriola, Phys. Rev. D 84 (2011) 074015, 1107.5631.
3. A.V. Belitsky and A.V. Radyushkin, Phys. Rept. 418 (2005) 1, hep-ph/0504030.
4. T. Feldmann, Eur. Phys. J. Special Topics 140 (2007) 135.
5. S. Boffi and B. Pasquini, Riv. Nuovo Cim. 30 (2007) 387, 0711.2625.
6. QCDSF, D. Brommel et al., Phys. Rev. Lett. 101 (2008) 122001, 0708.2249.
7. D. Brommel et al., PoS LAT2005 (2006) 360, hep-lat/0509133.
8. D. Brommel, Pion structure from the lattice, PhD thesis, University of Regensburg, Regensburg, Germany, 2007, DESY-THESIS-2007-023.
9. W. Broniowski and E.R. Arriola, Phys.Rev. D78 (2008) 094011, 0809.1744.
10. E. Ruiz Arriola, Phys. Lett. B253 (1991) 430.
11. D. Diakonov and V.Y. Petrov, Nucl. Phys. B272 (1986) 457.
12. B. Holdom, J. Terning and K. Verbeek, Phys. Lett. B245 (1990) 612.
13. R.M. Davidson and E. Ruiz Arriola, Phys. Lett. B348 (1995) 163.
14. R.M. Davidson and E. Ruiz Arriola, Acta Phys. Polon. B33 (2002) 1791, hep-ph/0110291.
15. W. Broniowski and E. Ruiz Arriola, Phys. Lett. B574 (2003) 57, hep-ph/0307198.
16. A.E. Dorokhov and L. Tomio, (1998), hep-ph/9803329.
17. M.V. Polyakov and C. Weiss, Phys. Rev. D60 (1999) 114017, hep-ph/9902451.
18. A.E. Dorokhov and L. Tomio, Phys. Rev. D62 (2000) 014016.
19. I.V. Anikin et al., Nucl. Phys. A678 (2000) 175.
20. M. Praszalowicz and A. Rostworowski, Acta Phys. Polon. B34 (2003) 2699, hep-ph/0302269.
21. A. Bzdak and M. Praszalowicz, Acta Phys. Polon. B34 (2003) 3401, hep-ph/0305217.
22. T. Nguyen et al., Phys. Rev. C83 (2011) 062201, 1102.2448.
23. L. Theussl, S. Noguera and V. Vento, Eur. Phys. J. A20 (2004) 483, nucl-th/0211036.
24. F. Bissey et al., Phys. Lett. B587 (2004) 189, hep-ph/0310184.
25. S. Noguera and V. Vento, Eur. Phys. J. A28 (2006) 227, hep-ph/0505102.
26. W. Broniowski, E. Ruiz Arriola and K. Golec-Biernat, Phys. Rev. D77 (2008) 034023, 0712.1012.
27. T. Frederico et al., Nucl. Phys. B (Proc. Supp.) 199 (2010) 264, 0911.1736.
28. T. Frederico et al., Phys. Rev. D80 (2009) 054021, 0907.5566.
29. S.V. Esaibegian and S.N. Tamarian, Sov. J. Nucl. Phys. 51 (1990) 310.
30. A.E. Dorokhov, Nuovo Cim. A109 (1996) 391.
31. V.Y. Petrov et al., Phys. Rev. D59 (1999) 114018, hep-ph/9807229.
32. I.V. Anikin, A.E. Dorokhov and L. Tomio, Phys. Lett. B475 (2000) 361, hep-ph/9909368.
33. M. Praszalowicz and A. Rostworowski, Phys. Rev. D64 (2001) 074003, hep-ph/0105188.
34. A.E. Dorokhov, JETP Lett. 77 (2003) 63, hep-ph/0212156.
35. E. Ruiz Arriola and W. Broniowski, Phys. Rev. D66 (2002) 094016, hep-ph/0207266.
36. E. Ruiz Arriola, Acta Phys. Polon. B33 (2002) 4443, hep-ph/0210007.
37. B.C. Tiburzi, Phys. Rev. D72 (2005) 094001, hep-ph/0508112.
38. W. Broniowski and E. Ruiz Arriola, Phys. Lett. B649 (2007) 49, hep-ph/0701243.
39. A. Courtoy and S. Noguera, Prog. Part. Nucl. Phys. 61 (2008) 170, 0803.3524.
40. P. Kotko and M. Praszalowicz, Acta Phys. Polon. B40 (2009) 123, 0803.2847.
41. B.U. Musch et al., Phys. Rev. D83 (2011) 094507, 1011.1213.
42. P. Hagler, Phys. Rept. 490 (2010) 49, 0912.5483.
43. M. Burkardt and S. Dalley, Prog. Part. Nucl. Phys. 48 (2002) 317, hep-ph/0112007.
44. S. Dalley, Phys. Rev. D64 (2001) 036006, hep-ph/0101318.
45. S. Dalley, Few Body Syst. 36 (2005) 69, hep-ph/0409139.
46. S. Dalley and B. van de Sande, Phys. Rev. D67 (2003) 114507, hep-ph/0212086.

47. P.J. Sutton et al., Phys. Rev. D45 (1992) 2349.
48. M. Gluck, E. Reya and I. Schienbein, Eur. Phys. J. C10 (1999) 313, hep-ph/9903288.
49. C. Best et al., Phys. Rev. D56 (1997) 2743, hep-lat/9703014.
50. M. Diehl and L. Szymanowski, Phys. Lett. B690 (2010) 149, 1003.4171.
51. N. Kivel and L. Mankiewicz, Phys. Lett. B458 (1999) 338, hep-ph/9905342.
52. N. Kivel and L. Mankiewicz, Nucl. Phys. B557 (1999) 271, hep-ph/9903531.
53. A. Manashov, M. Kirch and A. Schafer, Phys. Rev. Lett. 95 (2005) 012002, hep-ph/0503109.
54. M. Kirch, A. Manashov and A. Schafer, Phys. Rev. D72 (2005) 114006, hep-ph/0509330.

Bled Workshops
in Physics
Vol. 12, No. 1
p. 25

Proceedings of the Mini-Workshop
Understanding hadronic spectra
Bled, Slovenia, July 3 - 10, 2011

Spectroscopy of heavy baryons*

Joseph P. Day, Ki-Seok Choi, Willibald Plessas

Theoretical Physics, Institute of Physics, University of Graz, A-8010 Graz, Austria

Abstract. We report first results from a study of heavy-baryon spectroscopy within a relativistic constituent-quark model whose hyperfine interaction is based on Goldstone-boson-exchange dynamics.

1 Introduction

The relativistic constituent-quark model (RCQM) has become quite successful for the description of hadron properties at low energies. This is especially true for the RCQM based on Goldstone-boson-exchange (GBE) dynamics [1] with regard to baryons (for a short review see ref. [2]). So far the GBE RCQM has been restricted to baryons consisting of constituent quarks Q with flavors u, d, and s only, as it has been argued that their hyperfine interaction should be governed by GBE dynamics due to the spontaneous breaking of chiral symmetry (SBχS) of low-energy quantum chromodynamics (QCD) [3]. Regarding the other known baryons, i.e. the ones with flavors c and b, we still face the interesting questions after the light-heavy and heavy-heavy Q-Q interactions. It remains to be clarified, which kind of dynamics, gluon exchange and/or Goldstone-boson exchange, is dominant.

We have looked into these problems within the framework of the RCQM. Accepting the GBE RCQM in the $SU(3)_F$ sector, there are in principle three ways to add interactions for the light-heavy and heavy-heavy Q-Q interactions:

- employ GBE dynamics throughout,
- extend the $SU(3)_F$ GBE RCQM with one-gluon exchange (OGE) for the c and b flavors, and
- use a superposition of both the GBE and OGE hyperfine interactions beyond $SU(3)_F$.

According to our present experience the best performance of a universal RCQM for all $SU(5)_F$ baryons is achieved by the first way [4]. Here, we thus report results of a $SU(5)_F$ RCQM that is based on GBE dynamics for baryons of all five quark flavors.

* Talk delivered by J. Day

2 Theory

Our theoretical framework is relativistic quantum mechanics (RQM), which assumes a fixed number of relevant degrees of freedom and relies on an invariant mass operator $\hat{M} = \hat{M}_{\text{free}} + \hat{M}_{\text{int}}$ fulfilling all symmetry requirements of the Poincaré group. Here, the free and interaction parts of the mass operator are expressed in the rest frame of the baryon (i.e. for $\mathbf{P} = \sum_i^3 \mathbf{k}_i^2 = 0$) by

$$\hat{M}_{\text{free}} = \sum_{i=1}^{3} \sqrt{\hat{m}_i^2 + \hat{\mathbf{k}}_i^2}\,, \qquad \hat{M}_{\text{int}} = \sum_{i<j}^{3} \hat{V}_{ij} = \sum_{i<j}^{3} \left(\hat{V}_{ij}^{\text{conf}} + \hat{V}_{ij}^{\text{hf}}\right)\,, \tag{1}$$

where $\mathbf{k}_i$ represent the three-momenta of the individual quarks with rest masses m_i and the Q-Q potentials $\hat{V}_{ij}$ are composed of confinement and hyperfine interactions. By employing such a mass operator $\hat{M}^2 = \hat{P}^\mu \hat{P}_\mu$, with baryon four-momentum $\hat{P}_\mu = (\hat{H}, \hat{\mathbf{P}})$, the Poincaré algebra of all ten generators $\{\hat{H}, \hat{P}_i, \hat{J}_i, \hat{K}_i\}$, for $i = 1, 2, 3$,

$$\begin{array}{lll} [\hat{P}_i, \hat{P}_j] = 0, & [\hat{J}_i, \hat{H}] = 0, & [\hat{P}_i, \hat{H}] = 0, \\ [\hat{K}_i, \hat{H}] = i\hat{P}_i, & [\hat{J}_i, \hat{J}_j] = i\epsilon_{ijk}\hat{J}_k, & [\hat{J}_i, \hat{K}_j] = i\epsilon_{ijk}\hat{K}_k, \\ [\hat{J}_i, \hat{P}_j] = i\epsilon_{ijk}\hat{P}_k, & [\hat{K}_i, \hat{K}_j] = -i\epsilon_{ijk}\hat{J}_k, & [\hat{K}_i, \hat{P}_j] = i\delta_{ij}\hat{H}. \end{array}$$

is guaranteed.

3 The GBE RCQM

3.1 The $SU(3)_F$ Sector

The hyperfine interaction of the GBE RCQM for constituent quarks with flavors u, d, and s, confined by a linear potential $V_{ij}^{\text{conf}}(\mathbf{r}) = Cr$, reads

$$V^{\text{hf}}(\mathbf{r}) = \left[V_\pi(\mathbf{r}) \sum_{a=1}^{3} \lambda_i^a \lambda_j^a + V_K(\mathbf{r}) \sum_{a=4}^{7} \lambda_i^a \lambda_j^a + V_\eta(\mathbf{r}) \lambda_i^8 \lambda_j^8 + V_{\eta'}(\mathbf{r}) \lambda_i^0 \lambda_j^0\right] \boldsymbol{\sigma}_i \cdot \boldsymbol{\sigma}_j\,, \tag{2}$$

where $\mathbf{r}$ is the relative vector between constituent quarks i and j. The λ_i^a represent the $SU(3)_F$ Gell-Mann matrices of flavor a and the $\boldsymbol{\sigma}_i$ the $SU(2)$ Pauli spin matrices of the individual constituent quarks. The GBE is described by the exchange of the octet of pseudoscalar mesons π, K, and η, where due to the $U(1)$ anomaly also the singlet exchange η' is added. The corresponding regularized meson-exchange potentials, derived in instantaneous approximation, are expressed by

$$V_\gamma(\mathbf{r}) = \frac{g_\gamma^2}{2\pi} \frac{1}{12 m_i m_j} \left[\mu_\gamma^2 \frac{e^{-\mu_\gamma r}}{r} - \Lambda_\gamma^2 \frac{e^{-\Lambda_\gamma r}}{r}\right]\,, \qquad \gamma = \pi, K, \eta, \eta'\,, \tag{3}$$

with g_γ the quark-meson coupling constant, μ_γ the exchanged meson mass, and Λ_γ a cut-off parameter. The complete parameterization of the GBE RCQM can be found in ref. [1]. An extended version of it, including beyond spin-spin forces also all other interaction components stemming from GBE dynamics, was published in ref. [5].

3.2 Generalization to $SU(5)_F$

In the spirit of the ansatz (3) we have generalized the GBE RCQM to $SU(5)_F$ in order to cover also heavy baryons, containing the flavors c and b, in a universal model. Keeping the confinement potential unaltered, the extended hyperfine interaction is proposed to be

$$V^{hf}(\mathbf{r}) = \Bigg[V_\pi(\mathbf{r}) \sum_{a=1}^{3} \lambda_i^a \lambda_j^a + V_K(\mathbf{r}) \sum_{a=4}^{7} \lambda_i^a \lambda_j^a + V_{\eta_8}(\mathbf{r}) \lambda_i^8 \lambda_j^8 + \frac{2}{5} V_{\eta_0}(\mathbf{r}) + V_D(\mathbf{r}) \sum_{a=9}^{12} \lambda_i^a \lambda_j^a + V_{D_s}(\mathbf{r}) \sum_{a=13}^{14} \lambda_i^a \lambda_j^a + V_{\eta_{15}}(\mathbf{r}) \lambda_i^{15} \lambda_j^{15} + V_B(\mathbf{r}) \sum_{a=16}^{19} \lambda_i^a \lambda_j^a + V_{B_s}(\mathbf{r}) \sum_{a=20}^{21} \lambda_i^a \lambda_j^a + V_{B_c}(\mathbf{r}) \sum_{a=22}^{23} \lambda_i^a \lambda_j^a + V_{\eta_{24}}(\mathbf{r}) \lambda_i^{24} \lambda_j^{24} \Bigg] \boldsymbol{\sigma}_i \cdot \boldsymbol{\sigma}_j \ .$$

It contains the GBE in $SU(5)_F$, which is represented by the exchange of the 24-plet of pseudoscalar mesons plus the singlet η_0. The various regularized meson-exchange potentials have the same functional dependence as in Eq. (3). The detailed parameterization is given in a forthcoming paper [6].

3.3 Consistency of the Universal GBE RCQM

Since $SU(3) \subset SU(4) \subset SU(5)$, the generalized GBE RCQM should perform with similar or even better success as the corresponding $SU(3)_F$ model specifically for u-, d-, and s-flavor baryons. This is not immediately obvious, as the light- and strange-baryon sectors are now influenced by an altered singlet exchange, namely, η_0 that corresponds to $SU(5)_F$ rather than to $SU(3)_F$. In addition the exchanges of η_{15} and η_{24} come into play.

We thus present in Figs. 1 and 2 first a comparison of the spectroscopy of light and strange baryons, as yielded by the original $SU(3)_F$ and the extended $SU(5)_F$ GBE RCQMs. As becomes clearly evident, the $SU(5)_F$ GBE RCQM performs equally well, in some instances even better, than the original $SU(3)_F$ one. In particular, the new model also produces the right level orderings in the N and Λ excitation spectra due to the specific flavor dependence in the hyperfine interaction in Eq. (4).

3.4 Results for Heavy-Baryon Spectra

Next we present the predictions of the $SU(5)_F$ GBE RCQM for the spectra of c- and b-flavor baryons in comparison to experimental data available for states with at least 4- or 3-star status according to the PDG (see Fig. 3). It appears that all experimental results, for which also a definite J^P is known, are reproduced quite well.

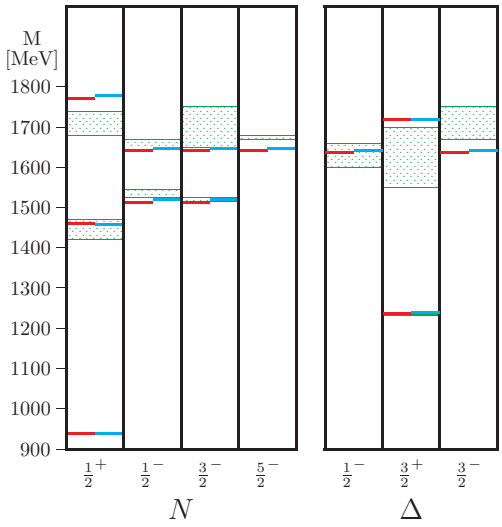

Fig. 1. N and Δ spectra of definite spin and parity J^P produced by the extended $SU(5)_F$ GBE RCQM (left/red levels) in comparison to the ones of the original $SU(3)_F$ GBE RCQM [1, 3] (right/blue levels) and to experimental data with their uncertainties (green boxes) from the PDG [7].

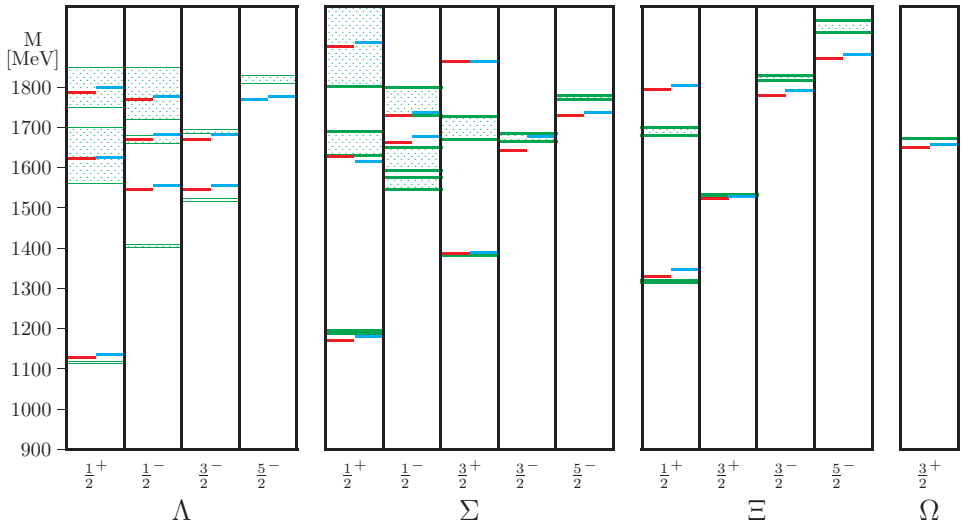

Fig. 2. Same as in Fig. 1 but for strange baryons.

In Fig. 4 we also present the predictions of the $SU(5)_F$ GBE RCQM for double-charm baryons. Here, there is only one measurement reported by the PDG, namely, the ground state of Ξ_{cc}. As can be seen from Fig. 4 and also the Table below, the theoretical level produced by the GBE RCQM remains at variance with the experimental data. For this comparison, however, one should bear in mind that the

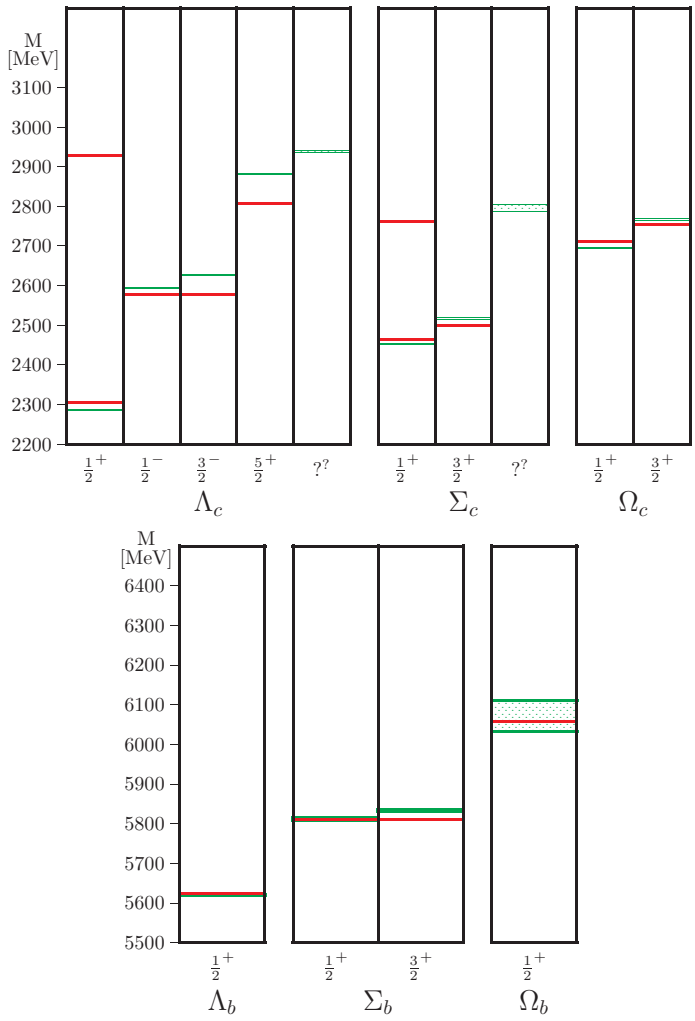

Fig. 3. Heavy-baryon spectra of definite J^P as produced by the extended $SU(5)_F$ GBE RCQM (solid/red levels) in comparison to experimental data with their uncertainties (dotted/green levels resp. boxes) reported by the PDG [7].

lowest Ξ_{cc} state with $J^P = \frac{1}{2}^+$ is only rated by 1 star by the PDG. Its measurement was only made once in 2002 by the SELEX collaboration [8], and since then has never been reproduced independently. In view of other theoretical works having investigated double-charm baryons, one may have some doubt about the measured mass of Ξ_{cc}. As is evident from the comparison in the Table below, for instance, the theoretical results from the RCQM of the Bonn group [11] and also the ones from the Bhaduri-Cohler-Nogami one-gluon-exchange model [9], reported in 2005 by Stancu and Richard [10] at the Bled Workshop, give mass values for

the Ξ_{cc} ground state quite similar to the one we have achieved. Further measurements of double-charm baryons would thus be highly welcome.

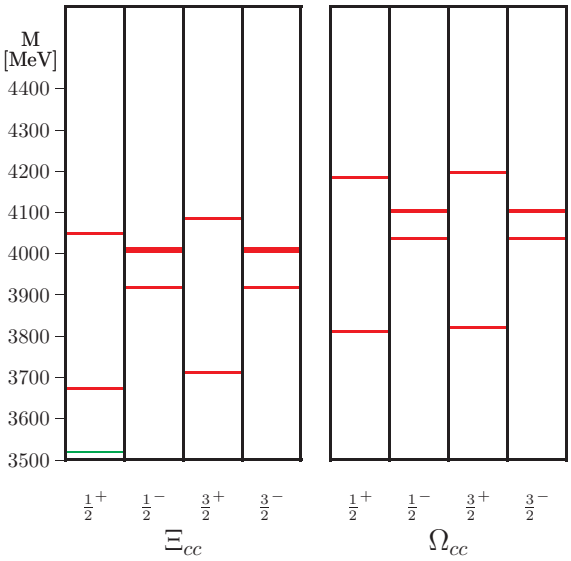

Fig. 4. Ξ_{cc} and Ω_{cc} spectra as produced by the extended $SU(5)_F$ GBE RCQM (solid/red levels) in comparison to experimental data reported only for the Ξ_{cc} ground state (dotted/green level/box) [7,8].

Baryon	J^P	Theory			Experiment [8]
		Ref. [10]	Ref. [11]	GBE RCQM	
Ξ_{cc}	$\frac{1}{2}^+$	3643	3642	3673	3518.9 ± 0.9
Ξ_{cc}	$\frac{3}{2}^+$	3724	3723	3711	-
Ξ_{cc}	$\frac{1}{2}^-$		3920	3919	-
Ξ_{cc}	$\frac{3}{2}^-$		3920	3919	-

Table 1. Comparison of the predictions by the GBE RCQM and other theoretical models for double-charm Ξ_{cc} ground and excited states vis-à-vis the experimental measurement reported by the SELEX collaboration.

4 Conclusion

We have constructed a universal RCQM for all baryons with flavors u, d, s, c, and b. It is based on a relativistically invariant mass operator describing systems

of three constituent quarks, confined by a linear potential according to QCD and interacting through hyperfine forces derived from GBE. This RCQM extends the previous GBE RCQM beyond $SU(3)_F$ and reproduces the phenomenologically known spectra with reasonable accuracy. For definitely pinning down the type of hyperfine interaction especially for light-heavy and heavy-heavy Q-Q subsystems more data in the sector of c- and b-flavor baryons would be highly desirable.

In future it will be very interesting, if the universal GBE RCQM discussed here will be able to describe also reactions involving heavy baryons with a similar good performance as has previously been found for the $SU(3)$ GBE RCQM in the cases of light and strange baryons.

Acknowledgments This work was supported by the Austrian Science Fund, FWF, through the Doctoral Program on *Hadrons in Vacuum, Nuclei, and Stars* (FWF DK W1203-N16). J.P.D. would like to thank Profs. Ica Stancu and Veljko Dmitrašinović for valuable discussions during the Workshop, giving him further insights into heavy-baryon spectroscopy.

References

1. L. Y. Glozman, W. Plessas, K. Varga, and R. F. Wagenbrunn, Phys. Rev. D **58**, 094030 (1998).
2. W. Plessas, PoS **LC2010**, 017 (2010); arXiv:1011.0156 [hep-ph].
3. L. Y. Glozman, Z. Papp, W. Plessas, K. Varga, and R. F. Wagenbrunn, Phys. Rev. C **57**, 3406 (1998).
4. J. P. Day, K. -S. Choi, and W. Plessas, arXiv:1108.3450 [hep-ph].
5. K. Glantschnig, R. Kainhofer, W. Plessas, B. Sengl, and R. F. Wagenbrunn, Eur. Phys. J. **A23**, 507 (2005).
6. J. P. Day, K. -S. Choi, and W. Plessas, to be published.
7. K. Nakamura *et al.* (Particle Data Group), J. Phys. G **37**, 075021 (2010).
8. M. Mattson *et al.* (SELEX Collaboration), Phys. Rev. Lett. **89**, 112001 (2002).
9. R. K. Bhaduri, L. E. Cohler, and Y. Nogami, Nuovo Cim. **A65**, 376 (1981).
10. J.-M. Richard and F. Stancu, in *Exciting Hadrons* (Proceedings of the Mini-Workshop, Bled, Slovenia, 2005), ed. by B. Golli, M. Rosina, and S. Sirca (DMFA, Zaloznistvo, Ljubljana, 2005), p. 25; [hep-ph/0511043].
11. S. Migura, D. Merten, B. Metsch, and H. -R. Petry, Eur. Phys. J. **A28**, 41 (2006).

BLED WORKSHOPS
IN PHYSICS
VOL. 12, NO. 1
p. 32

Proceedings of the Mini-Workshop
Understanding hadronic spectra
Bled, Slovenia, July 3 - 10, 2011

Baryons' anomalous magnetic moments in a $U_L(3) \times U_R(3)$ chiral symmetric theory*

V. Dmitrašinović[a], Hua-Xing Chen[b,c], Atsushi Hosaka[d]

[a] Institute of Physics, Belgrade University, Pregrevica 118, Zemun,
P.O.Box 57, 11080 Beograd, Serbia
[b] School of Physics and Nuclear Energy Engineering, Beihang University,
Beijing 100191, China
[c] Departamento de Física Teórica and IFIC, Centro Mixto Universidad de Valencia-CSIC,
Institutos de Investigación de Paterna, Aptdo. 22085, 46071 Valencia, Spain
[d] Research Center for Nuclear Physics, Osaka University, Ibaraki 567–0047, Japan

Three-quark nucleon interpolating fields in QCD have well-defined $SU_L(3) \times SU_R(3)$ and $U_A(1)$ chiral transformation properties, *viz.* $[(\mathbf{6},\mathbf{3}) \oplus (\mathbf{3},\mathbf{6})]$, $[(\mathbf{3},\overline{\mathbf{3}}) \oplus (\overline{\mathbf{3}},\mathbf{3})]$, $[(\mathbf{8},\mathbf{1}) \oplus (\mathbf{1},\mathbf{8})]$ and their "mirror" images, Ref. [13]. It is known, Ref. [3] that chiral mixing of the $[(\mathbf{6},\mathbf{3}) \oplus (\mathbf{3},\mathbf{6})]$ multiplet with one ordinary ("naive") and one "mirror" field belonging to the $[(\overline{\mathbf{3}},\mathbf{3}) \oplus (\mathbf{3},\overline{\mathbf{3}})]$ and $[(\mathbf{1},\mathbf{8}) \oplus (\mathbf{8},\mathbf{1})]$ multiplets allows fitting of the isovector ($g_A^{(3)}$) and the flavor-singlet (isoscalar) axial coupling ($g_A^{(0)}$) of the nucleon. The magnetic moments of baryons are, however, difficult to incorporate into such a chiral mixing scheme. In order to reproduce the anomalous magnetic moments of baryons, we construct all $SU_L(3) \times SU_R(3)$ chirally invariant one-derivative Pauli tensor one-$[(\mathbf{8},\mathbf{1}) \oplus (\mathbf{1},\mathbf{8})]$-meson-baryon interactions subject to chiral mixing. It turns out that there are (strong) selection rules: for example, there is only one one-derivative chirally symmetric interaction between $J = \frac{1}{2}$ fields belonging to the $[(\mathbf{6},\mathbf{3}) \oplus (\mathbf{3},\mathbf{6})]$ and the $[(\mathbf{3},\overline{\mathbf{3}}) \oplus (\overline{\mathbf{3}},\mathbf{3})]$ chiral multiplets. We also study the chiral anomalous magnetic interactions of the $[(\mathbf{3},\overline{\mathbf{3}}) \oplus (\overline{\mathbf{3}},\mathbf{3})]$ and $[(\mathbf{8},\mathbf{1}) \oplus (\mathbf{1},\mathbf{8})]$ baryon fields. Again, there are selection rules that allow only off-diagonal and no diagonal one-derivative chiral $SU_L(3) \times SU_R(3)$ interactions of this type, that also conserve the $U_A(1)$ symmetry. We use these interactions to calculate the F/D ratio for the anomalous magnetic moments of baryons as F/D=1/3, in close proximity to the experiment.

In this talk we report some as yet unpublished results [1] of our studies of the anomalous magnetic moments of the baryons in the chiral mixing approach. Recent studies [2, 3] point towards baryon chiral mixing (of $[(\mathbf{6},\mathbf{3}) \oplus (\mathbf{3},\mathbf{6})]$ with the $[(\mathbf{3},\overline{\mathbf{3}}) \oplus (\overline{\mathbf{3}},\mathbf{3})]$, $[(\mathbf{8},\mathbf{1}) \oplus (\mathbf{1},\mathbf{8})]$ chiral multiplets [1]) as a possible mechanism underlying the baryons' axial couplings. This finding is in line with the old current algebra results of Gerstein and Lee [4, 5] and of Harari [6, 7], updated to include

* Talk delivered by V. Dmitrašinović

[1] These multiplets are not limited to three-quark interpolators.

recently measured values of F and D couplings, Ref. [8], and extended to include the flavor-singlet coupling $g_A^{(0)}$ of the nucleon [9,10], which was not considered in the mid-1960's at all, presumably due to the lack of data. Our own starting point was the QCD interpolating fields' $U_A(1)$ chiral properties [11–13].

Even though the chiral mixing has been known for more than 40 years [14–17], the $SU_L(3) \times SU_R(3)$ chiral interactions necessary to describe the anomalous magnetic moments have not been discussed in print, only the problems associated with them [18]. It ought to be noted, however, that Gerstein and Lee [5] found a phenomenological chiral mixing scheme that led to acceptable anomalous magnetic moments of the nucleons. These authors did not try to construct a chiral Lagrangian that would reproduce such chiral mixing, however.

The present paper serves to provide a dynamical model of chiral mixing that is the "best" approximation to the phenomenological solution of both the (F, D) and the flavor-singlet axial coupling, and the anomalous magnetic moment problems, assuming only three-quark baryon interpolating fields.

In our previous publication [19] we found two solutions that fit the axial coupling data [2]: one that conserves the $U_A(1)$ symmetry (the Harari scenario) and another one that does not (the Gerstein-Lee scenario). Here we have shown that only the former scenario leads to nucleon anomalous magnetic moments that are in agreement with experiment.

Having made the first step, which was to reproduce the phenomenological mixing starting from a chiral effective model interaction, we turn to the next step, which is to look for a chiral dynamical source of the anomalous magnetic moments. One such mechanism is the simplest chirally symmetric *one-derivative* one-(ρ, a)-meson interaction Lagrangian; one-derivative because only thus one can couple the baryon magnetic moment (the Pauli current) to the ρ-field. Here we study vector meson couplings because photon couplings follow them under the vector meson dominance hypothesis which has been shown to work in the low energy region.

We have constructed all $SU_L(3) \times SU_R(3)$ chirally invariant one-derivative one-vector-meson-baryon interactions and then use them to calculate the baryons' magnetic moments as well as the non-derivative Dirac terms. There are severe chiral symmetry induced selection rules, see Table 1.

We used these interactions to relate the anomalous magnetic moments to the "physical" mixing angles determined from the axial couplings and the baryons' masses. In this way we found a unique solution that unequivocally points towards the Harari scenario as the phenomenologically correct one. Of course, the absolute values of the anomalous magnetic moments cannot be determined by mere use of the chiral symmetry, without dynamical caculations, but their F/D ratio can. The magnetic moment F/D ratio is predicted to be 1/3 by the chiral mixing interaction, the same value as in the non-relativistic quark model, or as in the SU(6) symmetry limit. This last fact is very curious and seems to require further thought.

[2] this does not preclude the existence of more complicated solutions.

Table 1. Allowed chiral invariant Pauli type interaction terms with one $(\mathbf{8},\mathbf{1})\oplus(\mathbf{1},\mathbf{8})$ vector meson field $\bar{N}\sigma^{\mu\nu}\partial_\nu M_\mu N$. In the first column we show the chiral representation of N, and the first row the chiral representation of $\bar{N}$. We use "[mir]" to denote the relevant mirror fields.

	$(\mathbf{8},\mathbf{1})\oplus(\mathbf{1},\mathbf{8})$	$(\mathbf{3},\bar{\mathbf{3}})\oplus(\bar{\mathbf{3}},\mathbf{3})$	$(\mathbf{6},\mathbf{3})\oplus(\mathbf{3},\mathbf{6})$	$(\mathbf{10},\mathbf{1})\oplus(\mathbf{1},\mathbf{10})$
$(\mathbf{1},\mathbf{8})\oplus(\mathbf{8},\mathbf{1})$[mir]	$2\times M_\mu$			M_μ
$(\mathbf{3},\bar{\mathbf{3}})\oplus(\bar{\mathbf{3}},\mathbf{3})$[mir]		M_μ, $M_\mu^\dagger$		
$(\bar{\mathbf{3}},\bar{\mathbf{6}})\oplus(\bar{\mathbf{6}},\bar{\mathbf{3}})$[mir]			M_μ, $M_\mu^\dagger$	
$(\mathbf{1},\overline{\mathbf{10}})\oplus(\overline{\mathbf{10}},\mathbf{1})$[mir]	M_μ			M_μ

	$(\mathbf{3},\bar{\mathbf{3}})\oplus(\bar{\mathbf{3}},\mathbf{3})$	$(\mathbf{6},\mathbf{3})\oplus(\mathbf{3},\mathbf{6})$
$(\bar{\mathbf{3}},\mathbf{3})\oplus(\mathbf{3},\bar{\mathbf{3}})$		M_μ
$(\bar{\mathbf{6}},\bar{\mathbf{3}})\oplus(\bar{\mathbf{3}},\bar{\mathbf{6}})$	$M_\mu^\dagger$	

The "Gerstein-Lee" scenario requires vanishing nucleon anomalous magnetic moments, in serious disagreement with experiment (here we ignore any and all chiral mixing in the vector meson sector, which also violates the $U_A(1)$-symmetry [20]). This goes to show that the "QCD $U_A(1)$ anomaly" probably does not play a role in the "nucleon spin problem" [9, 10], as was once widely thought [21]. In all likelihood the $U_A(1)$ anomaly provides only a (relatively) small part of the solution, associated with the higher Fock space components, whereas the largest part comes from the $U_A(1)$-symmetric chiral structure ("mixing") of the three-quark components of the nucleon.

The next step, left for the future, is to investigate the $SU(3)\times SU(3)\to SU(2)\times SU(2)$ symmetry breaking and the study of the chiral $SU(2)\times SU(2)$ properties of hyperons. Then one may consider explicit chiral symmetry breaking corrections to the axial and the vector currents, which are related to the $SU(3)\times SU(3)$ symmetry breaking meson-nucleon derivative interactions, not just the explicit $SU(3)$ symmetry breaking ones that have been considered thus far (see Ref. [8] and the previous subsection, above).

References

1. H. X. Chen, V. Dmitrasinovic and A. Hosaka, submitted to Phys. Rev. D (2011).
2. V. Dmitrasinovic, A. Hosaka and K. Nagata, Mod. Phys. Lett. A **25**, 233 (2010).
3. H. X. Chen, V. Dmitrasinovic and A. Hosaka, Phys. Rev. D **81**, 054002 (2010).
4. I. S. Gerstein and B. W. Lee, Phys. Rev. Lett. **16**, 1060 (1966).
5. I. S. Gerstein and B. W. Lee, Phys. Rev. **152**, 1418 (1966).
6. H. Harari, Phys. Rev. Lett. **16**, 964 (1966).
7. H. Harari, Phys. Rev. Lett. **17**, 56 (1966).
8. T. Yamanishi, Phys. Rev. D **76**, 014006 (2007).
9. W. Vogelsang, J. Phys. G **34**, S149 (2007).
10. S. D. Bass, "The Spin structure of the proton," World Scientific, Singapore, (2007).
11. K. Nagata, A. Hosaka and V. Dmitrasinovic, Mod. Phys. Lett. A **23**, 2381 (2008).

12. K. Nagata, A. Hosaka and V. Dmitrasinovic, Eur. Phys. J. C **57**, 557 (2008).
13. H. X. Chen, V. Dmitrasinovic, A. Hosaka, K. Nagata and S. L. Zhu, Phys. Rev. D **78**, 054021 (2008).
14. Y. Hara, Phys. Rev. **139**, B134 (1965).
15. W. A. Bardeen and B. W. Lee, Phys. Rev. **177**, 2389 (1969).
16. B. W. Lee, Phys. Rev. **170**, 1359 (1968).
17. S. Weinberg, Phys. Rev. **177**, 2604 (1969).
18. R. Dashen and M. Gell-Mann, Phys. Rev. Lett. **17**, 340 (1966).
19. H. X. Chen, V. Dmitrasinovic and A. Hosaka, Phys. Rev. D **83**, 014015 (2011).
20. V. Dmitrasinovic, Nucl. Phys. A **686**, 379 (2001).
21. H. q. Zheng,"Singlet axial coupling, proton structure and the parity doublet model," CERN-TH-6327-91 preprint (unpublished).

BLED WORKSHOPS
IN PHYSICS
VOL. 12, NO. 1
p. 36

Proceedings of the Mini-Workshop
Understanding hadronic spectra
Bled, Slovenia, July 3 - 10, 2011

On the way to a realistic description of hadron resonances*

Regina Kleinhappel, Willibald Plessas, Wolfgang Schweiger

Theoretical Physics, Institute of Physics, University of Graz,
Universitätsplatz 5, A-8010 Graz, Austria

We are in the course of developing a coupled-channel relativistic constituent-quark model (CC RCQM). Thereby it should become possible to describe hadron reactions more realistically. In particular, we focus on strong hadron resonance decays, where we want to include the coupling to the mesonic decay channels explicitly.

In this regard, promising results have already been obtained before in a toy model for quark-antiquark systems with a scalar interaction neglecting spin and flavor degrees of freedom [1, 2]. There we calculated the decay of a meson resonance into the ground state by emitting a pion in a fully relativistic manner. The RCQM was constructed in a coupled-channel formalism along Poincaré-invariant quantum mechanics in the point-form. It leads to the interacting mass operator in matrix form comprising the two channels

1. the confined quark-antiquark system, depending on the valence-quark degrees of freedom, described by the mass operator $\hat{M}_{\rm val}$ and
2. the decay channel, containing in addition the π as the decay product, described by the mass operator $\hat{M}_{\rm val,\pi}$:

$$\hat{\mathcal{M}} = \begin{pmatrix} \hat{M}_{\rm val} & \hat{K}^\dagger \\ \hat{K} & \hat{M}_{\rm val,\pi} \end{pmatrix} . \tag{1}$$

Here, the operator $\hat{K}$ provides the coupling to the decay channel by producing the π at an elementary quark/antiquark-π vertex. For simplicity, the mass operator in the first channel is assumed to be the free mass operator plus a confinement interaction of harmonic oscillator type. The mass operator $\hat{M}_{\rm val,\pi}$ in the second channel contains in addition the kinetic energy of the π.

We solved the eigenvalue problem of the matrix mass operator in Eq. (1) after a Feshbach reduction leading to the complex eigenvalue problem

$$\left[\hat{M}_{\rm val} + \hat{K}^\dagger \left(\mathcal{M} - \hat{M}_{\rm val,\pi} + i0\right)^{-1} \hat{K}\right] |\psi_{\rm val}\rangle = \mathcal{M}\, |\psi_{\rm val}\rangle \ . \tag{2}$$

The results for the mass eigenvalues are shown in Fig. 1 as a function of the coupling strength to the decay channel. For the definite value of $g^2/4\pi$=1.19, marked

* Talk delivered by R. Kleinhappel

by the vertical line, we obtained the ground state corresponding to a model ρ meson with real mass eigenvalue m and the first excitation as a true resonance with complex mass eigenvalue $\mathcal{M}$. The decay width of the latter is $\Gamma = 2\,\mathrm{Im}\,\mathcal{M} = 26$ MeV.

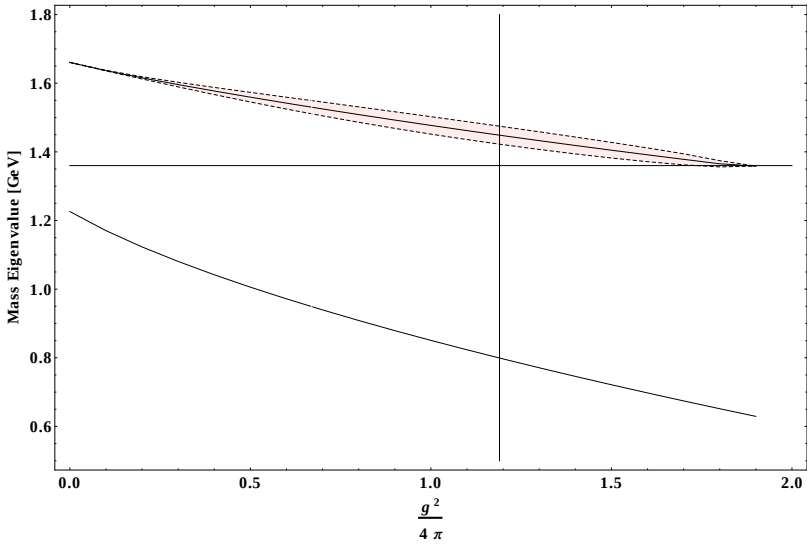

Fig. 1. Dependence of the mass-operator eigenvalues of the ground state (lower solid curve) and the first excited state (upper solid curve) on the coupling constant between the constituent (anti)quarks and the meson. For the resonant state it is also shown, how the decay width Γ – whose value is multiplied by a factor of 4 for better visibility – develops (shaded area). The vertical line indicates the particular coupling strength, where the mass eigenvalues of a model ρ ground state and an ω^* resonance are reproduced. The horizontal line marks the energy, where the decay width Γ vanishes; it is just the energy of the $Q\bar{Q}$ ground state with only confinement plus the π mass.

Beyond describing the spectrum more realistically, our model also allows to deduce meson vertex form factors from a microscopic approach. This has been done in ref. [3].

Currently, we are applying our approach to mesons, including spin and flavor degrees of freedom. At the same time we are improving the dynamics entering the valence and decay channels. Subsequently, the whole formalism will be extended to baryons. We expect that the notorious shortcomings of single-channel models, producing hadronic decay widths generally too small [4], will thereby be remedied.

Acknowledgments This work was supported by the Austrian Science Fund, FWF, through the Doctoral Program on *Hadrons in Vacuum, Nuclei, and Stars* (FWF DK W1203-N16).

References

1. R. Kleinhappel and W. Schweiger, in *Dressing Hadrons* (Proceedings of the Mini-Workshop, Bled, Slovenia, 2010), ed. by B. Golli, M. Rosina, and S. Sirca, DMFA, Ljubljana (2010), p. 33; arXiv:1010.3919
2. R. Kleinhappel and W. Schweiger, to appear in the Proceedings of the 14th International Conference on Hadron Spectroscopy, Munich, 2011; arXiv:1109.0127
3. R. Kleinhappel, Diploma Thesis, University of Graz, 2010
4. T. Melde, W. Plessas, and B. Sengl, Phys. Rev. D 77, 114002 (2008)

BLED WORKSHOPS
IN PHYSICS
VOL. 12, NO. 1
p. 39

Proceedings of the Mini-Workshop
Understanding hadronic spectra
Bled, Slovenia, July 3 - 10, 2011

The Schwinger model in point form*

D. Kupelwieser[a], W. Schweiger[a], and W. H. Klink[b]

[a] Institut für Physik, Universität Graz, A-8010 Graz, Austria
[b] Dept. Physics and Astronomy, The University of Iowa, Iowa City, IA 52242-1479, U.S.

Abstract. We attempt to solve the Schwinger model, i.e. massless QED in 1+1 dimensions, by quantizing it on a space-time hyperboloid $x_\mu x^\mu = \tau^2$. The Fock-space representation of the 2-momentum operator is derived and its algebraic structure is analyzed. We briefly outline a solution strategy.

1 Introduction

The Schwinger model is quantum electrodynamics of massless fermions in 1 space and 1 time dimension [1] and serves as a popular testing ground for non-perturbative methods in quantum field theory (QFT). It is an exactly solvable, super-renormalizable gauge theory that exhibits various interesting phenomena [2], such as confinement, which one would like to understand better in 1+3-dimensional QFTs. Originally it was solved by means of functional methods [1]. Later on also operator solutions were found [3] and spectrum and eigenstates of the theory were calculated by quantizing it at equal time $x^0 = \text{const.}$ [4, 5] or at equal light-cone time $x^+ = x^0 + x^1 = \text{const.}$ [6]. We rather attempt to solve the Schwinger model by means of canonical quantization on the space-time hyperboloid $x_0^2 - x_1^2 = \tau^2$. Each of these quantization hypersurfaces is associated with a particular form of relativistic Hamiltonian dynamics [7], namely the instant form, the front form and the point form, respectively.

The quantization surface in point form is a space-time hyperboloid which is invariant under the action of the Lorentz group. The kinematic (interaction independent) generators of the Poincaré group are therefore those of the Lorentz subgroup. All the interactions go into the components of the 2-momentum P^μ, i.e. the generators of space-time translations, which provide the dynamics of the system. One of the main virtues of point-form dynamics is obviously a simple behavior of wave functions and operators under Lorentz transformations. This has already been exploited in applications to relativistic few-body systems [8], but corresponding studies of interacting quantum field theories are still very sparse. The best-known paper is that of Fubini et al. [9], who deal with point-form QFT in 2-dimensional Euclidean space-time. We rather want to extend equal-τ quantization in Minkowski space-time, as it was worked out in Ref. [10] for free field theories, to the interacting case. The solution being known, the Schwinger model

* Talk delivered by D. Kupelwieser

would be an interesting example to test the point-form approach against other methods. The hope is then that point-form quantum field theory will eventually represent a useful alternative in the study of 4-dimensional quantum field theories.

The Lagrangian of the Schwinger model is

$$\mathcal{L} = \mathcal{L}_\gamma + \mathcal{L}_e + \mathcal{L}_{\text{int}} = \underbrace{-\frac{1}{4}F^{\mu\nu}F_{\mu\nu}}_{\text{photon part}} + \underbrace{\frac{i}{2}\bar{\psi}\overset{\leftrightarrow}{\not{\partial}}\psi}_{\text{fermion part}} + \underbrace{\frac{1}{2}e\bar{\psi}\not{A}\psi}_{\text{interaction part}} \tag{1}$$

with the 2×2 Dirac matrices being represented, as usual, in the Weyl basis, i.e. $\gamma^0 = \sigma_1$, $\gamma^1 = i\sigma_2$ and $\gamma^5 = \gamma^0\gamma^1 = -\sigma_3$.

2 The 2-Momentum Operator

2.1 The free part

This exposition follows closely Ref. [10] to which we refer for further details.

Fermions: In order to obtain the Fock-space representation of the free fermion 2-momentum operator, we Fourier-expand the Dirac field $\psi(x)$ in terms of plane waves using the fermion and antifermion annihilation (creation) operators $c^{(\dagger)}(p)$ and $d^{(\dagger)}(p)$ and the spinor basis $\{u(p), v(p)\}$. In the massless case, the spinors are ($p^0 = |p^1|$):

$$u(p) = \frac{1}{\sqrt{2p^0}}\begin{pmatrix} p^0 - p^1 \\ p^0 + p^1 \end{pmatrix} \qquad \text{and} \qquad v(p) = \frac{1}{\sqrt{2p^0}}\begin{pmatrix} p^1 - p^0 \\ p^1 + p^0 \end{pmatrix} . \tag{2}$$

The free fermion 2-momentum operator in point-form is then obtained from the stress-energy tensor $\Theta_e^{\mu\nu}$ by integrating over the space-time hyperboloid $x_\mu x^\mu = \tau^2$:

$$P_e^\mu = \int_{\mathbb{R}^2} \underbrace{2d^2x\,\delta\left(x^2 - \tau^2\right)\,\theta(x^0)\,x_\nu}_{\text{point-form "surface" element}}\,\Theta_e^{\nu\mu}\,, \quad \text{with} \quad \Theta_e^{\nu\mu} = \frac{i}{2}\bar{\psi}\gamma^\nu\overset{\leftrightarrow}{\partial}{}^\mu\psi\,. \tag{3}$$

Inserting now the plain-wave expansion for the fields and interchanging momentum and x integrations we are left with the covariant distribution

$$\begin{aligned} W_\nu(q) &= 2\int_{\mathbb{R}^2} d^2x\,\delta(x^2 - \tau^2)\,\theta(x^0)\,x_\nu\,e^{-iqx} \\ &= 2\pi\delta(q^2)\epsilon(q^0)q_\nu + 2\pi\theta(q^2)\delta(q^0)J_0(\tau\sqrt{q^2})g_{\nu 0} \\ &\quad -\frac{\pi\tau}{\sqrt{q^2}}\theta(q^2)\left[iY_1(\tau\sqrt{q^2}) + \epsilon(q^0)J_1(\tau\sqrt{q^2})\right]q_\nu \\ &\quad -\frac{2i\tau}{\sqrt{-q^2}}\theta(-q^2)K_1(\tau\sqrt{-q^2})\,q_\nu\,. \end{aligned} \tag{4}$$

When evaluating equation (3) for the free parts of the Lagrangian (1), W_ν is contracted with spinor products of the form $\bar{u}\gamma^\nu u$, $\bar{u}\gamma^\nu v$, etc. All the contractions

with q_ν vanish and only the term $\propto\ \theta(q^2)\delta(q^0)\,g_{\nu 0}$ survives. The result, as already shown by Biernat et al. [10] using a different trick to evaluate W_ν, is (after normal ordering)

$$P^\mu_e = \int \frac{dp^1}{2p^0}\, p^\mu \left(c^\dagger(p)\, c(p) + d^\dagger(p)\, d(p)\right), \tag{5}$$

i.e. the same as in instant form.

Photons: For the free photon 2-momentum operator we proceed in an analogous way. [1] The Fourier expansion of the vector potential $A^\mu(x)$ in terms of plane waves gives rise to the photon creation- and annihilation operators $a^\dagger_\kappa(k)$ and $a_\kappa(k)$ and to polarization vectors $\epsilon^\mu_\kappa(k)$, with $\kappa = 0, 1$ labeling the polarization. The polarization vectors are orthonormalized according to $\epsilon^\mu_{\kappa'}(k)\epsilon_{\kappa\mu}(k) = g_{\kappa'\kappa}$. In order to preserve the nice covariance properties of the point form, we work within the Lorenz gauge and use the Gupta-Bleuler quantization procedure. As a consequence there are no physical photons left. The 0- and the 1-component of the photon field are pure gauge degrees of freedom. Proceeding in analogy to the fermion part we find for the Fock-space representation of the free photon 2-momentum operator again the same result as for equal-time quantization, i.e.

$$P^\mu_\gamma = \sum_{\kappa=0}^{1} \int \frac{dk^1}{2k^0}\, k^\mu\, g^{\kappa\kappa} a^\dagger_\kappa(k)\, a_\kappa(k)\,. \tag{6}$$

2.2 The interaction part

Since there is no derivative in the interaction part of the Lagrangian (1), the interaction part of the stress-energy tensor is simply given by $\Theta^{\mu\nu}_{\text{int}} = -g^{\mu\nu}\,\mathcal{L}_{\text{int}}$. The interaction part of the 2-momentum operator is then

$$P^\mu_{\text{int}} = -\int_{\mathbb{R}^2} 2\, d^2x\, \delta(x^2 - \tau^2)\, \theta(x^0)\, x^\mu\, \mathcal{L}_{\text{int}}(x)\,. \tag{7}$$

One can check explicitly that the corresponding integral for the interaction part of the boost generator vanishes as expected [10].

To obtain the Fock-space representation of P^μ_{int} we proceed as before. The only difference is now that $W_\nu(q)$ does not provide a momentum conserving δ function. But this is not surprising. Both components of the momentum operator are interaction dependent so that one cannot expect momentum conservation at interaction vertices. But what one can do is to analyze the algebraic structure of P^μ_{int}. By appropriately collecting terms it can be cast into the form

$$P^\mu_{\text{int}} = -e \sum_{\kappa=0}^{1} \int \frac{dk^1}{2k^0} \left(\mathcal{A}(X^\mu_\kappa)(k)\, a_\kappa(k) + \mathcal{A}^\dagger(X^\mu_\kappa)(k)\, a^\dagger_\kappa(k)\right) \tag{8}$$

[1] See also Ref. [11] for a detailed derivation of the gluon 2-momentum operator.

with

$$\mathcal{A}(X^\mu_\kappa)(k) = \int \frac{dp^1}{2p^0} \int \frac{dp'^1}{2p'^0} \left(c^\dagger(p'), d(p)\right) X^\mu_{(\kappa)}(k, p', p) \begin{pmatrix} c(p) \\ d^\dagger(p) \end{pmatrix} \tag{9}$$

The distribution W^μ for different combinations of the momenta p, p' and k together with the different spinor products determines essentially the elements of the 2×2 matrix $X^\mu_{(\kappa)}(k, p', p)$.

3 The Eigenvalue Problem

Putting all the pieces together we finally end up with the eigenvalue problem

$$\left(P^\mu_e + P^\mu_\gamma + P^\mu_{\text{int}}\right)\left|\Psi\right\rangle = \mathcal{A}(E^\mu)\left|\Psi\right\rangle + \sum_{\kappa=0}^{1} \int \frac{dk^1}{2k^0} \Big(k^\mu g^{\kappa\kappa} a^\dagger_\kappa(k)\, a_\kappa(k) - e\mathcal{A}(X^\mu_\kappa)(k)\, a_\kappa(k) - e\mathcal{A}^\dagger(X^\mu_\kappa)(k)\, a^\dagger_\kappa(k) \Big) \left|\Psi\right\rangle = p^\mu \left|\Psi\right\rangle \tag{10}$$

which we want to solve non-perturbatively. Here we have also expressed the fermion kinetic energy in terms of the $\mathcal{A}$s to emphasize that the fermion creation and annihilation operators occur only in bilinear combinations. The argument E^μ is essentially a diagonal matrix containing $\pm\delta(p'^1 - p^1)$.

A possible strategy to solve this eigenvalue problem was proposed in Ref. [12]. The first step is to keep the number of modes finite. This could, e.g., be done without spoiling Lorentz-transformation properties by compactifying the x^1 direction such that one ends up with a deSitter space. A finite number of modes means also that only a finite number of fermion-antifermion pairs can be created. In order to keep the number of bosons finite the boson algebra is then considered as a contraction limit of another unitary algebra that restricts the number of bosons in any mode. In this way one ends up with a solvable algebraic problem that involves only a finite number of modes and a finite number of particles. The interesting question will be whether the well known results for Schwinger model are recovered upon performing the necessary contractions that restore the original theory.

Acknowledgments D. Kupelwieser acknowledges the support of the "Fonds zur Förderung der wissenschaftlichen Forschung in Österreich" (FWF DK W1203-N16).

References

1. J. S. Schwinger, Phys. Rev. **128** (1962) 2425
2. S. R. Coleman, R. Jackiw and L. Susskind, Ann. Phys. **93** (1975) 267
3. J. H. Lowenstein and J. A. Swieca, Ann. Phys. **68** (1971) 172
4. N. S. Manton, Ann. Phys. **159** (1985) 220
5. R. Link, Phys. Rev. **D42** (1990) 2103
6. F. Lenz, M. Thies, K. Yazaki, S. Levit, Annals Phys. **208** (1991) 1
7. P. A. M. Dirac, Rev. Mod. Phys. **21** (1949) 392

8. E. P. Biernat, W.H. Klink and W. Schweiger, Few Body Syst. **49** (2011) 149
9. S. Fubini, A. J. Hanson, R. Jackiw, Phys. Rev. **D7** (1973) 1732
10. E.P. Biernat, W. H. Klink, W. Schweiger and S. Zelzer, Annals Phys. **323** (2008) 1361
11. K. Murphy, PhD thesis, University of Iowa, 2009
12. W. H. Klink, "Point Form QFT on Velocity Grids I", arXiv:0801.4039 [nucl-th]

Bled Workshops
in Physics
Vol. 12, No. 1
p. 44

Proceedings of the Mini-Workshop
Understanding hadronic spectra
Bled, Slovenia, July 3 - 10, 2011

Electroweak structures of light and strange baryons*

Ki-Seok Choi[a] and W. Plessas[b]

[a] Department of Physics, Soongsil University, Seoul 156-743, Republic of Korea
[b] Theoretical Physics, Institute of Physics, University of Graz, A-8010 Graz, Austria

We have recently completed a study of the electromagnetic and axial form factors of all light and strange baryons in the framework of the relativistic constituent-quark model (RCQM). We have employed in the first instance the Goldstone-boson-exchange (GBE) RCQM [1, 2], but have also made analogous calculations with a typical one-gluon-exchange (OGE) RCQM, namely, the relativized model of Bhaduri, Cohler, and Nogami, as parameterized in ref. [3]. We have worked in the point form of Poincaré-invariant quantum mechanics.

Covariant predictions for the nucleon electromagnetic and axial as well as induced pseudoscalar form factors especially of the GBE RCQM had already been obtained about a decade ago [4–6]. They have been followed by detailed studies of the electric radii as well as magnetic moments of all light and strange baryons [7]. Also, our group has made comparative studies of point-form and instant-form calculations of the nucleon electromagnetic form factors [8], in order to find out the essential differences between the spectator-model constructions in either the instant and point forms [9]. More recently one has performed detailed investigations of the axial charges of the nucleon and N^* resonances [10]; this kind of studies have then also been extended to the axial charges of the whole octet and decuplet of light and strange baryons [11]. The axial charges are connected with the πNN coupling constant via the Goldberger-Treiman relation. Therefore it has been very interesting to study also the πNN as well as $\pi N\Delta$ interaction vertices [12]. With these investigations we have reached a microscopic description of the Q^2 dependences of the πNN and $\pi N\Delta$ form factors together with predictions for the corresponding coupling constants $f_{\pi NN}$ and $f_{\pi N\Delta}$, which were found in agreement with phenomenology.

In the spirit of the previous studies along the point-form construction of current operators we have recently extended our investigations to electromagnetic and axial form factors of the Δ and the hyperon ground states. This was the central focus of the dissertation of K.-S. C. [13]. Publications reporting these results are forthcoming [14]. Here we shortly summarize the main results as presented at the Workshop.

For the Δ and hyperon elastic electromagnetic and axial form factors there are no experimental data available. Such data exist only for some magnetic moments and electric radii. However, more and more results from lattice quantum

* Talk delivered by W. Plessas

chromodynamics (QCD) are appearing over the times. So, it has become possible to compare with lattice-QCD data and in some instances also with results from other theoretical approaches, such as, for example, chiral perturbation theory. Already in ref. [7] it was found that the predictions of the GBE RCQM for electric radii and magnetic moments of the Δ's and hyperons are in good agreement with existing experimental data for these observables. Now, it has turned out that the electromagnetic form factors produced by the GBE RCQM are quite congruent with insights gained from lattice QCD. This applies specifically to the Δ, Σ, Ξ, and Ω electromagnetic form factors; for Σ^* and Ξ^* no lattice-QCD results are yet available. For the axial form factors, we can compare to lattice-QCD data only for the Δ. Here too, the covariant predictions of the GBE RCQM agree or fall close to slightly scattered results from different lattice-QCD calculations.

Here, we should also like to add a note regarding the elastic electromagnetic form factors of the nucleons. While the corresponding predictions by the GBE RCQM have long been known [4,5], a deeper analysis of their behaviours regarding their flavor contents has recently come into the focus of interest. This is due to phenomenological data that have been extracted from a flavor decomposition of the world data on electromagnetic nucleon form factors [15]. A theoretical analysis of the individual flavor contributions to the form-factor predictions by the GBE RCQM has revealed that here again the theoretical results for the separate flavor parts are in good agreement with phenomenology in all respects [16] (see also the contribution by M. Rohrmoser et al. in these proceedings).

It is certainly remarkable that the parameter-free predictions of the GBE RCQM turn out to reproduce either experimental data or lattice-QCD results so closely. This is the more so, since the RCQM relies only on valence-quark degrees of freedom and does not include any explicit mesonic effects (specifically meson-dressing effects) or even contributions from configurations of more than three quarks. Judging from the present results one must conclude that such ingredients can only play a minor role. In all instances it has become evident that relativistic (boost) effects are most important. A fully relativistic treatment is thus mandatory in dealing with hadron reactions.

Acknowledgments This work was supported by the Austrian Science Fund, FWF, through the Doctoral Program on *Hadrons in Vacuum, Nuclei, and Stars* (FWF DK W1203-N16).

References

1. L. Y. Glozman, W. Plessas, K. Varga, and R. F. Wagenbrunn, Phys. Rev. D **58**, 094030 (1998).
2. L. Y. Glozman, Z. Papp, W. Plessas, K. Varga, and R. F. Wagenbrunn, Phys. Rev. C **57**, 3406 (1998).
3. L. Theussl, R. F. Wagenbrunn, B. Desplanques, and W. Plessas, Eur. Phys. J. A **12**, 91 (2001)
4. R. F. Wagenbrunn, S. Boffi, W. Klink, W. Plessas and M. Radici, Phys. Lett. B **511**, 33 (2001)

5. S. Boffi, L. Y. Glozman, W. Klink, W. Plessas, M. Radici and R. F. Wagenbrunn, Eur. Phys. J. A **14**, 17 (2002)
6. L. Y. Glozman, M. Radici, R. F. Wagenbrunn, S. Boffi, W. Klink and W. Plessas, Phys. Lett. B **516**, 183 (2001)
7. K. Berger, R. F. Wagenbrunn and W. Plessas, Phys. Rev. D **70**, 094027 (2004)
8. T. Melde, K. Berger, L. Canton, W. Plessas and R. F. Wagenbrunn, Phys. Rev. D **76**, 074020 (2007)
9. T. Melde, L. Canton, W. Plessas, and R. F. Wagenbrunn, Eur. Phys. J. A **25**, 97 (2005).
10. K. S. Choi, W. Plessas and R. F. Wagenbrunn, Phys. Rev. C **81**, 028201 (2010)
11. K. S. Choi, W. Plessas and R. F. Wagenbrunn, Phys. Rev. D **82**, 014007 (2010)
12. T. Melde, L. Canton and W. Plessas, Phys. Rev. Lett. **102**, 132002 (2009)
13. K.-S. Choi, PhD Thesis, Univ. of Graz (2011)
14. K.-S. Choi, W. Plessas, and R.F. Wagenbrunn, to be published
15. G. D. Cates, C. W. de Jager, S. Riordan, and B. Wojtsekhowski, Phys. Rev. Lett. **106**, 252003 (2011)
16. M. Rohrmoser, K. -S. Choi, and W. Plessas, arXiv:1110.3665 [hep-ph]

Bled Workshops
in Physics
Vol. 12, No. 1
p. 47

Proceedings of the Mini-Workshop
Understanding hadronic spectra
Bled, Slovenia, July 3 - 10, 2011

Analysis of flavor contributions to electromagnetic nucleon form factors*

Martin Rohrmoser[a], Ki-Seok Choi[b], and Willibald Plessas[a]

[a] Theoretical Physics, Institute of Physics, University of Graz,
Universitätsplatz 5, A-8010 Graz, Austria
[b] Department of Physics, Soongsil University, Seoul 156-743, Republic of Korea

Abstract. In view of a recently published flavor decomposition of the world experimental data on elastic electromagnetic form factors of the nucleons, we have performed a theoretical study of the individual flavor contributions to these observables in the framework of a relativistic constituent-quark model. We have found a surprisingly good agreement of our theory with all details of the experimental data in the range of momentum transfers $0 \leq Q^2 \lesssim 3.5\,\mathrm{GeV}^2$.

1 Introduction

Quite recently it has become possible to identify the various u- and d-flavor contributions to the elastic proton and neutron electromagnetic form factors G_E^p, G_M^p, G_E^n, and G_M^n from experiment [1]. The corresponding flavor separation of the experimental data covers the range of momentum transfers $0.30 \leq Q^2 \leq 3.41\,\mathrm{GeV}^2$. Interesting observations have been made on the behaviour of the flavor contributions and the total results for either the Sachs or Dirac and Pauli form factors.

It appears as a challenge for theory to reproduce the very detailed properties of the nucleon electromagnetic form factors as revealed by the experimental flavor decomposition of ref. [1]. We have put the relativistic constituent-quark model (RCQM) whose quark-quark hyperfine interaction is based on Goldstone-boson exchange (GBE) [2,3] to a test with the new experimental data base. The covariant predictions of the GBE RCQM for the elastic electromagnetic form factors have already been obtained over the past decade and were found in remarkably good agreement with experimental data in all instances for momentum transfers up to $Q^2 \sim 5\,\mathrm{GeV}^2$ [4–6].

The covariant form factors are most conveniently calculated in the point form of Poincaré-invariant quantum mechanics [7]. In our approach we have done so by applying a spectator model for the electromagnetic current operator [8]. Contrary to the case with other forms of relativistic quantum mechanics, the spectator-model character of the current operator in point form is preserved in all reference frames [9]. These features of the point-form spectator model (PFSM)

* Talk delivered by M. Rohrmoser

guarantee in particular the electromagnetic form factors to be manifestly covariant.

Some first results of our theoretical analysis of flavor contributions to the nucleon electromagnetic form factors can be found already in ref. [10]. Here, we give some more information about the formalism and present further detailed results.

2 Formalism

Our theoretical framework is relativistic quantum mechanics (RQM), which assumes a fixed number of relevant degrees of freedom. The nucleons N are thus considered as bound states of three constituent quarks Q. The RCQM is based on an invariant mass operator $\hat{M} = \hat{M}_{\text{free}} + \hat{M}_{\text{int}}$ fulfilling all symmetry requirements of the Poincaré group. The free and interaction parts of the mass operator are expressed in the rest frame of the nucleon (i.e. for $\mathbf{P} = \sum_i^3 \mathbf{k}_i^2 = 0$) by

$$\hat{M}_{\text{free}} = \sum_{i=1}^{3} \sqrt{\hat{m}_i^2 + \hat{\mathbf{k}}_i^2}\,, \qquad \hat{M}_{\text{int}} = \sum_{i<j}^{3} \hat{V}_{ij} = \sum_{i<j}^{3} \left(\hat{V}_{ij}^{\text{conf}} + \hat{V}_{ij}^{\text{hf}}\right)\,, \tag{1}$$

where $\mathbf{k}_i$ represent the three-momenta of the individual quarks with rest masses m_i and the Q-Q potentials $\hat{V}_{ij}$ are composed of confinement and hyperfine interactions. By employing such a mass operator $\hat{M}^2 = \hat{P}^\mu \hat{P}_\mu$, with baryon four-momentum $\hat{P}_\mu = (\hat{H}, \hat{\mathbf{P}})$, the Poincaré algebra of all ten generators $\{\hat{H}, \hat{P}_i, \hat{J}_i, \hat{K}_i\}$, for $i = 1, 2, 3$, is guaranteed.

For the GBE RCQM [2] one has assumed a linear confinement of a strength corresponding to the string tension of quantum chromodynamics (QCD) and a hyperfine interaction derived from GBE; the latter should account for the spontaneous breaking of chiral symmetry of low-energy QCD. Its specific feature is an explicit flavor dependence that allows to reproduce the baryon excitation spectra with an unprecedented accuracy [3]. The GBE RCQM has already been successfully applied to a number of different processes (for a short review see, e.g., ref. [11]).

Stepping out from the mass-operator eigenstates of the nucleons $|P, J, \Sigma\rangle = |M, V, J, \Sigma\rangle$, which are simultaneous eigenstates of the mass operator $\hat{M}$, the four-momentum operator $\hat{P}^\mu$ (where $\hat{P}^\mu = \hat{M}\hat{V}^\mu$, with the four-velocity operator $\hat{V}^\mu$), the total angular-momentum operator $\hat{J}$ and its z-component $\hat{\Sigma}$, one can define the invariant form factors $F^\mu_{\Sigma',\Sigma}$ by the matrix elements of the electromagnetic current operator between incoming and outgoing nucleon states

$$F^\mu_{\Sigma',\Sigma}(Q^2) = \frac{1}{2M} \langle V', M', J', \Sigma' | \hat{J}^\mu | V, M, J, \Sigma \rangle\,, \tag{2}$$

where Q^2 is the square of the space-like momentum transfer $Q^\mu = P'^\mu - P^\mu$. The elastic Sachs form factors are hereby obtained (for $M = M'$ and $J = J' = \frac{1}{2}$) in the following way:

$$G_E(Q^2) = F^0_{\frac{1}{2}\frac{1}{2}}(Q^2) \tag{3}$$

$$G_M(Q^2) = \frac{2M}{Q} F^1_{\frac{1}{2}-\frac{1}{2}}(Q^2)\,. \tag{4}$$

The Dirac and Pauli form factors are then obtained as

$$F_1(Q^2) = \frac{1}{1+\tau}\left[G_E(Q^2) + \tau G_M(Q^2)\right] \tag{5}$$

$$F_2(Q^2) = \frac{1}{1+\tau}\left[G_M(Q^2) - G_E(Q^2)\right] , \tag{6}$$

where $\tau = (\frac{Q}{2M})^2$. Details of the calculation of the current matrix elements of Eq. (2) can, e.g., be found in refs. [4–6, 9].

Following Eqs. (2)-(4), we can also write for the Sachs form factors

$$G_E(Q^2) = \frac{1}{2M}\left\langle V', M, \frac{1}{2}, \frac{1}{2}\right| \hat{J}^0 \left| V, M, \frac{1}{2}, \frac{1}{2}\right\rangle \tag{7}$$

$$G_M(Q^2) = \frac{1}{Q}\left\langle V', M, \frac{1}{2}, \frac{1}{2}\right| \hat{J}^1 \left| V, M, \frac{1}{2}, -\frac{1}{2}\right\rangle . \tag{8}$$

Next we define the contributions of flavors u and d to the Sachs form factors in a nucleon N as

$$G_E^{u,N}(Q^2) = \frac{3}{n_{u,N}}\frac{1}{2M}\left\langle V', M, \frac{1}{2}, \frac{1}{2}\right| \hat{J}^0_u \left| V, M, \frac{1}{2}, \frac{1}{2}\right\rangle \tag{9}$$

$$G_E^{d,N}(Q^2) = \frac{-3}{n_{d,N}}\frac{1}{2M}\left\langle V', M, \frac{1}{2}, \frac{1}{2}\right| \hat{J}^0_d \left| V, M, \frac{1}{2}, \frac{1}{2}\right\rangle \tag{10}$$

$$G_M^{u,N}(Q^2) = \frac{3}{n_{u,N}}\frac{1}{Q}\left\langle V', M, \frac{1}{2}, \frac{1}{2}\right| \hat{J}^1_u \left| V, M, \frac{1}{2}, -\frac{1}{2}\right\rangle \tag{11}$$

$$G_M^{d,p}(Q^2) = \frac{-3}{n_{d,N}}\frac{1}{Q}\left\langle V', M, \frac{1}{2}, \frac{1}{2}\right| \hat{J}^1_d \left| V, M, \frac{1}{2}, -\frac{1}{2}\right\rangle , \tag{12}$$

where $\hat{J}^{0,1}_f$ are the projections of the current-operator components $\hat{J}^{0,1}$ on flavors $f = u, d$ and $n_{f,N}$ are the numbers of quarks with flavors u and d in the proton or the neutron, respectively. A priori we thus have eight separate contributions to the full results of nucleon Sachs form factors. Under charge symmetry they are reduced to only four independent contributions, since we have the restricting relations for both the electric and magnetic form factors

$$G_{E,M}^{u,p}(Q^2) = 2G_{E,M}^{d,n}(Q^2) := G_{E,M}^{u}(Q^2) \tag{13}$$

$$2G_{E,M}^{d,p}(Q^2) = G_{E,M}^{u,n}(Q^2) := G_{E,M}^{d}(Q^2) . \tag{14}$$

This means that the Sachs form factors of the proton and neutron are constituted from their flavor parts as

$$G_E^p = \frac{2}{3}G_E^u - \frac{1}{3}G_E^d , \qquad G_E^n = \frac{2}{3}G_E^d - \frac{1}{3}G_E^u \tag{15}$$

$$G_M^p = \frac{2}{3}G_M^u - \frac{1}{3}G_M^d , \qquad G_M^n = \frac{2}{3}G_M^d - \frac{1}{3}G_M^u . \tag{16}$$

The inverse formulae read

$$G_E^u = 2G_E^p + G_E^n , \qquad G_E^d = G_E^p + 2G_E^n \tag{17}$$

$$G_M^u = 2G_M^p + G_M^n , \qquad G_M^d = G_M^p + 2G_M^n . \tag{18}$$

The corresponding flavor contributions to the nucleon Dirac and Pauli form factors are then given by

$$F_1^f(Q^2) = \frac{1}{1+\tau}\left[G_E^f(Q^2) + \tau G_M^f(Q^2)\right] \tag{19}$$

$$F_2^f(Q^2) = \frac{1}{1+\tau}\left[G_M^f(Q^2) - G_E^f(Q^2)\right] , \tag{20}$$

for f=u, d. The latter can also be expressed directly through the proton and neutron Dirac and Pauli form factors in the following way

$$F_i^u = 2F_i^p + F_i^n , \qquad F_i^d = 2F_i^n + F_i^p , \qquad i = 1, 2 . \tag{21}$$

3 Results

Here we present results for the flavor contributions to the nucleon Sachs as well as Dirac and Pauli form factors obtained from the GBE RCQM in the PFSM approach, i.e. through calculations in complete analogy to the previous studies of the nucleon electromagnetic structures [4–6, 9].

The individual flavor contributions to the proton and neutron electric as well as magnetic form factors, as published in the original refs. [4, 5], are shown in Fig. 1. As is nicely seen, not only the global results for all four form factors G_E^p, G_M^p, G_E^n, and G_M^n agree well with the world experimental data but also the separate flavor parts match the data extracted in ref. [1]. Slight differences to these data are only visible for the anyway very small d-flavor contribution to the magnetic form factor of the neutron.

In addition to the electromagnetic Sachs form factors as depicted in Fig. 1 we may also examine the flavor compositions of the nucleon electric radii r_E and magnetic moments μ. We recall that these quantities are defined through the behaviours of the electric and magnetic form factors at Q^2=0 in the following way

$$r_E^2 = -6\frac{dG_E(Q^2)}{dQ^2}\bigg|_{Q^2=0} , \qquad \mu = G_M(Q^2 = 0) . \tag{22}$$

In Tables 1 and 2 we present the individual flavor contributions to the nucleon electric radii and magnetic moments. It is interesting how the different parts contribute to build up the full results, which are again in quite reasonable agreement with experimental data.

The ratios of the Pauli to the Dirac form factors F_2/F_1 for the proton and neutron have been in the focus of many theoretical investigations because of scaling considerations. In ref. [1] the particular Q^2 dependences have been highlighted in comparison to the corresponding ratios for the separate flavor parts, i.e. F_2^f/F_1^f, for f=u, d. From the flavor decomposition of the experimental data it was found that both F_2^u/F_1^u and F_2^d/F_1^d become practically constant for momentum transfers $Q^2 \gtrsim 1.5\,\mathrm{GeV}^2$, much in contrast to F_2/F_1 for both the proton and the neutron. We depict the behaviour of the theoretical results obtained with the GBE RCQM in Figs. 2 and 3. Again it is found that the theoretical predictions are in reasonable agreement with the experimental data not only for the total results (Fig. 2) but also for the flavor-separated ratios (Fig. 3).

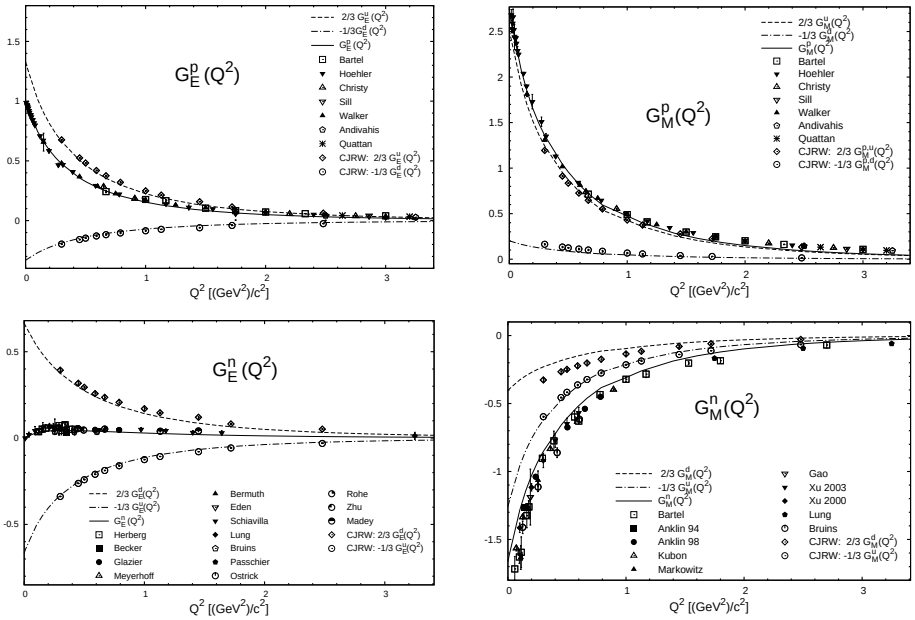

Fig. 1. u- and d-flavor contributions to the proton (upper panels) and neutron (lower panels) electric and magnetic form factors as predicted by the GBE RCQM in comparison to experimental data from ref. [1] (CJRW) and other experiments as indicated.

Table 1. u- and d-flavor contributions to the proton and neutron electric radii squared r_E^2 [fm^2].

	GBE RCQM			
	Flavor Contributions		Total	Experiment
	u	d		
p	1.0089	−0.1848	0.8241	0.769(28) [12]
				0.70869(113) [13]
n	0.3696	−0.5045	−0.1349	−0.1161(22) [12]

Table 2. u- and d-flavor contributions to the proton and neutron magnetic moments μ [n.m.].

	GBE RCQM			
	Flavor Contributions		Total	Experiment
	u	d		
p	2.4641	0.2343	2.6984	2.792847356(23) [12]
n	−0.4686	−1.2321	-1.7006	−1.9130427(5) [12]

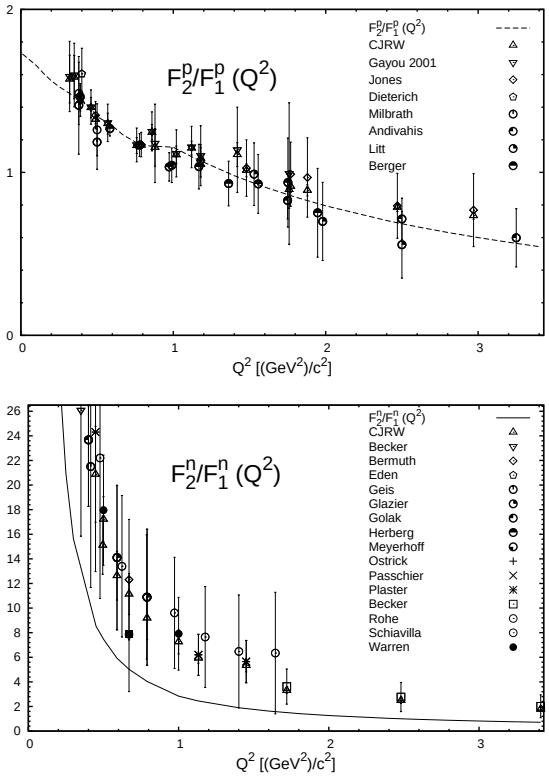

Fig. 2. Ratios of Pauli to Dirac form factors for the proton (left) and neutron (right) as predicted by the GBE RCQM in comparison to experimental data from ref. [1] and other experiments as indicated.

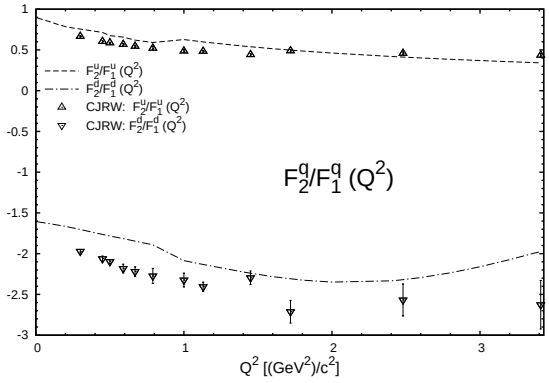

Fig. 3. Ratios of the u- and d-flavor contributions to the Pauli to Dirac form factors as predicted by the GBE RCQM in comparison to experimental data from ref. [1].

4 Conclusions

From the flavor analysis of elastic electromagnetic nucleon form factors we have learned that the RCQM, especially the one with GBE hyperfine forces, provides rather reasonable results in practically all instances. We attribute the successes mainly to:

- appropriate dynamics in the GBE RCQM,
- very precise nucleon wave functions from the GBE RCQM,
- mixed-symmetry spatial components in the nucleon wave functions,
- manifest covariance of the observables due to point-form Lorentz boosts,
- strict frame independence of the construction of the current operator,
- fulfillment of current conservation.

It is interesting to note that the GBE RCQM relies on three-quark configurations only. The underlying dynamics are just based on coupling valence-quark fields with Goldstone bosons. No explicit mesonic effects (e.g., so-called meson-cloud effects) or more-quark components are introduced beyond. From our previous studies we do know that relativistic (boost) effects are most important in the reproduction of the nucleon electromagnetic form factors [4, 5]. This is even true for the quantities extracted at or near zero momentum transfers, i.e. the magnetic moments and electric radii [6]. For the good performance of the GBE RCQM we identify as most important two special symmetry ingredients in our theory, namely, the spontaneous breaking of chiral symmetry of low-energy QCD and strict Lorentz invariance.

Acknowledgments This work was supported by the Austrian Science Fund, FWF, through the Doctoral Program on *Hadrons in Vacuum, Nuclei, and Stars* (FWF DK W1203-N16). The authors are grateful to B. Wojtsekhowski for providing them with an extensive experimental data base of elastic nucleon electromagnetic form factors. M.R. thanks the organizers of the Workshop for the generous support enabling him to participate in an exciting meeting with a lot of illuminating discussions.

References

1. G. D. Cates, C. W. de Jager, S. Riordan, and B. Wojtsekhowski, Phys. Rev. Lett. **106**, 252003 (2011)
2. L. Y. Glozman, W. Plessas, K. Varga, and R. F. Wagenbrunn, Phys. Rev. D **58**, 094030 (1998)
3. L. Y. Glozman, Z. Papp, W. Plessas, K. Varga, and R. F. Wagenbrunn, Phys. Rev. C **57**, 3406 (1998)
4. R. F. Wagenbrunn, S. Boffi, W. Klink, W. Plessas, and M. Radici, Phys. Lett. **B511**, 33 (2001)
5. S. Boffi, L. Glozman, W. Klink, W. Plessas, M. Radici, and R. Wagenbrunn, Eur. Phys. J. **A14**, 17 (2002)
6. K. Berger, R. F. Wagenbrunn, and W. Plessas, Phys. Rev. D **70**, 094027 (2004)

7. P. A. M. Dirac, Rev. Mod. Phys. **21**, 392 (1949)
8. T. Melde, L. Canton, W. Plessas, and R. F. Wagenbrunn, Eur. Phys. J. **A25**, 97 (2005)
9. T. Melde, K. Berger, L. Canton, W. Plessas, and R. F. Wagenbrunn, Phys. Rev. D **76**, 074020 (2007)
10. M. Rohrmoser, K. -S. Choi, W. Plessas, arXiv:1110.3665 [hep-ph]
11. W. Plessas, PoS **LC2010**, 017 (2010); arXiv:1011.0156 [hep-ph]
12. K. Nakamura et al. (Particle Data Group), J. Phys. **G37**, 075021 (2010)
13. R. Pohl et al., Nature **466**, 213 (2010)

Bled Workshops
in Physics
Vol. 12, No. 1
p. 55

Proceedings of the Mini-Workshop
Understanding hadronic spectra
Bled, Slovenia, July 3 - 10, 2011

A review of new data on compact stars from a Magnetar model of magnetised cores*

Vikram Soni[a] and N. D. Haridass[b]

[a] National Physical Laboratory and Jamia Millia University, New Delhi, India
[b] Indian Insitute of Science, Bangalore, India

Abstract. We have used the Magnetar model to identify some stars, in a sampling of a few high magnetic field pulsars, as magnetars. Thus this model throws up a lot of unexplored physics from the strongly interacting core to the plasma physics and the crustal solid state physics of huge magnetic fields.

Our understanding of neutron stars is at a crossroad. We have to understand many families of neutron stars, for example pulsars and magnetars, in one framework. This is what we have tried to do in this work.

Neutron stars are also the laboratory to understand the high density phase diagram for strong interactions. This work gives us a new understanding of the strong interactions that is linked intimately to astrophysical data.

Our Model Conclusions

In conclusion we enumerate some of the consequences of the model presented above:

i) Magnetars belong exclusively to the higher than pulsar mass population of neutron stars that are born with a high density magnetic core.

ii) The high density core is created by a strong interaction phase transition that aligns magnetic moments to create large dynamical $10^{16(17)}$ G magnetic fields at the surface of the core. Dynamical fields are 'permanent' unlike fields derived from currents.

iii) The core field is shielded by Lenz currents generated in the high conductivity plasma in and around it, but is gradually transported to the crust by ambipolar diffusion over a timescale of $\simeq 10^{5-6}$ years with interior temperatures of more than $\simeq 10^{8.5}$ K, - this results in a time delay before the field comes out to the surface. In old spun up binary neutron stars created by slow accretion (for example the large mass (almost 2 solar mass) binary neutron star, PSR J1614-2230), the lower interior temperatures inhibit transport of the core field to the crust.

iv) The strong magnetic field breaks through the crust as the shielding currents dissipate giving out a steady X-ray flux and several energetic flares.

v) This further implies that the surface field keeps increasing in magnitude till all shielding currents dissipate and the permanent dipolar core field is established.

* Talk delivered by V. Soni

vi) Neutron stars are also the laboratory to understand the high density phase diagram for strong interactions. The existence of the large mass (almost 2 solar mass) binary neutron star, PSR J1614-2230, very probably rules out soft equations of state, associated with quark matter (with/without condensate) cores.

We have found that all these phenomena are supported by extensive data and observations.

References

1. V. Soni and D. Bhattacharya, Phys. Lett. B **643** 2006.
2. D. Bhattacharya and V. Soni, arXiv (astro-ph) 0705.0592, 2007.
3. N. D. Hari Dass and V. Soni, *Magnetars from Magnetized Cores created by a Strong Interaction Phase Transition*, arXiv(astro-ph) 1012.1420, 2010.

Bled Workshops
in Physics
Vol. 12, No. 1
p. 57

Proceedings of the Mini-Workshop
Understanding hadronic spectra
Bled, Slovenia, July 3 - 10, 2011

Negative parity nonstrange baryons in large N_c QCD: quark excitation versus meson-nucleon scattering*

N. Matagne[a] and Fl. Stancu[b]

[a] Service de Physique Nucléaire et Subnucléaire, University of Mons, Place du Parc, B-7000 Mons, Belgium
[b] Institute of Physics, B5, University of Liège, Sart Tilman, B-4000 Liège 1, Belgium

Abstract. We show that the two complementary pictures of large N_c baryons - the single-quark orbital excitation about a symmetric core and the meson-nucleon resonance – are compatible for $\ell = 3$ SU(4) baryons. The proof is based on a simple Hamiltonian including operators up to order $\mathcal{O}(N_c^0)$ used previously in the literature for $\ell = 1$.

1 The status of the $1/N_c$ expansion method

The large N_c QCD, or alternatively the $1/N_c$ expansion method, proposed by 't Hooft [1] and implemented by Witten [2] became a valuable tool to study baryon properties in terms of the parameter $1/N_c$ where N_c is the number of colors. According to Witten's intuitive picture, a baryon containing N_c quarks is seen as a bound state in an average self-consistent potential of a Hartree type and the corrections to the Hartree approximation are of order $1/N_c$.

Ten years after 't Hooft's work, Gervais and Sakita [3] and independently Dashen and Manohar in 1993 [4] derived a set of consistency conditions for the pion-baryon coupling constants which imply that the large N_c limit of QCD has an exact contracted $SU(2N_f)_c$ symmetry when $N_c \to \infty$, N_f being the number of flavors. For ground state baryons the $SU(2N_f)$ symmetry is broken by corrections proportional to $1/N_c$ [5,6].

Analogous to s-wave baryons, consistency conditions which constrain the strong couplings of excited baryons to pions were derived in Ref. [7]. These consistency conditions predict the equality between pion couplings to excited states and pion couplings to s-wave baryons. These predictions are consistent with the nonrelativistic quark model.

A few years later, in the spirit of the Hartree approximation a procedure for constructing large N_c baryon wave functions with mixed symmetric spin-flavor parts has been proposed [8] and an operator analysis was performed for $\ell = 1$ baryons [9]. It was proven that, for such states, the $SU(2N_f)$ breaking occurs at order N_c^0, instead of $1/N_c$, as it is the case for ground and also symmetric excited states $[56, \ell^+]$ (for the latter see Refs. [10,11]). This procedure has been

* Talk delivered by I. Stancu

extended to positive parity nonstrange baryons belonging to the $[70, \ell^+]$ with $\ell = 0$ and 2 [12]. In addition, in Ref. [12], the dependence of the contribution of the linear term in N_c, of the spin-orbit and of the spin-spin terms in the mass formula was presented as a function of the excitation energy or alternatively in terms of the band number N. Based on this analysis an impressive global compatibility between the $1/N_c$ expansion and the quark model results for $N = 0, 1, 2$ and 4 [13] was found (for a review see Ref. [14]). More recently the $[70, 1^-]$ multiplet was reanalyzed by using an exact wave function, instead of the Hartree-type wave function, which allowed to keep control of the Pauli principle at any stage of the calculations [15]. The novelty was that the isospin-isospin term, neglected previously [9] becomes as dominant in Δ resonances as the spin-spin term in N^* resonances.

The purpose of this work is to analyze the compatibility between the $1/N_c$ expansion method in the so-called *quark-shell picture* and the *resonance or scattering picture* defined in the framework of chiral soliton models. Details can be found in Ref. [16].

2 Negative parity baryons

If an excited baryon belongs to a symmetric [**56**]-plet the three-quark system can be treated similarly to the ground state in the flavour-spin degrees of freedom, but one has to take into account the presence of an orbital excitation in the space part of the wave function [10,11]. If the baryon state is described by a mixed symmetric representation, [**70**] in SU(6) notation, the treatment becomes more complicated. In particular, the resonances up to 2 GeV belong to $[\mathbf{70}, 1^-]$, $[\mathbf{70}, 0^+]$ or $[\mathbf{70}, 2^+]$ multiplets and beyond to 2 GeV to $[\mathbf{70}, 3^-]$, $[\mathbf{70}, 5^-]$, etc.

In the following we adopt the standard way to study the [**70**]-plets which, as already mentioned, is related to the Hartree approximation [8]. An excited baryon is described by a symmetric core plus an excited quark coupled to this core, see *e.g.* [9, 12, 17, 18]. The core is treated in a way similar to that of the ground state. In this method each $SU(2N_f) \times O(3)$ generator is separated into two parts

$$S^i = s^i + S^i_c; \quad T^a = t^a + T^a_c; \quad G^{ia} = g^{ia} + G^{ia}_c; \quad \ell^i = \ell^i_q + \ell^i_c, \tag{1}$$

where s^i, t^a, g^{ia} and ℓ^i_q are the excited quark operators and S^i_c, T^a_c, G^{ia}_c and ℓ^i_c the corresponding core operators.

2.1 The quark-shell picture

In the quark-shell picture we use the procedure of Ref. [19], equivalent to that of Ref. [20], later extended in Ref. [21]. We start from the leading-order Hamiltonian including operators up to order $\mathcal{O}(N_c^0)$ which has the following form

$$H = c_1 \mathbb{1} + c_2 \ell \cdot s + c_3 \frac{1}{N_c} \ell^{(2)} \cdot g \cdot G_c \tag{2}$$

This operator is defined in the spirit of a Hartree picture (mean field) where the matrix elements of the first term are proportional to N_c on all baryons [2]. The

spin-orbit term $\ell \cdot s$ which is a one-body operator and the third term - a two-body operator containing the tensor $\ell^{(2)ij}$ of O(3) - have matrix elements of order $\mathcal{O}(N_c^0)$. The neglect of $1/N_c$ corrections in the $1/N_c$ expansion makes sense for the comparison with the scattering picture in the large N_c limit, described in the following section.

One can see that the Hamiltonian (2) reproduces the characteristic N_c scaling for the excitation energy of baryons which is N_c^0 [2].

The nucleon case In large N_c the color part of the wave function is antisymmetric so that the orbital-spin-flavor part must be symmetric to satisfy the Pauli principle. A quanta of orbital excitation requires the orbital part to be mixed symmetric, the lowest state having the partition $[N_c - 1, 1]$. We have the following $[N_c - 1, 1]$ spin-flavor (SF) states which form a symmetric state with the orbital $\ell = 3$ state of partition $[N_c - 1, 1]$

1. $[N_c - 1, 1]_{SF} = \left[\frac{N_c+1}{2}, \frac{N_c-1}{2}\right]_S \times \left[\frac{N_c+1}{2}, \frac{N_c-1}{2}\right]_F, \quad N_c \geq 3$
   with $S = 1/2$ and $J = 5/2, 7/2$
2. $[N_c - 1, 1]_{SF} = \left[\frac{N_c+3}{2}, \frac{N_c-3}{2}\right]_S \times \left[\frac{N_c+1}{2}, \frac{N_c-1}{2}\right]_F, \quad N_c \geq 3$
   with $S = 3/2$ and $J = 3/2, 5/2, 7/2, 9/2$.

They give rise to matrices of a given J either 2×2 or 1×1 depending on the multiplicity of J. States of symmetry $[N_c - 1, 1]_{SF}$ with $S = 5/2$, like for Δ (see below), which together with $\ell = 3$ could give rise to $J = 11/2$, are not allowed for N, by inner products of the permutation group [22]. Therefore the experimentally observed resonance $N(2600)I_{11/2}$ should belong to the $N = 5$ band ($\ell = 5$). For $N_c = 3$ the above states correspond to the $^2 8$ and $^4 8$ multiplets of SU(2) $\times$ SU(3) respectively.

The Δ case In this case the Pauli principle allows the following states

1. $[N_c - 1, 1]_{SF} = \left[\frac{N_c+1}{2}, \frac{N_c-1}{2}\right]_S \times \left[\frac{N_c+3}{2}, \frac{N_c-3}{2}\right]_F, \quad N_c \geq 3$
   with $S = 1/2$ and $J = 5/2, 7/2$,
2. $[N_c - 1, 1]_{SF} = \left[\frac{N_c+3}{2}, \frac{N_c-3}{2}\right]_S \times \left[\frac{N_c+3}{2}, \frac{N_c-3}{2}\right]_F, \quad N_c \geq 5$
   with $S = 3/2$ and $J = 3/2, 5/2, 7/2, 9/2$,
3. $[N_c - 1, 1]_{SF} = \left[\frac{N_c+5}{2}, \frac{N_c-5}{2}\right]_S \times \left[\frac{N_c+3}{2}, \frac{N_c-3}{2}\right]_F, \quad N_c \geq 7$
   with $S = 5/2$ and $J = 1/2, 3/2, 5/2, 7/2, 9/2, 11/2$.

As above, they indicate the size of a matrix of fixed J for the Hamiltonian (2). For example, the matrix of $\Delta_{5/2}$ is 3×3, because all three states can have $J = 5/2$. For $N_c = 3$ the first state belongs to the $^2 10$ multiplet. The other two types of states do not appear in the real world with $N_c = 3$. Note that both for N_J and Δ_J states the size of a given matrix equals the multiplicity of the corresponding state indicated in Table 1 of Ref. [21] for $\ell = 3$.

The Hamiltonian (2) is diagonalized in the bases defined above. Let us denote the eigenvalues either by $m_{N_J}^{(i)}$ or $m_{\Delta_J}^{(i)}$ with i = 1, 2 or 3, depending on how

many eigenvalues are at a fixed J. The Hamiltonian has analytical solutions, all eigenvalues being linear functions in the coefficients c_1, c_2 and c_3. It is remarkable that the 18 available eigenstates with $\ell = 3$ fall into three degenerate multiplets, like for $\ell = 1$. If the degenerate masses are denoted by m_2', m_3 and m_4 we have

$$m_2' = m^{(1)}_{\Delta_{1/2}} = m^{(1)}_{N_{3/2}} = m^{(1)}_{\Delta_{3/2}} = m^{(1)}_{N_{5/2}} = m^{(1)}_{\Delta_{5/2}} = m^{(1)}_{\Delta_{7/2}}, \tag{3}$$

$$m_3 = m^{(2)}_{\Delta_{3/2}} = m^{(2)}_{N_{5/2}} = m^{(2)}_{\Delta_{5/2}} = m^{(1)}_{N_{7/2}} = m^{(2)}_{\Delta_{7/2}} = m^{(1)}_{\Delta_{9/2}}, \tag{4}$$

$$m_4 = m^{(3)}_{\Delta_{5/2}} = m^{(2)}_{N_{7/2}} = m^{(3)}_{\Delta_{7/2}} = m^{(1)}_{N_{9/2}} = m^{(2)}_{\Delta_{9/2}} = m^{(1)}_{\Delta_{11/2}}, \tag{5}$$

where

$$m_2' = c_1 N_c - 2c_2 - \frac{3}{4}c_3, \tag{6}$$

$$m_3 = c_1 N_c - \frac{1}{2}c_2 + \frac{15}{16}c_3, \tag{7}$$

$$m_4 = c_1 N_c + \frac{3}{2}c_2 - \frac{5}{16}c_3. \tag{8}$$

The notation m_2' is used to distinguish this eigenvalue from m_2 of Ref. [19].

In the following subsection we shall see that the scattering picture gives an identical pattern of degeneracy in the quantum numbers, but the resonance mass is not quantitatively defined. Therefore only a qualitative compatibility can be established.

2.2 The meson-nucleon scattering picture

Here we are concerned with nonstrange baryons, as above, and look for a degeneracy pattern in the resonance picture. The starting point in this analysis are the linear relations of the S matrices $S^{\pi}_{LL'RR'IJ}$ and S^{η}_{LRJ} of π and η scattering off a ground state baryon in terms of K-amplitudes. They are given by the following equations [19,21]

$$S^{\pi}_{LL'RR'IJ} = \sum_K (-1)^{R'-R}\sqrt{(2R+1)(2R'+1)}(2K+1)\begin{Bmatrix} K & I & J \\ R' & L' & 1 \end{Bmatrix}\begin{Bmatrix} K & I & J \\ R & L & 1 \end{Bmatrix} s^{\pi}_{KLL'}, \tag{9}$$

and

$$S^{\eta}_{LRJ} = \sum_K \delta_{KL}\delta(LRJ)s^{\eta}_K, \tag{10}$$

where $s^{\pi}_{KL'L}$ and s^{η}_K are the reduced amplitudes. The notation is as follows. For π scattering R and R′ are the spin of the incoming and outgoing baryons respectively (R =1/2 for N and R = 3/2 for Δ), L and L′ are the partial wave angular momentum of the incident and final π respectively (the orbital angular momentum L of η remains unchanged), I and J represent the total isospin and total angular momentum associated to a given resonance and K is the magnitude of the *grand spin* $\mathbf{K} = \mathbf{I} + \mathbf{J}$. The 6j coefficients imply four triangle rules $\delta(LRJ)$, $\delta(R1I)$, $\delta(L1K)$ and $\delta(IJK)$.

These equations were first derived in the context of the chiral soliton model [23,24] where the mean-field breaks the rotational and isospin symmetries, so that J and I are not conserved but the *grand spin* K is conserved and excitations can be labelled by K. These relations are exact in large N_c QCD and are independent of any model assumption.

The meaning of Eq. (9) is that there are more amplitudes $S^{\pi}_{LL'RR'IJ}$ than there are $s^{\pi}_{KLL'}$ amplitudes. The reason is that the IJ as well as the RR' dependence is contained only in the geometrical factor containing the two 6j coefficients. Then, for example, in the πN scattering, in order for a resonance to occur in one channel there must be a resonance in at least one of the contributing amplitudes $s^{\pi}_{KLL'}$. But as $s^{\pi}_{KLL'}$ contributes in more than one channel, all these channels resonate at the same energy and this implies degeneracy in the excited spectrum. From the chiral soliton model there is no reason to suspect degeneracy between different K sectors.

From the meson-baryon scattering relations (9) and (10) three sets of degenerate states have been found for $\ell = 1$ orbital excitations [19]. There is a clear correspondence between these sets and the three towers of states [19, 20] of the excited quark picture provided by the symmetric core + excited quark scheme [9]. They correspond to $K = 0, 1$ and 2 in the resonance picture. But the resonance picture also provides a $K = 3$ due to the amplitude s^{π}_{322}. As this is different from the other $s^{\pi}_{KL'L}$, in Ref. [19] it was interpreted as belonging to the $N = 3$ band.

Here we extend the work of Ref. [19, 21] to $\ell = 3$ excited states which belong to the $N = 3$ band. The partial wave amplitudes of interest and their expansion in terms of K-amplitudes from Eqs. (9) and (10) can be found in Tables I-III of Ref. [16]. They correspond to $L = L' = 2$, $L = L' = 4$ and $L = L' = 6$ respectively. From those tables one can infer the following degenerate towers of states with their contributing amplitudes

$$\Delta_{1/2},\quad N_{3/2},\quad \Delta_{3/2},\quad N_{5/2},\quad \Delta_{5/2},\quad \Delta_{7/2},\qquad (s^{\pi}_{222}, s^{\eta}_{2}), \tag{11}$$

$$\Delta_{3/2},\quad N_{5/2},\quad \Delta_{5/2},\quad N_{7/2},\quad \Delta_{7/2},\quad \Delta_{9/2},\quad (s^{\pi}_{322}, s^{\pi}_{344}), \tag{12}$$

$$\Delta_{5/2},\quad N_{7/2},\quad \Delta_{7/2},\quad N_{9/2},\quad \Delta_{9/2},\quad \Delta_{11/2},\quad (s^{\pi}_{444}, s^{\eta}_{4}), \tag{13}$$

$$\Delta_{7/2},\quad N_{9/2},\quad \Delta_{9/2},\quad \Delta_{11/2},\quad (s^{\pi}_{544}, s^{\pi}_{566}), \tag{14}$$

$$\Delta_{9/2},\quad \Delta_{11/2},\quad (s^{\pi}_{666}, s^{\eta}_{6}) \tag{15}$$

associated to $K = 2, 3, 4, 5$ and 6 respectively.

We can compare the towers (11)-(15) with the quark-shell model results of (3)-(5). The first observation is that the agreement of (11) ($K = 2$) with (3), of (12) ($K = 3$) with (4) and of (13) ($K = 4$) with (5) is perfect regarding the quantum numbers. Second, we note that the resonance picture can have poles with $K = 5, 6$ which infer the towers (14) and (15). They have no counterpart in the quark-shell picture for $\ell = 3$. But there is no problem because the poles with $K = 5, 6$ can belong to a higher band, namely $N = 5$ ($\ell = 5$) without spoiling the compatibility.

Comparing these results with those of Ref. [21] one can conclude that one can associate a common $K = 2$ to $\ell = 1$ and $\ell = 3$. For this value of K the triangular rule $\delta(K\ell 1)$ proposed in Ref [21] is satisfied. The quark-shell picture brings however more information than the resonance picture due to the fact that it implies an

energy dependence via the ℓ dependence which measures the orbital excitation. Note that m_2' is different from m_2 of $\ell = 1$ [19, 20]. Because in the resonance picture they stem from the same amplitude s^{π}_{222}, one expects that this amplitude possesses two poles at two distinct energies, in order to have compatibility. Thus the number of poles of the reduced amplitudes s^{π}_{KLL} remains an open question.

We anticipate that a similar situation will appear for every value of K associated to two distinct values of ℓ, satisfying the $\delta(K\ell 1)$ rule, for example, for $K = 4$ which is common to $\ell = 3$ and $\ell = 5$.

3 Conclusions

We have compared two alternative pictures for baryon resonances consistent with large the N_c QCD limit and found that the two pictures are compatible for $\ell = 3$ excited states, as it was the case for $\ell = 1$. The quark-shell picture is practical and successful in describing known resonances and in predicting other members of the excited octets and decuplets. But the extended symmetry $SU(2N_f) \times O(3)$ where O(3), which is essential to include orbital excitations, does not have a direct link to large N_c. On the other hand the scattering picture is close to experimental analysis but it is not clear where the pole positions should lie. It is however very encouraging that the two pictures give sets of degenerate states with identical quantum numbers when one works at order $\mathcal{O}(N_c^0)$. It is a qualitative proof that the spin-flavor picture is valid and useful for baryon phenomenology.

References

1. G. 't Hooft, Nucl. Phys. **72** (1974) 461.
2. E. Witten, Nucl. Phys. **B160** (1979) 57.
3. J. L. Gervais and B. Sakita, Phys. Rev. Lett. **52** (1984) 87; Phys. Rev. **D30** (1984) 1795.
4. R. Dashen and A. V. Manohar, Phys. Lett. **B315** (1993) 425; ibid **B315** (1993) 438.
5. R. F. Dashen, E. Jenkins and A. V. Manohar, Phys. Rev. **D51** (1995) 3697.
6. E. Jenkins, Ann. Rev. Nucl. Part. Sci. **48** (1998) 81; AIP Conference Proceedings, Vol. 623 (2002) 36, arXiv:hep-ph/0111338; PoS E **FT09** (2009) 044 [arXiv:0905.1061 [hep-ph]].
7. D. Pirjol and T. M. Yan, Phys. Rev. D **57** (1998) 1449.
8. J. L. Goity, Phys. Lett. **B414** (1997) 140.
9. C. E. Carlson, C. D. Carone, J. L. Goity and R. F. Lebed, Phys. Rev. **D59** (1999) 114008.
10. J. L. Goity, C. Schat and N. N. Scoccola, Phys. Lett. **B564** (2003) 83.
11. N. Matagne and F. Stancu, Phys. Rev. **D71** (2005) 014010.
12. N. Matagne and F. Stancu, Phys. Lett. **B631** (2005) 7.
13. C. Semay, F. Buisseret, N. Matagne and F. Stancu, Phys. Rev. D **75** (2007) 096001.
14. F. Buisseret, C. Semay, F. Stancu and N. Matagne, Proceedings of the Mini-workshop Bled 2008, Few Quark States and the Continuum", Bled Workshops in Physics, vol. 9, no. 1, eds. B. Golli, M. Rosina and S. Sirca. arXiv:0810.2905 [hep-ph].
15. N. Matagne and F. Stancu, Nucl. Phys. A **811** (2008) 291.
16. N. Matagne and F. Stancu, Phys. Rev. **D84** (2011) 056013.
17. C. L. Schat, J. L. Goity and N. N. Scoccola, Phys. Rev. Lett. **88** (2002) 102002; J. L. Goity, C. L. Schat and N. N. Scoccola, Phys. Rev. **D66** (2002) 114014.

18. N. Matagne and F. Stancu, Phys. Rev. **D74** (2006) 034014; Nucl. Phys. Proc. Suppl. **174** (2007) 155.
19. T. D. Cohen and R. F. Lebed, Phys. Rev. Lett. **91**, 012001 (2003); Phys. Rev. **D67** (2003) 096008.
20. D. Pirjol and C. Schat, Phys. Rev. **D67** (2003) 096009.
21. T. D. Cohen and R. F. Lebed, Phys. Rev. **D68** (2003) 056003.
22. F. Stancu, "Group theory in subnuclear physics," Oxford Stud. Nucl. Phys. **19** (1996) 1.
23. A. Hayashi, G. Eckart, G. Holzwart and H. Walliser, Phys. Lett. **147B** (1984) 5.
24. M. P. Mattis and M. E. Peskin, Phys. Rev. **D32** (1985) 58; M. P. Mattis, Phys. Rev. Lett. **56** (1986) 1103; Phys. Rev. **D39** (1989) 994; Phys. Rev. Lett. **63** (1989) 1455; M. P. Mattis and M. Mukerjee, Phys. Rev. Lett. **61** (1988) 1344.

Bled Workshops
in Physics
Vol. 12, No. 1
p. 64

Proceedings of the Mini-Workshop
Understanding hadronic spectra
Bled, Slovenia, July 3 - 10, 2011

News from Belle

M. Bračko*

University of Maribor, Smetanova ulica 17, SI-2000 Maribor, Slovenia
and J. Stefan Institute, Jamova cesta 39, SI-1000 Ljubljana, Slovenia

Abstract. This paper reports on some of the latest spectroscopic measurements performed with the experimental data collected by the Belle spectrometer, which has been operating at the KEKB asymmetric-energy e^+e^- collider in the KEK laboratory in Tsukuba, Japan.

1 Introduction

The Belle detector [1] at the asymmetric-energy e^+e^- collider KEKB [2] has accumulated about 1 ab^{-1} of data by the end of its operation in June 2010. The KEKB collider, called a *B-factory*, most of the time operated near the $\Upsilon(4S)$ resonance, while at the end of its operation it was running mainly at the $\Upsilon(5S)$ resonance. Large amount of collected experimental data and excellent detector performance enabled many interesting spectroscopic results, including discoveries of new hadronic states and studies of their properties. This report covers most recent and interesting spectroscopic measurements—performed with either charmonium(-like) and bottomonium(-like) states.

2 Charmonium and Charmonium-like States

2.1 η_c and $\eta_c(2S)$ in B meson decays

There has been a renewed interest in charmonium spectroscopy since 2002. The attention to this field was drawn by the discovery of the two missing $c\bar{c}$ states below the open-charm threshold, $\eta_c(2S)$ and $h_c(1P)$ [3,4] with $J^{PC}=0^{-+}$ and 1^{+-}, respectively.

Still, many questions about the lightest charmonium states have been unanswered. For example, the width of the $\eta_c(1S)$ has been determined with large discrepancies between experiments with different production mechanisms: in J/ψ and $\psi(2S)$ radiative decays $\Gamma_{\eta_c} \simeq 15$ MeV, while in B meson decays or $\gamma\gamma \to \eta_c$ processes, $\Gamma_{\eta_c} \simeq 30$ MeV [5]. In a recent Belle analysis [6] a data sample of 535 million of $B\overline{B}$ pairs is used for the study of $B^+ \to K^+\eta_c(\to K_S K^\pm\pi^\mp)$ decays[1]. The mass and the width of the η_c were determined by a 2-dimensional fit of the invariant mass

* Representing the Belle Collaboration.
[1] In this review, the inclusion of charge-conjugated states is always implied.

Γ_{η_c} [MeV]	Production Mechanism	Measured by
$35.1\pm3.1^{+1.0}_{-1.6}$	B decays	Belle [6]
$30.5\pm1.0\pm0.9$	$\psi' \to \gamma\eta_c$	BESIII [7]
$28.1\pm3.2\pm2.2$	$\gamma\gamma \to \eta_c$	Belle [8]
$31.7\pm1.2\pm0.8$	$\gamma\gamma \to \eta_c$	BABAR [9]
$36.3^{+3.7}_{-3.6}\pm4.4$	B decays	BABAR [10]

Table 1. Recent measurements of the η_c width.

$M_{inv}(K_S K\pi)$ vs. the angle between K_S and K^+ from B^+ in the η_c centre-of-mass system. Since η_c is a pseudoscalar meson, the angular distribution should be flat, but significant P- and D-wave components from non-resonant charmless B background decays are also observed. By including the above angle into the fit, the interference with the background seems to be correctly taken into account, and as a result the measured η_c width, listed in Table 1, is found to be consistent with other recent measurement. The η_c mass is determined to be $(2985.4\pm1.5^{+0.2}_{-2.0})$ MeV.

The same study [6] is performed also for the $\eta_c(2S)$ meson. For this first radially excited 0^{-+} $c\overline{c}$ state the width measurement is important, because the potential model predictions are less reliable due to the vicinity of the $D^0\overline{D}^0$ threshold. The analysis shows, that here the interference with the non-resonant background is even larger as in the case of the η_c. The measured width is $\Gamma_{\eta_c(2S)}=(6.6^{+8.4}_{-5.1}{}^{+2.6}_{-0.9})$ MeV for the fit with interference and $(41.1\pm12.0^{+6.4}_{-10.9})$ MeV, when the interference is not taken into account, *i.e.* for the fit of the invariant mass only. The factor 5 smaller width of the $\eta_c(2S)$ when compared to the η_c can be explained only by the wave function differences, since both states decay hadronically via two gluons. With the new measurement, the error on the world average of the $\eta_c(2S)$ width is decreased for almost a factor of 2.

2.2 The $X(3872)$ news

The story about new charmonium-like states (so called "XYZ" states) began in 2003, when Belle reported on $B^+ \to K^+J/\psi\pi^+\pi^-$ analysis, where a new state decaying to $J/\psi\pi^+\pi^-$ was discovered [11]. The new state, called $X(3872)$, was soon confirmed and also intensively studied by the CDF, DØ and *BABAR* collaborations [12–20]. So far it has been established that this narrow state ($\Gamma = (3.0^{+1.9}_{-1.4} \pm 0.9)$ MeV) has a mass of (3872.2 ± 0.8) MeV, which is very close to the $D^0\overline{D}^{*0}$ threshold [5]. The intensive studies of several $X(3872)$ production and decay modes suggest two possible J^{PC} assignments, 1^{++} and 2^{-+}, and establish the $X(3872)$ as a candidate for a loosely bound $D^0\overline{D}^{*0}$ molecular state. However, results provided substantial evidence that the $X(3872)$ state must contain a significant $c\overline{c}$ component as well.

Recently, Belle performed a study of $B \to (c\overline{c}\gamma)K$ using the final data sample with 772 million of $B\overline{B}$ pairs collected at the $\Upsilon(4S)$ resonance [21]. Pure $D^0\overline{D}^{*0}$

Experiment [Reference]	Measured X(3872) mass [MeV]
CDF [24]	3871.61±0.16±0.19
BaBar (B^+) [25]	3871.4±0.6±0.1
BaBar (B^0) [25]	3868.7±1.5±0.4
DØ [12]	3871.8±3.1±3.0
Belle [23]	3871.84±0.27±0.19
LHCb [26]	3871.96±0.46±0.10
Updated World Average	3871.67±0.17

Table 2. Measurements of the X(3872) mass. First error is due to limited statistics, while the second corresponds to systematic uncertainties.

molecular model [22] predicts $\mathcal{B}(X(3872) \to \psi'\gamma)$ to be less than $\mathcal{B}(X(3872) \to J/\psi\gamma)$. Results by the *BABAR* collaboration [20] show that $\mathcal{B}(X(3872) \to \psi'\gamma)$ is almost three times that of $\mathcal{B}(X(3872) \to J/\psi\gamma)$, which is inconsistent with the pure molecular model, and can be interpreted as a large $c\overline{c} - D^0\overline{D}^{*0}$ admixture. We observe $X(3872) \to J/\psi\gamma$ together with an evidence for $\chi_{c2} \to J/\psi\gamma$ in $B^\pm \to J/\psi\,\gamma K^\pm$ decays, while in our search for $X(3872) \to \psi'\gamma$ no significant signal is found. We also observe $B \to \chi_{c1}K$ decays in both, charged as well as neutral B decays. The obtained results suggest that the $c\overline{c}$-$D^0\overline{D}^{*0}$ admixture in $X(3872)$ may not be as large as discussed above.

New results for the $X(3872) \to J/\psi\pi^+\pi^-$ decay modes in $B^+ \to K^+X(3872)$ and $B^0 \to K^0$ $(\to \pi^+\pi^-)X(3872)$ decays are obtained with the complete Belle data set of 772 million $B\overline{B}$ pairs collected at the $\Upsilon(4S)$ resonance [23]. The results for the $X(3872)$ mass and width are obtained by a 3-dimensional fit to distributions of the three variables: beam-constrained-mass $M_{bc} = \sqrt{(E^{cms}_{beam})^2 - (p^{cms}_B)^2}$ (with the beam energy E^{cms}_{beam} and the B-meson momentum p^{cms}_B both measured in the centre-of-mass system), the invariant mass $M_{inv}(J/\psi\pi^+\pi^-)$ and the energy difference $\Delta E = E^{cms}_B - E^{cms}_{beam}$ (where E^{cms}_B is the B-meson energy in the centre-of-mass system). As a first step, the fit is performed for the reference channel $\psi' \to J/\psi\pi^+\pi^-$, and the resolution parameters are then fixed for the fit of the X(3872). The mass, determined by the fit, is listed in Table 2 in comparison to other precise measurements. Including the new Belle result, the updated world-average mass of the X(3872) is m_X=(3871.67±0.17) MeV. If the X(3872) is an S-wave $D^{*0}\overline{D}^0$ molecular state, the binding energy E_b would be given by the mass difference $m(X) - m(D^{*0})$-$-m(D^0)$. With the current value of $m(D^0)+m(D^{*0})$=(3871.79 ± 0.30) MeV [5], a binding energy of E_b=(−0.12±0.35) MeV can be calculated, which is surprisingly small and would indicate a very large radius of the molecular state.

The best upper limit for the $X(3872)$ width was 2.3 MeV (with 90% C.L.), obtained by previous Belle measurement [11]. The 3-dimensional fits are more sensitive to the natural width, which is smaller than the detector resolution ($\sigma \sim$4 MeV). Due to the fit sensitivity and the calibration performed on the reference channel

$\psi' \to J/\psi\pi^+\pi^-$, the updated upper limit for the $X(3872)$ width is about 1/2 of the previous value: $\Gamma(X(3872)) < 1.2$ MeV at 90% C.L.

Previous studies performed by several experiments suggested two possible J^{PC} assignments for the $X(3872)$, 1^{++} and 2^{-+}. In the recent Belle analysis [21], the $X(3872)$ quantum numbers were also studied with the full available data sample collected at the $\Upsilon(4S)$ resonance. Although at the current level of statistical sensitivity it is not possible to distinguish completely between the two possible quantum number assignments, the study shows that quantum numbers $J^{PC}=1^{++}$ seem to be slightly preferable for the $X(3872)$ state.

3 Bottomonium and Bottomonium-like States

An interesting question is whether in the $b\overline{b}$ systems there exist analogous "XYZ" states, predicted by many of the models proposed to explain the charmonium-like exotic states. Also, even for regular bottomonium states there are a lot of unanswered questions. Some of the answers are expected to be given by analyses of the Belle data sample of 121 fb^{-1}, collected at the energy of the $\Upsilon(5S)$ resonance.

The Belle collaboration used a data sample at the CM energy around the $\Upsilon(5S)$ mass 10.89 GeV, and found large signals for decays into $\pi^+\pi^-\Upsilon(1S)$, $\pi^+\pi^-\Upsilon(2S)$ and $\pi^+\pi^-\Upsilon(3S)$ final states [33]. If these transitions are only from the $\Upsilon(5S)$ resonance, then the corresponding partial widths are between 0.5 and 0.9 MeV. These values are more than two orders of magnitude larger than the corresponding partial widths for $\Upsilon(4S)$, $\Upsilon(3S)$ and $\Upsilon(2S)$ decays to $\pi^+\pi^-\Upsilon(1S)$. Recent CLEO-c results for the process $e^+e^- \to h_c(1P)\pi^+\pi^-$ showed that its rate is comparable to the process $e^+e^- \to J/\psi\pi^+\pi^-$ at $\sqrt{s} = 4170$ MeV and found an indication of even higher transition rate at the $Y(4260)$ energy [34]. Analogously, these results imply that the $h_b(mP)$ production might be enhanced in the region of the Y_b and motivate a search for the $h_b(mP)$ in the $\Upsilon(5S)$ data. $h_b(1P)$ and $h_b(2P)$ states are observed in the missing mass spectrum of $\pi^+\pi^-$ pairs for the $\Upsilon(5S)$ decays, with significances of 5.5σ and 11.2σ, respectively [35]. This is the first observation of the $h_b(1P)$ and $h_b(2P)$ spin-singlet bottomonium states in the reaction $e^+e^- \to h_b(mP)\pi^+\pi^-$ at the $\Upsilon(5S)$ energy.

Comparable rates of $h_b(1P)$ and $h_b(2P)$ production indicate a possible exotic process that violates heavy quark spin-flip and this motivates a further study of the resonant structure in $\Upsilon(5S) \to h_b(mP)\pi^+\pi^-$ and $\Upsilon(5S) \to \Upsilon(nS)\pi^+\pi^-$ decays [36]. Due to the limited statistics, only the study of $M(h_b(mP)\pi)$ distribution is possible for $h_b(mP)\pi^+\pi^-$, while in the case of $\Upsilon(nS)\pi^+\pi^-$ decay modes the Dalitz plot analysis can be performed. As a result, two charged bottomonium-like resonances, $Z_b(10610)$ and $Z_b(10650)$, are observed with signals in five different decay channels, $\Upsilon(nS)\pi^\pm$ $(n = 1, 2, 3)$ and $h_b(mP)\pi^\pm$ $(m = 1, 2)$. The averaged values for the mass and widths of the two states are calculated to be: $M(Z_b(10610)) = (10608.4 \pm 2.0)$ MeV, $\Gamma(Z_b(10610)) = (15.6 \pm 2.5)$ MeV and $M(Z_b(10650)) = (10653.2 \pm 1.5)$ MeV, $\Gamma(Z_b(10650)) = (14.4 \pm 3.2)$ MeV. The measured masses are only a few MeV above the thresholds for the open beauty channels $B^*\overline{B}$ (10604.6 MeV) and $B^*\overline{B}^*$ (10650.2 MeV), which could indicate a molecular nature of the two observed states. Angular analysis of charged pion

distributions favors the $J^P = 1^+$ spin-parity assignment for both $Z_b(10610)$ and $Z_b(10650)$.

4 Summary and Conclusions

The Belle experiment at the KEKB collider provides an excellent environment for charm and charmonium spectroscopy. As a result, many new particles have already been discovered during the Belle operation, and some of them are mentioned in this report. Some recent Belle results also indicate that analogs to exotic charmonium-like states can be found in $b\overline{b}$ systems. As the operation of the experiment has just finished in June 2010, more interesting results on charmonium(-like) and bottomonium(-like) spectroscopy can still be expected from Belle in the near future.

References

1. Belle Collaboration, *Nucl. Instrum. Methods* A **479**, 117 (2002).
2. S. Kurokawa and E. Kikutani, *Nucl. Instrum. Methods* A **499**, 1 (2003), and other papers included in this Volume.
3. Belle Collaboration, *Phys. Rev. Lett.* **89**, 102001 (2002).
4. Cleo Collaboration, *Phys. Rev. Lett.* **95**, 102003 (2005).
5. K. Nakamura *et al.* (Particle Data Group), *J. Phys.* G **37**, 075021 (2010).
6. Belle Collab., arXiv:1105.0978v2 [hep-ex], to appear in *Phys. Lett.* B.
7. BESIII Collab., preliminary results, presented at XIV International Conference on Hadron Spectroscopy (Hadron2011), Munich, Germany.
8. Belle Collaboration, *Eur. Phys. J.* C **53**, 1 (2008).
9. BaBar Collaboration, *Phys. Rev.* D **81**, 052010 (2010).
10. BaBar Collaboration, *Phys. Rev.* D **78**, 012006 (2008).
11. Belle Collaboration, *Phys. Rev. Lett.* **91**, 262001 (2003).
12. CDF Collaboration, *Phys. Rev. Lett.* **93**, 072001 (2004); DØ Collaboration, *Phys. Rev. Lett.* **93**, 162002 (2004); *BABAR* Collaboration, *Phys. Rev.* D **71**, 071103 (2005).
13. Belle Collaboration, arXiv:hep-ex/0505037, arXiv:hep-ex/0505038; submitted to the Lepton-Photon 2005 Conference.
14. Belle Collaboration, *Phys. Rev. Lett.* **97**, 162002 (2006).
15. *BABAR* Collaboration, *Phys. Rev.* D **74**, 071101 (2006).
16. Belle Collaboration, arXiv:0809.1224v1 [hep-ex]; contributed to the ICHEP 2008 Conference.
17. Belle Collaboration, arXiv:0810.0358v2 [hep-ex]; contributed to the ICHEP 2008 Conference.
18. CDF Collaboration, *Phys. Rev. Lett.* **98**, 132002 (2007).
19. *BABAR* Collaboration, *Phys. Rev.* D **77**, 011102 (2008).
20. *BABAR* Collaboration, *Phys. Rev. Lett.* **102**, 132001 (2009).
21. Belle Collaboration, *Phys. Rev. Lett.* **107**, 091803 (2011).
22. E. S. Swanson, *Phys. Rep.* **429**, 243 (2006).
23. Belle Collaboration, *Phys. Rev.* D **84**, 052004(R) (2011).
24. CDF Collaboration, *Phys. Rev. Lett.* **103**, 152001 (2009).
25. *BABAR* Collaboration, *Phys. Rev.* D **77**, 111101(R) (2008).

26. LHCb Collab., Proc. XIX International Workshop on Deep-Inelastic Scattering and Related Subjects (DIS2011), LHCb-CONF-2011-021.
27. Belle Collaboration, *Phys. Rev. Lett.* **100**, 142001 (2008).
28. *BABAR* Collaboration, *Phys. Rev.* D **79**, 112001 (2009).
29. Belle Collaboration, *Phys. Rev.* D **80**, 031104 (2009).
30. Belle Collaboration, *Phys. Rev.* D **78**, 072004 (2008).
31. *BABAR* Collaboration, *Phys. Rev.* D **74**, 091103 (2006).
32. BES Collaboration, *Phys. Rev. Lett.* **100**, 102003 (2008).
33. Belle Collaboration, *Phys. Rev. Lett.* **100**, 112001 (2008); *Phys. Rev.* D **82**, 091106 (2010).
34. CLEO-c Collaboration, *Phys. Rev. Lett.* **107**, 041803 (2011).
35. Belle Collab., arXiv:1103.3419 [hep-ex], submitted to *Phys. Rev. Lett.*
36. Belle Collaboration, arXiv:1105.4583 [hep-ex].

Bled Workshops
in Physics
Vol. 12, No. 1
p. 70

Proceedings of the Mini-Workshop
Understanding hadronic spectra
Bled, Slovenia, July 3 - 10, 2011

Electroproduction of mesons in a chiral quark model

B. Golli

Faculty of Education, University of Ljubljana, 1000 Ljubljana, Slovenia and Jožef Stefan Institute, 1000 Ljubljana, Slovenia

Motivation This work is a continuation of a joint project on the description of baryon resonances performed by the Coimbra group (Manuel Fiolhais, Luis Alvarez Ruso, Pedro Alberto) and the Ljubljana group (Simon Širca and B. G.)

The pion- and photon-induced meson production on nucleons are important tools to study the hadron dynamics in the first and second resonance region. One of the main challenges is to understand the interplay of quark and meson degrees of freedom. While several models of nucleon excited states spanning from the non-relativistic models based solely the quark degrees of freedom to models involving only mesonic degrees of freedom are able to successfully describe the pion elastic and non-elastic scattering in the resonance region, electro-production of mesons represents a much more severe test which may be able to disentangle the properties originating in the (valence, constituent) quark degrees of freedom from those of the meson cloud. One of the most widely recognized example is electro-excitation of the $\Delta(1232)$ resonance where the pion cloud contributes $\sim 45\,\%$ to the magnetic dipole amplitude, and strongly dominates the electric quadrupole amplitude. Similarly, the behaviour of the pion electro-excitation amplitude in the Roper region can be explained by assuming a relatively strong contribution of the pion cloud. However, in the second resonance region, such a conclusion is less transparent because of the presence of other channels. To avoid ambiguities, we need to develop a method in which the strong and the EM processes are treated in a unified approach without too many adjustable parameters.

The method In order to study the interplay of quark and meson degrees of freedom, we have developed a method that incorporates the nucleon and its excited states calculated in different chiral quark models into a coupled channel approach involving different meson-baryon channels as well as the photon-nucleon channel. The conceptual foundations of our approach in chiral quark models date back to the paper [1], in which we demonstrated the above mentioned importance of the pion cloud in electro-production of pions in the region of the $\Delta(1232)$.

In [2] we have generalized our approach used in our previous studies of the resonances (see e.g. [1], [3], [4] and [5]). The generalized method incorporates excited baryons represented as quasi-bound quark-model states into a coupled channel framework using the K-matrix formalism. It can be applied to meson

scattering as well as to electro and weak-production of mesons. Our method assumes a class of chiral quark models in which mesons couple linearly to the quark. In such a case it is possible to write down an exact expression for the K matrix (and, consequently, for the T matrix) in terms of the principal-value states corresponding to the meson-baryon channels possessing the proper asymptotic behaviour. The construction respects the symmetry of the K matrix and hence ensures the unitarity of the S matrix.

The strong and the weak points The main *advantages* of our method can be summarized in

- Baryons are treated as composite particles from the very beginning; the strong and electro-weak form-factors are derived from baryon internal structure and not inserted a posteriori; as a consequence the method introduces a much smaller number of free parameters.
- The physical resonances appear as linear superpositions of bare resonances.
- The bare quark-meson and quark-photon vertices are modified through meson loops as well as through mixing of resonances and coupling to the background.
- The meson cloud around baryons is included in a consistent way also in the asymptotic states.
- The method yields a symmetric K matrix and hence respects the unitarity of the S matrix.

The present *limitations* of the method are primarily the absence of meson-meson interaction and the nucleon-meson four-point interaction which can be introduced only in an approximate way. This is a consequence of our assumption about the meson-quark interaction discussed above. Our method is therefore primarily intended to describe the processes in the region of resonances rather than in the energy region close to the threshold where other methods are anyway superior.

The Roper resonance In [2] and [6] we have considered the scattering and the pion electro-production in the region of the $N(1440)$ and of its $I = \frac{3}{2}$ partner, the $\Delta(1600)$. As the underlying quark model we have taken the Cloudy bag Model, primarily because of its simplicity. A good agreement with the observed scattering amplitude and the M_{1-} electro-production amplitude is found provided the $\pi\Delta$ and the σN channels of comparable strength are included in the multichannel calculation. The results strongly support the hypothesis that the pion cloud plays an important role in the case of the electro-excitation of $N^*(1440)$ resonance, especially in the region of low Q^2 (long-range effects). In this region the quark contribution is small and positive, while the pion contribution and the vertex corrections due to meson loops are large and negative. At intermediate Q^2, these two effects are responsible for the zero crossing of the amplitude. At higher Q^2 (short-range physics) the quark core takes over, rendering the amplitude positive.

The S11 resonances In recent years there have been substantial efforts to understand the peculiar nature of the lightest of the S11 resonances, the $N(1535)$, due to its position just above the ηN threshold and the large branching ratio to the ηN channel. The extension of the approach to the low-lying negative-parity resonances requires the inclusion of new channels involving the s- and d-wave pions, the η and the ρ mesons, and the $K\Lambda$ channel. In [7–9] we have used an SU(3) extension of the Cloudy Bag Model taking f_η and f_K from the meson sector, while for the other model parameters we have used the same values as in the case of the positive-parity resonances, adding only the mixing parameter between the two bare-quark states corresponding to $N(1535)$ and $N(1650)$, and their bare masses. We have obtained a good overall agreement with the available experimental results for the partial widths of the $N(1535)$ and the $N(1650)$ resonances as well as for the pion, η-meson and kaon electroproduction amplitudes. In particular, the excellent agreement with the data for η production strongly supports our conjecture about the dominance of the genuine three-quark configuration in the $N^*(1535)$ state. While the cross-section for pion-induced production of K^+ appears to be over-estimated in our model, the photo-production amplitude is smaller than predicted by phenomenological analyses. This discrepancy remains an open question and represents a challenge for further investigation.

References

1. M. Fiolhais, B. Golli, S. Širca, Phys. Lett. B **373**, 229 (1996)
2. B. Golli and S. Širca, Eur. Phys. J. A **38**, (2008) 271.
3. P. Alberto, M. Fiolhais, B. Golli, and J. Marques, Phys. Lett. B **523**, 273 (2001).
4. B. Golli, S. Sirca, L. Amoreira, M. Fiolhais Phys.Lett. B553 (2003) 51-60
5. P. Alberto, L. Amoreira, M. Fiolhais, B. Golli, and S. Širca, Eur. Phys. J. A **26**, 99 (2005).
6. B. Golli, S. Širca, and M. Fiolhais, Eur. Phys. J. A **42**, 185 (2009)
7. B. Golli, S. Širca, Eur. Phys. J. A **47** (2011) 61.
8. B. Golli, talk given at the Sixth International Workshop on Pion-Nucleon Partial-Wave Analysis and the Interpretation of Baryon Resonances, 2327 May, 2011, Washington, DC, U.S.A., `http://gwdac.phys.gwu.edu/pwa2011/Thursday/b_golli.pdf`
9. Simon Širca, Bojan Golli, Manuel Fiolhais and Pedro Alberto, in Proceedings of the XIV International Conference on Hadron Spectroscopy, 13-17 June 2011 Munich, Germany, edited by S. Paul, N. Brambilla, and B. Grube, `http://arxiv.org/abs/1109.0163`.

BLED WORKSHOPS
IN PHYSICS
VOL. 12, NO. 1
p. 73

Proceedings of the Mini-Workshop
Understanding hadronic spectra
Bled, Slovenia, July 3 - 10, 2011

Scattering phase shift and resonance properties*

S. Prelovšek[a,b], C. B. Lang[c] and D. Mohler[d]

[a] J. Stefan Institute, Jamova 39, 1000 Ljubljana, Slovenia
[b] Department of Physics, University of Ljubljana, Jadranska 19, 1000 Ljubljana, Slovenia
[c] Institut für Physik, FB Theoretische Physik, Universität Graz, A-8010 Graz Austria
[d] TRIUMF, 4004 Wesbrook Mall Vancouver, BC V6T 2A3, Canada

Abstract. We describe the method for extracting the elastic scattering phase shift from a lattice simulation at an introductory level, for non-lattice practitioners. We consider the scattering in a resonant channel, where the resulting phase shift $\delta(s)$ allows the lattice determination of the mass and the width of the resonance from a Breit-Wigner type fit. We present the method for the example of P-wave $\pi\pi$ scattering in the ρ meson channel.

1 Introduction

The determination of the strong decay width of a hadronic resonance in lattice QCD is a much more demanding task than the determination of its approximate mass. The only available method (that was applied up to now) was proposed by Lüscher [1] and is rather indirect. It applies for the case when the resonance appears in the elastic scattering of two hadrons $H_1H_2 \to R \to H_1H_2$.

- First, the energy spectrum E_n of the system of two interacting hadrons H_1H_2 enclosed in a few-fermi box has to be determined. The system is illustrated in Fig. 1. The spectrum in a finite box E_n is discrete and few (one or two) lowest energy levels have to be determined by lattice simulation.
- The shift of the energy E_n with respect to the non-interacting energy $E_{H1}(\mathbf{p_1})+E_{H2}(\mathbf{p_2})$ ($E_{Hi}(\mathbf{p_i}) = \sqrt{m_i^2 + \mathbf{p_i}^2}$) gives info on the interaction between H_1 and H_2. Lüscher derived a rigorous relation between the energy shift $E_n - E_{H1} - E_{H2}$ and the elastic phase shift $\delta(s)$ for H_1H_2 scattering in continuum [1]. The measured energies E_n can be used to extract the phase shift $\delta(s)$ evaluated at $s = E_n^2 - \mathbf{P}^2$, where E_n is the energy of the system and $\mathbf{P}$ its total momentum. In order to extract $\delta(s)$ at several different values of s, the simulations are done for several choices of total momenta $\mathbf{P}$ of the H_1H_2 system, which leads to different values of $s = E_n^2 - \mathbf{P}^2$.
- The resulting dependence of $\delta(s)$ as a function of s can be used to extract the mass m_R and the width Γ_R of the resonance R, which appears in the elastic channel $H_1H_2 \to R \to H_1H_2$. For this purpose, the $\delta(s)$ can be fitted with a Breit-Wigner form or some other phenomenologically inspired form, which depend on m_R and Γ_R.

* Talk delivered by S. Prelovšek

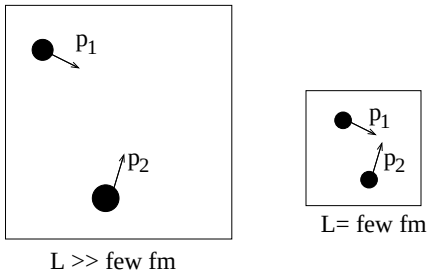

Fig. 1. The energy of two hadrons in a box of size L. On the left, $L \gg$ fm and $E(L) \simeq E_{H1}(\mathbf{p_1}) + E_{H2}(\mathbf{p_2})$. On the right, $L \simeq$ few fm and energy gets shifted due to their interaction, i.e. $E(L) \simeq E_{H1}(\mathbf{p_1}) + E_{H2}(\mathbf{p_2}) + \Delta E(L)$.

The described method, needed for the determination of the resonance width Γ_R, is rather challenging. It requires very accurate determination of a few lowest energy levels of the system H_1H_2, since the resulting phase shift depends ultimately on the energy shift. Among all the meson resonances, this method has been up to now rigorously applied only to ρ resonance. Although Lüscher proposed the method already in late 80's [1], the first lattice attempt to employ it to hadronic resonances had to wait until 2007 [2]. Since then, several studies of ρ have been carried out [3,4], with the most up to date ones [5–7].

This talk briefly describes the method to extract $\delta(s)$, m_R and Γ_R on an example of $\pi\pi$ scattering in the ρ channel. It is based on a recent simulation [6], which is the statistically most accurate determination of any strong meson width on one lattice ensemble. The purpose of this talk is to highlight the main physical reasoning, which lies behind the lattice extraction of $\delta(s)$, m_R and Γ_R, omitting most of technical details.

The sections follow the order of steps required, which are listed as items in the introduction. Section II describes the determination of spectrum E_n of the coupled system $H_1H_2 \leftrightarrow R$. The Section III described why E_n allow one to extract the elastic phase shift $\delta(s)$. The extraction of the resonance parameters m_R and Γ_R from the phase shift $\delta(s)$ is done in Section IV. We end with conclusions.

2 Spectrum of two hadrons in a finite box

The ρ meson is a resonance in $\pi\pi$ scattering in P-wave, and has quantum numbers $I^G(J^{PC}) = 1^+(1^{--})$. The total momentum $\mathbf{P}$ of the coupled $\pi\pi - \rho$ system can have values $\frac{2\pi}{N_L}\mathbf{d}$, $d \in Z^3$ due to the periodic boundary condition in the spatial direction, and we use the following three choices

$$\mathbf{P} = (0,0,0) \ , \ \tfrac{2\pi}{N_L}(0,0,1) \ , \ \tfrac{2\pi}{N_L}(1,1,0) \quad \text{and permutations} \ . \tag{1}$$

This enables us to obtain several values of $s = E_n^2 - \mathbf{P}^2$ for the system, thereby allowing the determination of $\delta(s)$ for these values of s without changing the spatial volume.

Our simulation is performed on an ensemble of 280 [8] gauge configurations with dynamical u/d quarks, where the valence and dynamical quarks employ improved Wilson-Clover action. The corresponding pion mass is $m_\pi a = 0.1673 \pm 0.0016$ or $m_\pi = 266 \pm 4$ MeV. The lattice spacing is $a = 0.1239 \pm 0.0013$ fm and we employ a rather small volume $N_L^3 \times N_T = 16^3 \times 32$, which allows us to use the costly full distillation method [9] for evaluating the quark contractions.

On the lattice, the discrete energies of the system E_n can be extracted after computing the dependence of the correlation matrix $C_{ij}(t_f, t_i)$ on Euclidean time $t_f - t_i$

$$C_{ij}(t_f, t_i) = \langle 0|\mathcal{O}_i(t_f)\, \mathcal{O}_j^\dagger(t_i)|0\rangle = \sum_n \langle \mathcal{O}_i|n\rangle\langle n|\mathcal{O}_j^\dagger\rangle\, e^{-E_n(t_f - t_i)}\,. \tag{2}$$

The analytical expression on the right is obtained by inserting the complete set $\sum_n |n\rangle\langle n|$ of physical states n with given quantum numbers. The interpolators O_i have the quantum numbers of the system in question. In our case the interpolators have quantum numbers $J^{PC} = 1^{--}$ and $|I, I_3\rangle = |1, 0\rangle$ and total three-momentum $\mathbf{P}$. They have to couple well to the $\pi\pi$ state and the quark-antiquark resonance ρ.

For each choice of $\mathbf{P}$ (1), we use 16 interpolators, listed in detail in Eq. (21) of [6]. We employ fifteen interpolators of quark-antiquark type

$$\mathcal{O}_i^{\bar{q}\,q}(t) = \sum_{\mathbf{x}}\, e^{i\mathbf{P}\mathbf{x}}\, \tfrac{1}{\sqrt{2}}[\bar{u}\mathcal{F}_i u\,(t, \mathbf{x}) \;+\; \bar{d}\mathcal{F}_i d\,(t, \mathbf{x})]\,, \tag{3}$$

where $\mathcal{F}_i$ denotes different color-spin-space structures with the same resulting quantum number $J^{PC} = 1^{--}$ and $|I, I_3\rangle = |1, 0\rangle$. We use also one $\pi(\mathbf{p_1})\pi(\mathbf{p_2})$ interpolator, where each pion is projected to a definite momentum

$$\begin{aligned} \mathcal{O}^{\pi\pi}(t) &= \tfrac{1}{\sqrt{2}}[\pi^+(\mathbf{p_1})\pi^-(\mathbf{p_2}) - \pi^-(\mathbf{p_1})\pi^+(\mathbf{p_2})]\,, \quad \mathbf{p_1} + \mathbf{p_2} = \mathbf{P}\,, \\ \pi^\pm(\mathbf{p_i}) &= \sum_{\mathbf{x}}\, e^{i\mathbf{p_i}\mathbf{x}}\, \bar{q}\gamma_5\tau^\pm q\,(t, \mathbf{x}) \end{aligned} \tag{4}$$

In practice, the $\pi\pi$ interpolator is the most important among our 16 interpolators, since it couples to the scattering state much better than the quark-antiquark interpolators. Let us note that all other lattice studies aimed at Γ_ρ used at most one quark-antiquark and one $\pi\pi$ interpolator, which may not always allow for reliable extraction of the first excited energy level E_2.

Given the 16 interpolators, we compute the 16×16 correlation matrix $C_{ij}(t_f, t_i)$ for all initial and final time-slices $t_i, t_f = 1, .., N_T = 32$. The needed Wick contractions that enter the correlation matrix with our $\bar{q}q$ and $\pi\pi$ interpolators are depicted in Fig. 2. The contributions (a,c,e) in Fig. 2 cannot be evaluated solely from the quark propagator from one point $(t_i, \mathbf{x}_i)$ to all other points of the lattice (such a propagator allowed most of the spectroscopy studies in the past). The contributions (a,c,e) require the propagators from all and to all points on the lattice, which is too costly to evaluate in practice. We use the recently proposed distillation method for this purpose [9], which enables the exact computation of the required contractions.

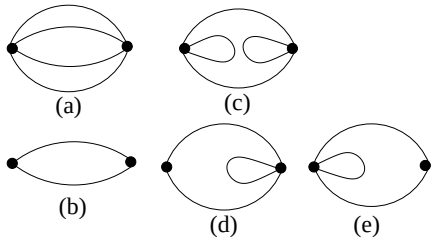

Fig. 2. Contractions for $I = 1$ correlators with $\bar{q}q$ (3) and $\pi\pi$ (4) interpolators.

P	level n	$E_n\, a$	$s\, a^2$	δ
$\frac{2\pi}{L}(0,0,0)$	1	0.5107(40)	0.2608(41)	130.56(1.37)
$\frac{2\pi}{L}(0,0,0)$	2	0.9002(101)	0.8103(182)	146.03 (6.58) [*]
$\frac{2\pi}{L}(0,0,1)$	1	0.5517(26)	0.1579(29)	3.06 (0.06)
$\frac{2\pi}{L}(0,0,1)$	2	0.6845(49)	0.3260(69)	156.41(1.56)
$\frac{2\pi}{L}(1,1,0)$	1	0.6933(33)	0.1926(49)	6.87(0.38)
$\frac{2\pi}{L}(1,1,0)$	2	0.7868(116)	0.3375(191)	164.25(3.53)

Table 1. The results for two lowest levels $n = 1, 2$ of the coupled $\pi\pi - \rho$ system with three choices of total momentum **P** on our lattice with $m_\pi a = 0.1673 \pm 0.0016$, $L = 16a$ and the lattice spacing $a = 0.1239 \pm 0.0013$ fm. The energy levels E_n are obtained by multiplying $E_n a$ with $a^{-1} \simeq 1.6$ GeV. The invariant mass squared of the system is $s = E_n^2 - \mathbf{P}^2$, but the dimensionless value in the table $s\, a^2$ is obtained using the discretized version of this relation [6].

We average the resulting correlators (i) over all initial time slices t_i at fixed time separation $t_f - t_i$, (ii) over all directions of momenta **P** (1) and (iii) over all directions of the ρ meson polarization.

The time dependence $t_f - t_i$ of the correlators $C_{ij}(t_f, t_i)$ (2) contains the information on the energies of the system E_n, and several methods for extracting E_n from C_{ij} are available. We extract two lowest energy levels $E_{n=1,2}$ of the system from the 16×16 correlation matrix $C_{ij}(t_f, t_i)$ using the so called variational method [10], which is the most established among the available methods. Table 1 displays the extracted lowest two energies $E_{n=1,2}$ of the coupled $\pi\pi - \rho$ system for our three choices of total momenta **P** (1).

The spectrum E_n in Table 1 for our finite box is the main result of this section. Each energy level corresponds to a different value of $s = E_n^2 - \mathbf{P}^2$, as calculated from E_n and **P** in the Table 1. In fact, the table lists values of s obtained from the discrete lattice version of the dispersion relation, which takes into account part of the corrections to $s = E_n^2 - \mathbf{P}^2$ due to finite lattice spacing [6].

3 Extraction of the phase shifts from energy levels

Let us consider the case when the resonance R can strongly decay only to two spinless hadrons H_1 and H_2, so one has elastic scattering of H_1 and H_2. We point out that the non-elastic case, when a resonance can decay strongly to several final states (i.e. H_1H_2 and $H_1'H_2'$), is much more challenging for a lattice study.

Suppose one encloses two hadrons $H_1(p_1)$ $H_2(p_2)$ with three-momenta p_1 and p_2 into a large box of size $L \gg$ fm and measures their energy. In a large box, they hardly interact and their energy is equal to sum of individual energies $E^{non-int} = E_{H1}(p_1)+E_{H2}(p_2)$ with $E_H(p) = \sqrt{m_H^2 + p^2}$. Now, let's force $H_1(p_1)$ and $H_2(p_2)$ to interact by decreasing the size of the box to L of a few fm. The energy of the system $E(L) = E_{H1}(p_1) + E_{H2}(p_2) + \Delta E(L)$ is shifted with respect to $E^{non-int}$: it will increase ($\Delta E(L) > 0$) if the interaction is repulsive and decrease ($\Delta E(L) < 0$) if the interaction is attractive. This simple physical reasoning indicates that the energy shift $\Delta E(L)$ gives info on the interaction.

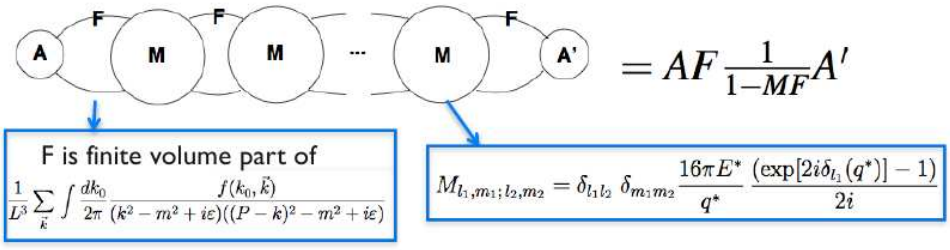

Fig. 3. The scattering of two interacting particles as series of the interaction vertex $M(\delta_L)$ and the scattering of non-interacting particles F at finite L [11].

In fact, the energy shift $\Delta E(L)$ and the energy itself $E(L)$ do not only give us "some" info on the interaction. According to the seminal analytic work of Lüscher [1], $E(L)$ or $\Delta E(L)$ rigorously tells us the value of the elastic scattering phase shift of H_1H_2 scattering at $L \to \infty$, i.e. $\delta(L = \infty)$:

$$\text{Luscher method :} \qquad E(L) \longrightarrow \delta(s, L = \infty) \qquad s = E(L)^2 - \mathbf{P}^2 \tag{5}$$

The derivation and the resulting formulae between $E(L)$ and δ are lengthy and rather complicated, but let us briefly explain at least why $E(L)$ contains info on $\delta(L = \infty)$. A nice and clear quantum-filed theory derivation is given in [11] and the main message is illustrated in Fig. 3. The scattering of two interacting spinless hadrons H_1H_2 at finite L (for degenerate case $m_{H1} = m_{H2} = m$) is represented in QFT by series of:

- scattering of two non-interacting hadrons at finite L, represented by F. The expression F contains sums over the loop momenta **k**, which are allowed in a finite box L with periodic boundary conditions in space. Here $f(k_0, \mathbf{k})$ stands for dependence of the vertices on the left and right on k_0 and **k**.

- the interaction vertex M with four hadron legs. This vertex depends on the elastic phase shift δ_l (at infinite volume) for the case of elastic scattering in the l-th partial wave.

The physical scattering requires resummation of the bubbles in Fig. 3, with non-interacting parts F and the interacting parts M, giving $AF\frac{1}{1-MF}A'$. The positions of the poles of the sum $AF\frac{1}{1-MF}A'$ obviously depend on M and therefore on δ_l. The positions of the poles dictate the possible energy levels of the system $E_n(L)$, so the energy levels $E_n(L)$ depend on M and therefore on δ_l.

The purpose of the above illustration was just to indicate why $E_n(L)$ depend on δ_l. In the case of $\pi\pi$ with $J^P = 1^-$, the relevant wave has $l = 1$ and we denote the corresponding phase by $\delta \equiv \delta_1$. The complete analytic relations between $E_n(L)$ and $\delta(s)$ needed for our case of the $\pi\pi$ scattering with $J^{PC} = 1^{--}$ and $I = 1$ are provided in [6] (for every $|\mathbf{P}|$ a different form of relation applies). These allow to extract δ for each of our six energy levels in Table 1 and the resulting phase shifts are given in the same Table.

The presented Lüscher formalism applies only for the case of elastic scattering. The $\pi\pi$ state is the only scattering state in this channel for energies when 4π state cannot be created, i.e., when $s = E_n^2 < (4m_\pi)^2$. For our $m_\pi a = 0.1673$ this is valid for all six levels, with the exception of the level E_1 at $\mathbf{P} = 0$, which is above 4π inelastic threshold. As the Lüscher analysis is not valid above the inelastic threshold, we omit this level from further analysis.

The resulting scattering phase shifts for five values of s are shown in Fig. 4. This is the main result of the lattice study; the resonance properties will be obtained by fitting $\delta(s)$ in the next section.

Note that the resulting phases are determined with a relatively good precision, which is better than in other available lattice studies of ρ at comparable u/d quark masses. The good precision can be traced back to various advanced techniques we used: the distillation method for evaluating contractions, usage of a large interpolator basis and average over all initial time slices, directions of momenta $\mathbf{P}$ and polarizations of ρ.

4 Extracting resonance mass and width from the phase shift

The phase shift $\delta(s)$ in Fig. 4, obtained directly from the lattice study, can be used to extract the properties of the resonance, in our case the ρ. The phase shift has a typical resonance shape: it passes from $\delta \simeq 0^\circ$ to $\delta \simeq 180^\circ$: the point where it crosses 90° gives the position of the resonance ($s = m_\rho^2$), while the steepness of the rise gives its width Γ_ρ. In particular, δ is related to resonance parameters by expressing the scattering amplitude a_l in terms of δ on one hand, and with Breit-Wigner form in the vicinity of the resonance on the other hand

$$a_1 = \frac{-\sqrt{s}\,\Gamma(s)}{s - m_\rho^2 + i\sqrt{s}\,\Gamma(s)} = \frac{e^{2i\delta(s)} - 1}{2i} \,. \tag{6}$$

Relation (6) can be conveniently re-written as

$$\sqrt{s}\,\Gamma(s)\,\cot\delta(s) = m_\rho^2 - s \,. \tag{7}$$

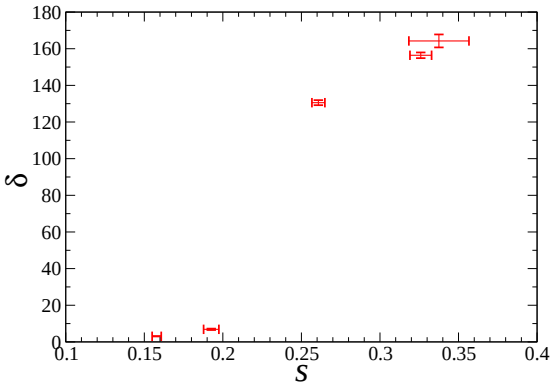

Fig. 4. The $\pi\pi$ phase shift $\delta(s)$ (in degrees) for five different values of dimensionless $sa^2 = (E_n a)^2 - (\mathbf{P}a)^2$, extracted from our lattice study [6]. The s is obtained by multiplying sa^2 with $(a^{-1})^2 \simeq (1.6\ GeV)^2$.

	lattice (this work [6]) $m_\pi \simeq 266$ MeV	exp [PDG]
m_ρ	792 ± 12 MeV	775 MeV
$g_{\rho\pi\pi}$	5.13 ± 0.20	5.97

Table 2. Our lattice results for the resonance parameters [6], compared to the experimental values.

The decay width significantly depends on the phase space and therefore on m_π, so the decay width extracted at $m_\pi \simeq 266$ MeV could not be directly compared to the measured width. So, it is customary to extract the $\rho \to \pi\pi$ coupling $g_{\rho\pi\pi}$ instead of the width, where the width

$$\Gamma(s) = \frac{p^{*3}}{s}\frac{g^2_{\rho\pi\pi}}{6\pi}\,, \qquad \Gamma_\rho = \Gamma(m^2_\rho) \tag{8}$$

depends on the phase space for a P-wave decay and the coupling $g_{\rho\pi\pi}$. The coupling is expected to be only mildly dependent on m_π, which was explicitly confirmed in the lattice studies [5,7] and analytic study [12]. In (8), p^* denotes the pion momentum in the center-of-momentum frame and we extract it from s using a discretized version of relation $\sqrt{s} = 2\sqrt{m_\pi^2 + p^{*2}}$ [6]. Inserting $\Gamma(s)$ (8) into (7), one obtains an expression for $\delta(s)$ in terms of two unknown parameters: m_ρ and $g_{\rho\pi\pi}$. We fit these two parameters using five values of $\delta(s)$ given in Fig. 4 and Table 1, and we get the values of resonance parameters in Table 2 with small statistical errors.

The resulting ρ-meson mass in Table 2 is slightly higher than in experiment, as expected due to $m_\pi = 266\ MeV > m_\pi^{exp}$. The coupling $g_{\rho\pi\pi}$ is rather close to the value $g^{exp}_{\rho\pi\pi}$ derived from the experimental width Γ^{exp}_ρ.

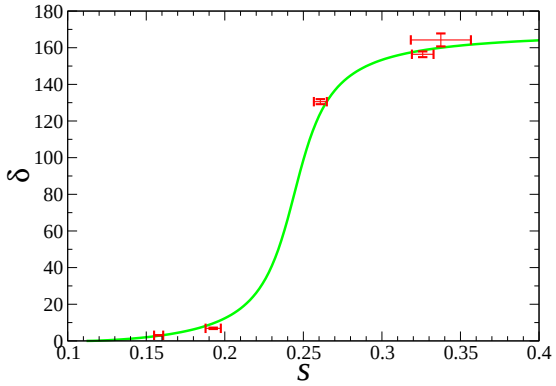

Fig. 5. The crosses are the $\pi\pi$ phase shift $\delta(s)$ (in degrees) for five different values of dimensionless $sa^2 = (E_n a)^2 - (\mathbf{P}a)^2$, extracted from our lattice study [6]. The line is the Breit-Wigner fit (7,8) for the resulting m_ρ and $g_{\rho\pi\pi}$ in Table 2. The physical value of s is obtained by multiplying sa^2 with $(a^{-1})^2 \simeq (1.6\ GeV)^2$.

5 Comparison to other lattice and analytical studies

The comparison of our results for m_ρ and Γ_ρ to two recent lattice studies [5,7] is compiled in Fig. 8 of [7]. Our result has the smallest error on a given ensemble, demonstrating that accurate lattice determination m_R and Γ_R for (some) resonances is possible now. The other two lattice studies are done for two [7] and four [5] pion masses and explicitly demonstrate mild dependence of $g_{\rho\pi\pi}$ on m_π. The discussion concerning the (dis)agreement of the three lattice studies is given in [7] and will be extended in [13].

The comparison of our $\delta(s)$ to the prediction of the lowest non-trivial order of unitarized Chiral Perturbation Theory [14] is given by the solid line in 6, which has been recalculated for our $m_\pi = 266$ MeV in [15]. The lowest[1] order prediction does not depend on unknown LECs and agrees reasonably well with our lattice result, given by the bullets.

6 Conclusions

We highlighted the main physical reasoning, which lies behind the lattice extraction of elastic phase shifts $\delta(s)$ and the resonance parameters m_R and Γ_R. The purpose was to present the general principle of the method and omit the technical details. The method was presented on the example of $\pi\pi \to \rho \to \pi\pi$ scattering. This example demonstrates that a proper first-principle treatment of some hadronic resonances on the lattice is now possible.

[1] One cannot make a fair comparison between out lattice result and the next-to-lowest order prediction, since it depends on a number of LECs, and some of them have been fixed using m_ρ from another lattice study, which gets a significantly higher m_ρ.

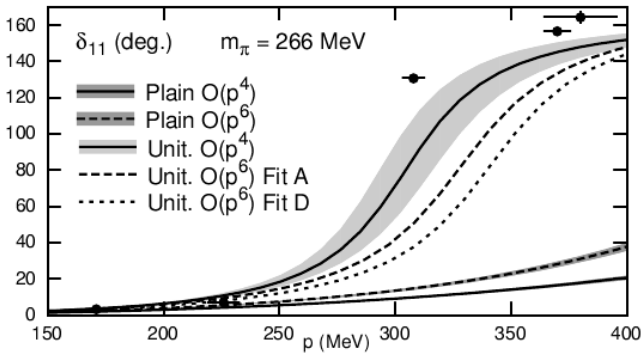

Fig. 6. The $\pi\pi$ phase shift in the ρ channel $\delta_{11}(p) \equiv \delta(p^*)$ at $m_\pi = 266$ MeV: the solid line (indicated by "Unit $O(p^4)$") gives prediction of the lowest order of Unitarized Chiral Perturbation Theory [14, 15], while bullets are our lattice data.

Acknowledgments We would like to kindly thank Anna Hasenfratz for providing the gauge configurations used for this work. We would like to thank Xu Feng, Naruhito Ishizuka, Jose Pelaez, Gerrit Schierholz and Richard Woloshyn for valuable discussions. The calculations have been performed on the theory cluster at TRIUMF and on local clusters at the University of Graz and Ljubljana. We thank these institutions for providing support. This work is supported by the Slovenian Research Agency, by the European RTN network FLAVIAnet (contract number MRTN-CT-035482) and by the Natural Sciences and Engineering Research Council of Canada (NSERC).

References

1. M. Lüscher, Commun. Math. Phys. 105 (1986) 153; Nucl. Phys. B 354 (1991) 531; Nucl. Phys. B 364 (1991) 237.
2. S. Aoki *et al.*, CP-PACS coll., Phys. Rev. D 76 (2007) 094506.
3. M. Göckeler *et al.*, QCDSF coll., PoS LAT (2008) 136, arXiv:0810.5337.
4. J. Firson *et al.*, BMW coll., arXiv:1011.3413.
5. X. Feng, K. Jansen and D.B. Renner, Phys. Rev. D (2011) 094505.
6. C.B. Lang, D. Mohler, S. Prelovsek and M. Vidmar, Phys. Rev. D 84 (2011) 054503, arXiv:1105.5636.
7. S. Aoki *et al.*, PACS-CS coll., arXiv:1106.5365.
8. A. Hasenfratz *et al.*, Phys. Rev. D 78 (2008) 054511, Phys. Rev. D78 (2008) 014515.
9. M. Peardon *et al.*, Phys. Rev. D 80 (2009) 054506, arXiv:0905.2160.
10. M. Lüscher and U. Wolff, Nucl. Phys. B 339 (1990) 222; B. Blossier *et al.*, JHEP 0904 (2009) 094, arXiv:0902.1265 [hep-lat]
11. C. Kim, C. Sachrajda and S. Sharpe, Nucl. Phys. B727 (2005) 218, hep-lat/0507006.
12. J. Pelaez and G. Rios, Phys. Rev. D 82 (2010) 114002, arXiv:1010.6008.
13. C.B. Lang, D. Mohler and S. Prelovsek, to be prepared for the LAT2011 proceedings.
14. J. Nebreda, J.R. Pelaez and G. Rios, Phys. Rev. D 83 (2011) 094011, arXiv:1101.2171;
15. J. Nebreda, J. R. Pelaez and G. Rios, arXiv:1108.5980

Bled Workshops
in Physics
Vol. 12, No. 1
p. 82

Proceedings of the Mini-Workshop
Understanding hadronic spectra
Bled, Slovenia, July 3 - 10, 2011

The pion cloud of the nucleon in the constituent quark picture ⋆

Bogdan Povh[a] and Mitja Rosina[b,c]

[a] Max-Planck-Institut für Kernphysik, Postfach 103980, D-69029 Heidelberg, Germany
[b] Faculty of Mathematics and Physics, University of Ljubljana, Jadranska 19, P.O. Box 2964, 1001 Ljubljana, Slovenia
[c] J. Stefan Institute, 1000 Ljubljana, Slovenia

Abstract. The importance of the pion cloud in the nucleon has been demonstrated in the study of the magnetic polarizabilities, electroexcitation, spin properties of the nucleon and, more recently, in deep inelastic scattering. The model in which the pion cloud of the nucleon is generated by the $qq\bar{q}$ component in the constituent quark has been successful in explaining the spin properties and the flavor asymmetric sea of the nucleon. We show that the same parameters yield the pion in $p \to n\pi^+$ and $p \to p\pi^0$ fluctuation in agreement with the observed value in the ($e + p \to e+$ forward neutron+X) experiment.

1 Introduction

First we review some evidence for the role of the pion cloud in explaining nucleon observables. As examples of low-energy processes, we quote the magnetic polarizabilities [1] and electroexcitation of the nucleon [2–4]. The pion cloud acts as a coil and gives a diamagnetic contribution while the virtual excitation of the N-like quark core into the Δ-like quark core acts as a paramagnet. The magnetic polarizability of the nucleon results from an approximate cancellation between these two contributions. Without the pion cloud, the paramagnetic contribution would dominate and give much too large magnetic polarizability. In the electroexcitation of the nucleon into Δ and into the Roper resonance, the linear σ-model with quarks and the cloudy bag model help us understand why (40 - 50)% of the dominant M1 ampliutude and 100% of the E2 amplitude is due to pion cloud.

The question arises, whether the same amplitude of the pion cloud (or equivalently, the same probability of pion fluctuation) can explain also observables measured at higher energies where the stucture functions of quarks play a role and pion is seen through its contribution to the corresponding quark and antiquark structure function.

2 Pion cloud in quarks can explain nucleon observables

The notion of the constituent quark applies generally to the massive quark dressed by gluons, the constituent of the nucleon. This non-relativistic model with three

⋆ Talk delivered by M. Rosina

massive constituent quarks works well for the hadronic masses and the magnetic moments. It breaks down if the spin properties of the baryons are considered. The improved version, the chiral constituent quark model is surprisingly succesful in explaining the spin properties of nucleons and hyperons. In the simplest form applied to the nucleon the chiral constituent quark is composed of a massive quark accompanied by a quark-antiquark pair coupled to the spin-parity quantum numbers of the pion $J^\pi = 0^-$. In the following we write the pion symbol as a shortcut to the quark-antiquark pair coupled to the pion quantum numbers. This simple model has been first applied by Eichten et al. [5] to explain the flavor asymmetry of the sea quarks and further elaborated by Baumgärtner et al. [6] and Pirner [7] in the interpretation of the spin properties of the nucleon. It is related to the three-flavour extension proposed by Cheng and Li [8]. Explicitly written, the chiral constituent up-quark (u) structure is

$$|u\rangle = \sqrt{(1 - \frac{3}{2}\,a)}\,|\mathbf{u}\rangle - \sqrt{a}|\mathbf{d}\pi^+\rangle + \sqrt{\frac{a}{2}}\,|\mathbf{u}\pi^0\rangle, \tag{1}$$

and of the down quark (d)

$$|d\rangle = \sqrt{(1 - \frac{3}{2}\,a)}\,|\mathbf{d}\rangle + \sqrt{a}|\mathbf{u}\pi^-\rangle - \sqrt{\frac{a}{2}}\,|\mathbf{d}\pi^0\rangle. \tag{2}$$

The basis of pure flavour quarks is denoted by boldface **u** and **d**.

At $Q^2 \approx 0$ gluons do not appear as an explicit degree of freedom and the nucleon is composed of quarks and quark-antiquark pairs. Thus in the lowest order the Fock state of the constituent quark has the form (1 and 2), where in the second and third term the quark-antiquark pair is coupled to the $J^\pi = 0^-$ quantum nummbers of the pion. This simple structure of the chiral constituent quark (1) has two attractive features. Firstly, as we will show, the chiral constituent quark reproduces the experimental results of the deep inelastic scattering and axial-vector beta decays of the neutron quantitatively; secondly, this model complies with our picture of the origin of the quark mass by the chiral symmetry breaking mechanism of Nambu and Jona-Lasino [9]. Dressing the light quark by gluons is inevitably accompanied by creation of the Goldstone boson, the pion. The Goldstone pion is an inherent part of the constituent quark.

The parameter a of (1, 2) is usually determined from the value of the axial vector coupling constant $g_A = 1.269 \pm 0.003$ [11] yielding $a = 0.239 \pm 0.002$. The parameter a measures the probability of the constituent quark to be in the state accompanied with a charged pion. Furthermore, with the probability $a/2$ the constituent quark is in a state component with the neutral pion. Thus the total probability of finding a pion in the constituent quark amounts thus to slightly more than one third. The large probability of the pion in the constituent quark is best manifested in the measurements of the quark polarization in the deep inelastic scattering. Not only that one third of the constituent quark with the pion does not contribute to the spin polarization, but even more, with the oppositely oriented quarks reduces the total quark polarization to one third of what would be without the pions. The loss of the angular momentum because of the oppositely

oriented quark is compensated by the orbital angular momentum of the pion in the p-state. The comparison of the experimental results of the deep inelastic scattering with the prediction of the chiral constituent-quark model is given in [10]. It is also worthwhile to mention that the valence-quark distribution does not peak at Bjorken $x = 0.3$ but it is softer and peaks at $x = 0.2$ corresponding to five and not three constitunts of the proton even before gluons can get excited. Eichten et al. ([5]) ascribe these quark-antiquark pairs to an asymmetric sea.

We consider also other observables which depend strongly on the pions in the nucleon: the Gottfried sum rule I_G (with corrections discussed in [10]), the integrals of the spin structure functions of proton I_p and deuteron I_d and the quark spin polarization $\Delta\Sigma$ [12,13]. They have larger error bars than g_A, but they agree reasonably well eith the model (Table 1.). The new experimental value for $\Delta\Sigma$ supports even more our assumption that the main contribution to the spin reduction comes from the pion fluctuation.

observable	model value	
$g_A = 1.269 \pm 0.003$	$\frac{5}{3}(1-a)$	$=$ input
$I_G = 0.216 \pm 0.033$	$\frac{1}{3}(1-2a)$	$= 0.174 \pm 0.002$
$I_p = 0.120 \pm 0.017$	$\frac{5}{18}(1-2a)$	$= 0.145 \pm 0.002$
$I_d = 0.043 \pm 0.006$	$\frac{5}{36}(1-3a)$	$= 0.039 \pm 0.001$
$\Delta\Sigma = 0.330 \pm 0.064$	$(1-3a)$	$= 0.283 \pm 0.006$

Table 1. The π^+ probability $a = 0.239 \pm 0.002$ is used to calculate different observables

3 The proton contains a neutron plus pion component

Let us consider the matrix element $\langle n\pi^+|p\rangle$.

Inserting for constituent quarks our chiral quarks it is evident that the $\langle n\pi^+|$ has an overlapp with a Fock component of the proton. The result of the explicit calculation is

$$|\langle n\pi^+|p\rangle|^2 = |\langle d\pi^+|u\rangle|^2 = (1 - \frac{3}{2}\,a)\,a = 0.15. \tag{3}$$

The result (3) means that the constituent u quark has a component of the d quark and a pion. Although the proton has two u quarks there is no factor 2 in the amplitude, due to the flavor-spin-color structure of the nucleon. The flavor-spin wavefunction of the proton has a mixed symmetry combined into a symmetric flavor-spin function:

$$|p\rangle = \sqrt{\frac{1}{2}}\ \begin{array}{|c|c|}\hline 1&2\\\hline 3\\\cline{1-1}\end{array}_{\,f} \times \begin{array}{|c|c|}\hline 1&2\\\hline 3\\\cline{1-1}\end{array}_{\,s} + \sqrt{\frac{1}{2}}\ \begin{array}{|c|c|}\hline 1&3\\\hline 2\\\cline{1-1}\end{array}_{\,f} \times \begin{array}{|c|c|}\hline 1&3\\\hline 2\\\cline{1-1}\end{array}_{\,s}. \tag{4}$$

A similar expression stays for the neutron. Since the combined wavefunction is symmetric under all permutations it is enough to look at the contribution of the

particles 1 and 2. In the first term of the proton wavefunction the particles 1 and 2 are symmetric and can both be u quarks and contribute constructively to the matrix element with a factor of two. In the second term the interference is destructive and the contribution cancels. Thus only the first term contributes to the matrix element. Since both in proton and in neutron the first term appears with a factor $\sqrt{1/2}$, the factor two is canceled out. This qualitative explanation can be verified by writing down the three-quark wavefunctions explicitly.

This can be seen even easier in the isospin formalism. In the act of producing a positive pion, the corresponding u quark loses one unit of charge, it becomes a d quark. This can be described with the operator $\sum_i t_-(i) = T_-$ where $T_- = T_x - iT_y$. We conveniently took the sum over all three quarks since the third quark, d, contributes zero anyway. The expectation value is $< TM-1|T_-|TM >= \sqrt{T(T+1)-M(M-1)}$ which for proton $(T = 1/2, M = 1/2)$ gives in fact the factor 1. It is instructive to compare with Δ^+ $(T = 3/2, M = 1/2)$ in the process $ep\rightarrow\ e\Delta X$ where one gets the factor 2, pointing out that the two u quarks are always symmetric and interfere constructively. Of course, for the squared amplitude, we get the additional factor a since only the π^+-dressed component of the u-quark contributes, and the factor $(1-\frac{3}{2}a)$ for the naked component of the final d-quark.

4 Experimental test of the pion fluctuation

The pion fluctuation of nucleon is well known in the classical nuclear physics as anomalously large pion-nucleon coupling constant $g^2/4\pi = 13.6$. Many of the nucleon properties are ascribed to the pion cloud of the nucleon [14]. Hovewer, there is no direct way of determinig experimentally the probability of finding a pion fluctuation in the proton. The best way is to calculate the pion flow by using the pion-nucleon coupling constant and the form factor assuming that the pion is emitted by a proton [15], [16]

$$f_{\pi^+/p}(x_L, t) = \frac{1}{2\pi}\frac{g^2_{p\pi n}}{4\pi}(1-x_L)^{1-2\alpha(t)}\frac{-t}{(m_\pi^2-t)^2}|G(t)|^2. \tag{5}$$

The pion flow is related to the measured cross section by

$$\mathbf{d}\sigma^{\gamma^* p\rightarrow nX} = f_{\pi^+/p}(x_L, t)\cdot \mathbf{d}\sigma^{\gamma^*\pi^+\rightarrow X} \tag{6}$$

where the $(\gamma^*\pi^+ \rightarrow X)$ DIS cross section is assumed to be 2/3 of the $(\gamma^* p \rightarrow X)$ DIS cross section in the cited analysis, with corrections due to absorption [10].

Obviously the pion is not emitted by a proton but by a quark. But as we showed above the state of the pion is dictated by the proton wave function and the pion form factor simulated well the assumption that the emission is from the proton. In the series of experiments [17]- [18], [19] measuring the spectrum of the forward neutrons in the reaction (e+p→e+forward n+X) has been shown that the high energy end of the neutron spectrum is consistent with the assumption that the deep inelastic scattering takes place on the pion. Thus we are justified to

say that the forward neutron is the signature of the reaction taking place on the pion and that the total probability of finding a pion in ep→nπ^+ fluctuation can be obtained by integrating over the variables of the pion flow.

The analysis depends to some extent on the estimation of pion flux $f_{\pi^+/p}$. The analysis has been elaborated in [10] and the quoted results are $\langle n\pi^+|p\rangle^2 = 0.165 \pm 0.01$ and 0.175 ± 0.01, respectively, for the two form factors best fitting to the experiment in [15] and [16].

5 Conclusion

The pion fluctuation p→n+π^+ and p→p+π^0 is an artifact of the quark-antiquark pairs of the constituent quarks. The impressive agreement between the measured and the calculated ratios between the probability of the pion fluctuation and the probability of finding a quark-antiquark pair of the constituent quark is a strong support of the constituent quark model.

In this section we stress the difference between the notion of the quark-antiquark pairs coupled to the pion quantum numbers being part of the constituent quarks and the pions of the proton. While the quark-antiquark pairs are implied by the experimental values of g_A, the integrated spin structure functions and the violation of the Gottfried summ rule, the fluctuating pions are identified by the characteristic energy and p_T distribution of the neutron spectra in the ep $\rightarrow$ nπ^+ reaction.

Eichten et al. [5] have named the quark-antiquark pairs of the constituent quark the asymmetric quark sea. This name emphasizes hopefully sufficiently the difference of their origin as compared to the normal quark sea.

For the value $a = \langle \mathbf{d}\pi^+|u\rangle^2 = 0.24$ each quark contains 0.36 quark-antiquark pairs. Summing up the quark-antiquark pairs one obtains about one quark-antiquark pair per nucleon. Using this value of a gives $\langle n\pi^+|p\rangle^2 = 0.15$. This number corresponds well with the experimental value of $\langle n\pi^+|p\rangle^2 = 0.165 \pm 0.01$ or 0.175 ± 0.01. It follows that in ≈ 0.26 cases the proton is a neutron+ π^+ or a proton+π^0. This means that about one quater of the nucleon's quark-antiquark pairs show up as the pion fluctuation.

Acknowledgments We wish to thank A. Bunyatyan for the discussions of the analysis on the forward neutron spectra and K. Rith for pointing us out the new results on spin-polarization data in DIS.

References

1. B. Golli and R. Sraka, Phys. Lett. B **312** (1993) 24-29.
2. M. Fiolhais, B. Golli and S. Širca, Phys. Lett. B **373** (1996) 229-234.
3. B. Golli and S. Širca, Eur. Phys. J. A **38** (2008) 271-286.
4. B. Golli, S. Širca and M. Fiolhais, Pion electro-production in the Roper region in chiral quark models, Eur. Phys. J. A **42** (2009) 185-193.
5. E.J.Eichten, I.Hinchliffe and C.Quigg, Phys. Rev. D **45** (1992) 2269.

6. S. Baumgaertner, H. J. Pirner, K. Koenigsmann, B. Povh, Z. Phys. A **353** (1996) 397.
7. H. J. Pirner, Prog. Part. Nucl. Phys. **36** (1996) 19-28.
8. T. P. Cheng and Ling-Fong Li, Phys. Rev. Lett. **74** (1995) 2872-2875.
9. S.P. Klevansky, Rev. Mod. Phys. **64** (1992) 694.
10. A. Bunyatyan and B. Povh, Eur. Phys. J. A **27** 2006 359-364.
11. K. Nakamura et al. (Particle Data Group), J. Phys. G **37** (2010) 075021.
12. K. Rith, Prog. Part. Nucl. Phys. **49** (2002) 245.
13. A. Airapetian et al., Phys. Rev. D **75** (2007), 012007.
14. A. W. Thomas, Prog. Theor. Phys. **168** (2007) 614
15. B. Kopeliovich, B. Povh and I. Potashnikova, Z. Phys. C **73** (1996) 125, [hep-ph/9601291].
16. H. Holtmann *et al.*, Phys. Lett. B **338** (1994) 363.
17. C. Adloff *et al.* [H1 Collaboration], Eur. Phys. J. C **6** (1999) 587, [hep-ex/9811013].
18. A. Aktas *et al.* [H1 Collaboration], Eur. Phys. J. C **41** (2005) 273, [hep-ex/0501074].
19. S. Chekanov *et al.* [ZEUS Collaboration], Phys. Lett. B **610** (2005) 199, [hep-ex/0404002], and references therein.

Bled Workshops
in Physics
Vol. 12, No. 1
p. 88

Proceedings of the Mini-Workshop
Understanding hadronic spectra
Bled, Slovenia, July 3 - 10, 2011

Recent experimental results from MAMI (Mainz), ELSA (Bonn), and JLab*

S. Širca[a,b]

[a] Faculty of Mathematics and Physics, University of Ljubljana, Slovenia
[b] Jožef Stefan Institute, Ljubljana, Slovenia

Abstract. In the past year a large set of new data on photo- and electro-production of mesons on nucleons and light nuclei has emerged, both near threshold and throughout the nucleon resonance region. Some of the most recent results from the three leading experimental facilities, MAMI (Mainz, Germany), ELSA (Bonn, Germany), and Jefferson Lab (Newport News, USA) relevant to this workshop are presented.

1 π and η photo-production on protons

In conjunction with the development of polarized target techniques and polarimetry capabilities, production of single mesons by real photon beams has recently become the richest source of information on nucleon dynamics from the meson production threshold and throughout the nucleon resonance region. The basic quantities that can be measured when polarization is exploited, are:

$$\sigma\,,T\,,$$

when the photon beam and the target are both unpolarized, and when the beam is unpolarized and the target is polarized along the y-direction, respectively;

$$\Sigma\,,H\,,P\,,G\,,$$

with linearly polarized beam and no target polarization, and with target polarized along x-, y- and z-directions, respectively;

$$F\,,E\,,$$

when the beam is circularly polarized and the target polarization is along the x- and z-directions, respectively. (The z-axis points along the beam; the z- and x-axes span the meson production plane; the y-axis is perpendicular to it.) In addition to resolving the spin (helicity) structures, so-called complete experiments can be performed for which measurements of the same observables have to be performed in different reaction channels, so that isospin decomposition can be done as well. Such measurements are also underway.

* Talk delivered by S. Širca

With the Crystal Ball and TAPS detectors at ELSA, preliminary results for Σ (beam-helicity asymmetry) in the $\vec{\gamma}p \to p\pi^0$ and $\vec{\gamma}p \to p\eta$ processes have been obtained at $E_\gamma = 1050\,\mathrm{MeV}$ as a function of the pion emission angle θ [1,2]. Almost the complete angular range has been covered at this energy. Apart from a few modest unresolved deviations between the ELSA and older GRAAL data sets [3] at extreme backward angles, all data are in excellent agreement with the MAID and SAID analyses, as well as the Bonn-Gatchina Partial-Wave Analysis (PWA). Moreover, there is a new precise unpolarized data set for η photoproduction from MAMI [4] which provides precise cross sections up to 400 MeV above threshold. Very sturdy results have been obtained on the angular expansion coefficients A_1, A_2, and A_3, which will be of great help in improving various PWA.

On the other hand, measurements of Σ in single-pion photo-production have also been performed at Jefferson Lab within the CLAS Collaboration in the g8b group of experiments, and here the agreement with respect to the theory (in particular MAID) is not as good. Largest deviations are observed at forward angles where Σ is typically underestimated by theory. Because both final channels on the proton target ($p\pi^0$ and $n\pi^+$) have been measured, different sensitivities to $N^\star$ and Δ resonances could be probed. This is a very comprehensive and large data set encompassing all angles and photon energies from 1000 to 2000 MeV.

At ELSA, Σ has also been determined at $\theta = 110^\circ$ as a function of E_γ ranging from about 700 to 1200 MeV, indicating that the $P_{11}(1440)$, $D_{13}(1520)$ and $F_{15}(1680)$ resonances are all needed (at least within the MAID model) to reproduce the energy dependence of Σ.

Most recently, similar-quality results have been obtained at ELSA for the double-polarization asymmetry G in $\vec{\gamma}\vec{p} \to p\eta$ (energy dependence at $\theta = 110^\circ$), as well as for G in the $\vec{\gamma}\vec{p} \to p\eta$ process. In the $p\eta$ channel, at $E_\gamma = 950$ and 1050 MeV, the preliminary data on G appears to be in rough agreement with the Bonn-Gatchina PWA and MAID, but is underestimated by SAID at 1050 MeV.

2 Electro-excitation of nucleon resonances

The focus of investigations of nucleon resonance excitations has recently shifted away from the Delta region to the first and second resonance regions. The bulk of the new data comes from the CLAS Collaboration and EBAC (Excited Baryons Analysis Center) at Jefferson Lab.

The most spectacular advances have been made regarding the Roper resonance $N^*(1440)$. The transverse and scalar helicity couplings extracted from a wealth of previous single-pion production data [5,6] and the most recent two-pion data set [7] are in excellent mutual agreement. In the framework of the EBAC analysis, this allows for a model-independent determination of the N^* electromagnetic couplings for Q^2 up to $\approx 4\,\mathrm{GeV}^2$. It is now clear that the transverse helicity amplitude $A_{1/2}$ crosses zero in the vicinity of $Q^2 \approx 0.5\,\mathrm{GeV}^2$ and that the structure of the Roper can evidently be explained in terms of a quark core as a first radial excitation of three dressed quarks, plus external meson-baryon dressing. (The CLAS12 project will test these findings to much higher $Q^2 \approx 12\,\mathrm{GeV}^2$.)

There are also new data on helicity amplitudes for the electro-excitation of the $N^*(1535)$ resonance on the proton, extracted from both the $n\pi^+$ and the $p\eta$ channel, both of which, again, are in good agreement between each other in the transverse case (while there are no $p\eta$ data in the scalar case). Note that this is the first extraction ever of $S_{1/2}(Q^2)$ up to $Q^2 \approx 4\,\mathrm{GeV}^2$.

With the present data on $A_{1/2}$ extending to relatively high values of Q^2, it is now possible to investigate (or rather, speculate) whether transitions to the regime of perturbative QCD occur. The main motivation behind these scaling studies is to observe the transition to photon interactions with the dressed quarks. The Q^2 dependence of the product $Q^3A_{1/2}(Q^2)$ has been studied as function of Q^2 in the P11 channel (Roper), the S11 channel ($N^*(1535)$) and the D13 channel ($N^*(1520)$). Apparently $Q^3A_{1/2}(Q^2)$ flattens out at Q^2 as low as $\approx 3\,\mathrm{GeV}^2$, persisting to $Q^2 \approx 4\,\mathrm{GeV}^2$ where the data ceases. But although this plateau is appealing, extensions to higher Q^2 are needed to confirm it.

3 π, $\pi\pi$, and η photo-production on deuterons

Most interesting experiments have been performed on the deuteron, in particular single-π^0 and single-η photo-production. The reaction mechanisms for π^0 photo-production are

$$\gamma + \mathrm{d} \longrightarrow \begin{cases} \pi^0 + \mathrm{p(n)} \;;\; \mathrm{quasi-free\ on\ p}\,, \\ \pi^0 + \mathrm{n(p)} \;;\; \mathrm{quasi-free\ on\ n}\,, \\ \pi^0 + \mathrm{d} \quad\;\; ;\; \mathrm{coherent}\,. \end{cases}$$

For $E_\gamma > 500\,\mathrm{MeV}$, the coherent contribution is negligible. Practically all measurements focus on that region, where the sum of the exclusive processes on the proton and the neutron should almost exactly add up to the quasi-free inclusive result. This process has been previously measured at MAMI/A2 [8] and LNS Sendai [9], but has now been superseded by a much lovelier data set [10].

Single-meson production on deuterons has important ramifications regarding the inclusion of D13, F15, and D15 resonances in unitary-isobar models and partial-wave analyses, as the proton and neutron channels exhibit distinct sensitivities to these ingredients. Two-pion production on the proton and the deuteron (allowing for the extraction of the corresponding neutron channel contribution) is relevant in the very same sense [11]. New preliminary data on $\gamma p \to p\pi^0\pi^0$ and $\gamma n \to n\pi^0\pi^0$ from the CB/TAPS @ MAMI Collaboration has become available, indicating that the electro-magnetic excitation of the F15 is relatively stronger on the proton, while the excitation of the D15 is stronger on the neutron. Helicity asymmetries for these two processes have also been measured.

But of the recent data sets, one of the most exciting and puzzling is that on quasi-free η photo-production on the deuteron,

$$\gamma + \mathrm{d} \to \eta + \mathrm{n(p)}\,,$$

acquired by the CB/TAPS Collaboration at ELSA. The differential cross-section for this process exhibits a narrow structure at $W \approx 1.65\,\mathrm{GeV}$, regardless of the

emission angle (specifically, it has been most often shown at $-0.9 < \cos\theta < -0.5$, $-0.3 < \cos\theta < 0.1$, and $0.1 < \cos\theta < 0.5$). The structure has been observed previously at LNS Sendai, by the GRAAL Collaboration [12], but now high precision data by the CBELSA/TAPS Collaboration has become available [13], clearly identifying the structure at

$$W = 1660\,\mathrm{MeV}\,, \qquad \Gamma = (25 \pm 12)\,\mathrm{MeV}\,.$$

Because the excess cross-section appears in the rescaled neutron cross-section as compared to the free-proton and quasi-free proton cases, this structure has become known as the "neutron anomaly". The reasons for the anomaly remain unknown, although several explanations have been offered. It may be an interference effect of the S11(1650) and P11(1710) resonances; it may be caused by a non-strange penta-quark; but it could also be generated by a $K\Sigma$ threshold enhancement of the neutron cross-section as a consequence of the pion loops. Note that while the ηp cross-section is $\approx 80\,\%$ S-wave, the nature of the ηn is not so well known.

At ELSA, quasi-free η photo-production has also been measured on ^{3}He nuclei. The idea behind replacing the deuteron by ^{3}He is that these nuclei have different nucleon momentum distributions (in the deuteron case, it peaks at $\approx$ 40 MeV, while it is maximal at ≈ 70 MeV in ^{3}He). This should generate different proton/neutron cross-section contributions in the processes

$$\gamma + {}^3\mathrm{He} \longrightarrow \eta + \mathrm{p(pn)}\,,$$
$$\gamma + {}^3\mathrm{He} \longrightarrow \eta + \mathrm{n(pp)}\,.$$

Apparently the broad structure at $W \approx 1.65$ GeV persists, with $\Gamma = (45 \pm 11)$ MeV, which is comparable to the experimental resolution.

References

1. D. Elsner et al. (CB/TAPS @ ELSA Collaboration), Eur. Phys. J. A **39** (2009) 373.
2. A. Thiel et al. (CB/TAPS @ ELSA Collaboration), submitted for publication.
3. O. Bartalini et al. (GRAAL Collaboration), Eur. Phys. J. A **26** (2005) 399.
4. E. F. McNicoll et al. (CB @ MAMI Collaboration), Phys. Rev. C **82** (2010) 035208.
5. M. Dugger et al. (CLAS Collaboration), Phys. Rev. C **79** (2009) 065206.
6. I. Aznauryan, V. Burkert et al., Phys. Rev. C **80** (2009) 055203.
7. V. Mokeev, AIP Conf. Proc. **1374** (2011) 349.
8. B. Krusche et al. (A2 Collaboration), Eur. Phys. J. A **6** (1999) 309.
9. H. Shimizu, NNR Workshop 2009, Edinburgh, June 8-10, 2009 (unpublished).
10. M. Dieterle et al. (A2 Collaboration), contribution to the Hadron 2011 Conference, Munich, June 13-17, 2011, arXiv:1108.6241 [nucl-ex].
11. H. Arenhövel, A. Fix, L. Tiator, Eur. Phys. J. A **25** (2005) 115.
12. A. Kuznetsov et al. (GRAAL Collaboration), Phys. Lett. B **647** (2007) 23.
13. I. Jaegle et al. (CBELSA/TAPS Collaboration), Eur. Phys. J. A **47** (2011) 89.

BLEJSKE DELAVNICE IZ FIZIKE, LETNIK 12, ŠT. 1, ISSN 1580-4992

BLED WORKSHOPS IN PHYSICS, VOL. 12, NO. 1

Zbornik delavnice 'Razumevanje hadronskih spektrov',
Bled, 3. – 10. julij 2011

Proceedings of the Mini-Workshop 'Understanding hadronic spectra',
Bled, July 3 – 10, 2011

Uredili in oblikovali Bojan Golli, Mitja Rosina, Simon Širca

Publikacijo sofinancira Javna agencija za knjigo Republike Slovenije

Tehnični urednik Tadeja Šekoranja

Založilo: DMFA – založništvo, Jadranska 19, 1000 Ljubljana, Slovenija

Natisnila tiskarna Bori v nakladi 120 izvodov

Publikacija DMFA številka 1853

Brezplačni izvod za udeležence delavnice